11/12/95 10:00 202 767 4906 AFOSR/NA

REPORT DOCUMENTATION PAGE

Form Approved
OMB No. 0704-0188

1. AGENCY USE ONLY (Leave blank)	2. REPORT DATE	3. REPORT TYPE AND DATES COVERED
	July 1995 FINAL	March 21, 1994 - June 30, 1995

4. TITLE AND SUBTITLE EXPERIMENTAL INVESTIGATION OF THREE-DIMENSIONAL VORTEX-AIRFOIL INTERACTION IN A SUPERSONIC STREAM

5. FUNDING NUMBERS
F49620-94-1-0210
2307/A5

6. AUTHOR(S)
Iraj M. Kalkhoran

7. PERFORMING ORGANIZATION NAME(S) AND ADDRESS(ES)
Polytechnic University
Six Metrotech Center
Brooklyn, New York 11201

8. PERFORMING ORGANIZATION REPORT NUMBER
POLY-AE 95-3

9. SPONSORING/MONITORING AGENCY NAME(S) AND ADDRESS(ES)
Dr. Leonidas Sakell
AFOSR/NA
110 Duncan Avenue
Bolling AFB, DC 20332-0001
NA

10. SPONSORING/MONITORING AGENCY REPORT NUMBER
F49620-94-1-0210

AFOSR-TR-95
0564

11. SUPPLEMENTARY NOTES

12a. DISTRIBUTION/AVAILABILITY STATEMENT
Unlimited
Approved for public release, distribution unlimited

12b. DISTRIBUTION CODE

13. ABSTRACT (Maximum 200 words)

An experimental study of the interaction between stream-wise vortices and a two-dimensional surface was conducted in a Mach 2.5 flow. The influence of oblique shock wave intensity on the inherently three-dimensional interaction was examined for vortices of variable strength. Planar laser sheet visualizations of the flowfield generated by the interaction at several distances downstream of the wedge leading edge were performed in order to gain an understanding of vortex behavior at distances further downstream. Results indicated that the interaction of a moderate strength vortex with an oblique shock wave leads to the formation of a steady separated shock structure upstream of the oblique shock front. Planar laser sheet visualization of the flowfield revealed an expansion of the vortex core in crossing a strong oblique shock front. The vortical structure was observed to persist along the entire chord of the shock generating wedge but was seen to diffuse with distances downstream of the wedge leading edge. Measurements of the vortex center above the wedge surface indicated that immediately downstream of the normal portion of the bulged-forward shock wave the vortex center was parallel to the direction of the free stream flow.

14. SUBJECT TERMS			15. NUMBER OF PAGES 80
			16. PRICE CODE
17. SECURITY CLASSIFICATION OF REPORT Unclassified	18. SECURITY CLASSIFICATION OF THIS PAGE Unclassified	19. SECURITY CLASSIFICATION OF ABSTRACT Unclassified	20. LIMITATION OF ABSTRA Unlimited

NSN 7540-01-280-5500

Standard Form 298 (Rev. 2-89)
Prescribed by ANSI Std. Z39-18
298-102

TABLE OF CONTENTS

I. ABSTRACT	1
II. INTRODUCTION	2
III. EXPERIMENTAL PROGRAM	5
i. Wind Tunnel and Test Conditions	5
ii. Vortex Generators	5
IV. VORTEX SURVEY	6
i. Computational Calibration of the Conical Probes	6
ii. Experimental Results	7
V. OBLIQUE SHOCK WAVE/VORTEX INTERACTION	9
i. Weak Interactions Results	9
ii. Strong Interaction Results	11
VI. PLANAR LASER SHEET VISUALIZATION DURING THE OBLIQUE SHOCK WAVE/VORTEX INTERACTION	14
VII. CONCLUSIONS	15
VIII. RECOMMENDATIONS FOR FUTURE WORK	16
IX. REFERENCES	16
X. APPENDICES	
A. PERSONNEL SUPPORTED	36
B. CONFERENCE PAPERS	37
C. JOURNAL PUBLICATIONS	78

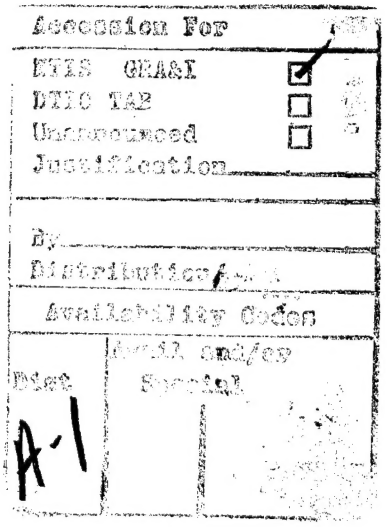

Experimental Investigation of Three-Dimensional Vortex-Airfoil Interaction in A Supersonic Stream

Iraj M. Kalkhoran
Department of Aerospace Engineering
Polytechnic University, Brooklyn NY 11201

I. ABSTRACT

An experimental study of the interaction between stream-wise vortices and a two-dimensional surface was conducted in a Mach 2.5 flow. The experimental scheme involved positioning an instrumented two-dimensional wedge downstream of a semi-span wing so that the trailing tip vortex from the wing interacted with the wedge surface. The experiments were designed to simulate interaction of streamwise vortices with aerodynamic surfaces. The influence of oblique shock wave intensity on the inherently three-dimensional interaction was examined for vortices of variable strength. Planar laser sheet visualizations of the flowfield generated by the interaction at several distances downstream of the wedge leading edge were performed in order to gain an understanding of vortex behavior at distances further downstream. Results indicated that the interaction of a moderate strength vortex with an oblique shock wave leads to the formation of a steady separated shock structure upstream of the oblique shock front. The scale of the structure increased with shock wave intensity and showed a close resemblance to the unsteady vortex distortion observed during the head-on interaction of stream-wise vortices with a wedge leading edge reported in previous studies. Planar laser sheet visualization of the flowfield revealed an expansion of the vortex core in crossing a strong oblique shock front. The vortical structure was observed to persist along the entire chord of the shock generating wedge but was seen to diffuse with distances downstream of the wedge leading edge. Measurements of the vortex center above the wedge surface indicated that immediately downstream of the normal portion of the bulged-forward shock wave the vortex center was parallel to the direction of the free stream flow. On the other hand, the vortex traveled parallel to the wedge surface at distances downstream of the wedge mid-chord position.

In order to characterize the properties of the generated vortices, an experimental survey of the wing tip vortices was conducted. The measurement technique involved using small scale 4-hole and 5-hole conical probes combined with a numerical calibration of the probes. The survey was performed 2.25 chords downstream of a semi-span rectangular wing at angles of attack of 5.7 and 10.4 degrees. Combination of 4-hole conical probe measurements with independent pitot pressure measurements indicated a significant Mach number and total pressure deficit in the core regions of supersonic wing tip vortices, combined with an asymmetric 'Burger like' swirl distribution.

II. INTRODUCTION

Concentrated streamwise vortices occur in many aeronautical applications such as the flow past airfoils and slender bodies at sufficiently high angles of incidence. They are formed by the separation and subsequent roll up of the thin viscous sheet near a surface which once away from the surface then convects downstream with the surrounding flow. This concentrated rotational region contained in a generally irrotational flow may then interact with other components of an aircraft or body of interest. For example, the vortices shed by the forebody or canards of a high speed aircraft flying at angle of attack (Fig. 1(a)) may pass over or strike its wings and aft control surfaces leading to loss of lift, increased drag or changes in the pitching moment characteristics of the aircraft. Another deleterious possibility is the ingestion of streamwise vortices by the air intake systems (Fig. 1b) resulting in decreased engine performance or blockage of the engine intake. The flowfields generated by such encounters are in general three-dimensional in nature and at supersonic speeds exhibit strong compressibility effects due to the presence of shock waves.

The strength of streamwise vortices steadily increases with the angle of incidence of the wing or body until a drastic disruption to its structure occurs, commonly called 'vortex breakdown'.[1-4] This phenomenon is characterized by a sudden increase in the size of the vortex, the appearance of a stagnation point on its axis and the presence of large scale unsteadiness. It is well known that in low speed flow vortex breakdown may also be precipitated in a streamwise vortex by the application of a sufficiently strong adverse pressure gradient.[5] A considerable number of investigations have been reported in this area including several review articles by Hall,[6] Liebovitch[7] and most recently by Delery.[8] In supersonic flows it has been experimentally demonstrated that vortex breakdown can result from the interaction of sufficiently strong streamwise vortices with normal shock waves.[9-11] The interaction of vortices with shock waves and in particular supersonic vortex breakdown has been investigated by a few authors, but has only recently attracted serious attention.

Shock wave/vortex interactions are generally separated into two distinct classifications; normal shock wave/vortex interactions and oblique shock wave/vortex interactions (Fig. 2). Interaction of a vortex with a normal shock wave always results in a change from supersonic flow (a supercritical region incapable of admitting upstream wave propagation) to subsonic flow (a subcritical region that allows upstream propagating waves). The interaction of a vortex with an oblique shock wave does not necessarily involve a supercritical to subcritical transition, as in most cases the flow remains supersonic behind the shock wave. A simple examination of the shock wave/vortex interaction problem indicates that the governing simulation parameters are the free stream Mach number and Reynolds number, a vortex intensity parameter defined by $\Gamma V_\infty/l$ (where l is an appropriate characteristic length), and a shock strength parameter such as the density ratio across the shock. For the oblique shock wave/vortex interaction the shock wave inclination angle is also an important parameter, since for these encounters the downstream flow properties depend on the component of Mach number normal to the

shock.

Introduction of a stream-wise vortex upstream of an otherwise planar shock wave will in general lead to curvature of the shock front due to gradients in Mach number and stagnation pressure in the vortex. Examining the geometry of the normal shock wave/vortex interaction (Fig. 2(a)), if the shock wave remained normal to the freestream during the interaction, the vortex swirl would be at all times tangent to the shock wave and therefore have no effect upon it. However as the shock wave deforms in response to axial Mach number and stagnation pressure gradients in the vortex core, the swirl will contribute to the shock curvature in a non-uniform manner depending on the local component of swirl Mach number (M_t) normal to the shock front. It is clear therefore that the interaction of a stream-wise vortex with a normal shock wave will in general lead to a three dimensional curvature of the shock front. For the special case of an axi-symmetric streamwise vortex, in which the Mach number and stagnation pressure vary in an axi-symmetric manner, the curved shock front degenerates to an axi-symmetric form. Examining the geometry of the oblique shock wave/vortex interaction (Fig. 2(b)), the fact that the undisturbed shock front is not normal to the free stream introduces an extra 'non-symmetric' element to the shock wave curvature produced by a given stream-wise vortex. A three-dimensional curvature of the shock front will always occur in this case, even if the incoming vortex is axi-symmetric. In summary, all shock wave/vortex interactions include a three-dimensional curvature of the shock wave, which for the special case of the interaction between an axi-symmetric stream-wise vortex and a normal shock wave degenerates to an axi-symmetric form.

A first step in the analysis of any shock wave/vortex interaction is the determination of the three-dimensional curved shock front. Given that this non-trivial task has been accomplished, the changes in the vortex properties across the shock wave are of interest, in particular the change in its vorticity. Fundamental studies by Hays[9] demonstrated that the vorticity jump across a general three dimensional curved shock is given by:

$$\delta\zeta_n = 0 \tag{1}$$

$$\delta\zeta_t = n \times [\nabla_t(\rho V_n)\delta\rho^{-1} - (\rho V_n)^{-1} V_t \cdot \nabla_t V_t \delta(\rho)] \tag{2}$$

where $\mathbf{n}$ is the unit vector normal to the discontinuity surface, the subscript t indicates the component of vector quantities tangent to the shock surface, and the velocity vector $\mathbf{V}$ for the flowfield is given by:

$$\mathbf{V} = \mathbf{n}V_n + \mathbf{V}_t \tag{3}$$

It is clear from these equations that there is no vorticity jump normal to the shock surface and that the vorticity jump tangent to the shock surface depends only on the density jump across the shock and the upstream properties. Due to the shock wave

curvature inherent in all shock wave/vortex interactions, a stream-wise vortex will undergo a change in its vorticity for both normal and oblique shock wave/vortex interactions alike.

Previous experimental and numerical studies relevant to the interaction problem have concentrated on the interaction of streamwise vortices with normal shock waves. Delery et al[10] carried out a wind tunnel study of the interaction between streamwise vortices of constant axial Mach number and normal shock waves, reporting some shock-induced modifications to both the structure and the trajectory of vortices. Their results indicated that interactions in which vortex breakdown occurred lead to negative axial velocity at the vortex axis, a considerable reduction in maximum tangential velocity, and an increase in the radius of the vortex core. Based on these experiments they established a vortex breakdown limit as a function of vortex swirl rate and shock wave intensity. A numerical study reported with the experiments[10] using the steady axi-symmetric Euler equations predicted a similar breakdown limit, but was not able to accurately calculate flow structure downstream of the breakdown.

Interaction of vortices with normal shock waves was also studied experimentally by Metwally et al,[11] and Cattafesta et al,[12] both of whom reported a strong influence of vortex swirl rate and Mach number on the interaction, a vortex breakdown, and an oscillating upstream shock propagation. Based on their experiments, Metwally et al[11] suggested a hypothetical supersonic vortex breakdown model consisting of a region of reversed flow as well as a stagnation point downstream of a bulged-forward shock wave. The interaction of streamwise vortices with normal shock waves in an inlet type configuration was experimentally investigated by Zatoloka et al.[13] They reported development of a stagnation zone as a result of the encounter and also showed some distorted shock patterns. Experiments involving the head-on interaction of wing tip vortices with the leading edge of a shock generating wedge were reported by Kalkhoran.[14] This interaction is different from the studies mentioned above, as a stagnation point is forced to occur in the flow at the wedge leading edge. It was observed during these experiments that the encounter resulted in formation of an unsteady detached shock front far upstream of the wedge leading edge. This structure was reported to instantaneously form a conical slip surface separating an internal subsonic flow from a surrounding supersonic region. No free standing stagnation point or flow recirculation was reported. It was not clear from these experiments whether the detected unsteadiness was due to an observed unsteady in-wash of the incoming tip vortex or whether the unsteadiness was a feature of the head-on interaction.

The aforementioned studies all involved interaction of concentrated stream-wise vortices with normal shock waves. Previous studies of the oblique shock wave/vortex interaction problem include a numerical study by Corpening and Anderson[15] in which the steady three-dimensional Euler equations were used to study interaction of vortices with oblique shock waves at Mach numbers of 2.28 and 5.0. They observed no vortex breakdown or appreciable alteration of vortex strength as a result of interactions, but did report a deformation of the planar shock into a three-dimensional convex-concave shock

shape. An experimental study of the interaction between streamwise vortices and oblique shock waves was reported by Kalkhoran and Sforza.[16] In this study a tip vortex from a rectangular wing interacted with the oblique shock wave generated by a 27^{o} two dimensional wedge in a Mach 3 stream. Vortex strength and separation distance between the vortex and the wedge leading edge were varied while the shock strength remained constant. An unsteady interaction was observed and time averaged wedge surface pressure measurements were presented showing significant suction on the forward portions of the wedge. An unsteady in-wash of the incoming tip vortex was observed in a similar fashion to reference 14.

The oblique shock wave/vortex interaction study reported here has been conducted at Mach 2.5 with a similar experimental configuration to that used in reference 16. The experimental scheme involved positioning an instrumented two-dimensional wedge downstream of a semi-span wing so that the trailing tip vortex from the wing interacted with the oblique shock wave formed over the wedge surface. The essential aim of the study was to examine the effect of shock strength on oblique shock wave/vortex interaction, a facet of the shock wave/vortex interaction problem not previously addressed. Furthermore, the study was designed to investigate vortex distortion phenomenon during oblique shock wave/vortex interaction, since numerical solutions of the problem[15,17] have not indicated any vortex distortion or breakdown as a result of such encounters. Modifications to the experimental configuration of reference 16 included a simpler vortex generator wing geometry, the inclusion of a variable angle shock generating wedge, and the installation of miniature high frequency pressure transducers at the wedge surface. In addition, the study has been conducted in a Mach 2.5 wind tunnel[18] of larger size than the Mach 3 facility used for the previous studies[14,16].

III. EXPERIMENTAL PROGRAM

i. Wind Tunnel and Test Conditions

The current investigation was conducted in Polytechnic University's 15 x 15 in^2 supersonic blowdown wind tunnel facility.[18] It is an intermittent blowdown wind tunnel with a square test section of 38.1 cm x 38.1 cm (15 in x 15 in) and is capable of producing unit Reynolds numbers in the range of 26 x 10^6 to 22 x 10^7 per meter (8 x 10^6 to 66 x 10^6 per foot) over a Mach number range from 1.75 to 4.0. The experimental studies reported here were conducted at a nominal test section Mach number of 2.49. The stagnation pressure and temperature for these experiments were 0.45 MPa (65 psia) and 290 K respectively, resulting in a unit Reynolds number of 4.3 x 10^7 per meter (1.3 x 10^7 per foot). A typical test time for the experiments was three seconds.

ii. Vortex Generators

The vortex-generator was a rectangular half-wing with a diamond shaped cross section (8 degree half angle), a chord length of 50.8mm (2 in), a span of 165.1 mm (6.5 in) and angle of attack capability from 0 to 10 degrees. The shock wave-generator was a

two-dimensional wedge section with an included angle of 20^{o}, a chord-wise length of l=76.3 mm (3.0 in) and a span of 178.2 mm (7.0 in).

IV. VORTEX SURVEY

Multi-hole conical probes have traditionally been the instrument of choice for measurements in three-dimensional supersonic flowfields. The drawbacks of conventional conical probes are their relatively slow time response, of the order of 1 second, and the time consuming experimental calibration procedure. An alternative to this is the generation of probe calibration curves using a numerical flow solver which was used during the present investigation.

Two small scale conical probes were used in for the current study. Each probe had a diameter of 3.2 mm (0.125 in) and a half angle of 30 degrees. The 5-hole conical probe included four equally spaced static pressure orifices on the cone surface (denoted a, b, c and d), together with a total pressure orifice placed centrally on a blunted nose (denoted e). The 4-hole conical probe included four equally spaced static pressure orifices on the cone surface but had negligible nose bluntness. Geometry of the conical probes used for vortex mapping of the present investigation is shown in Fig. 3. The spherical co-ordinate system shown in Fig. 4 is used for the current work. The z direction is parallel with the free stream and the probe axis, while the x and y directions are horizontal and vertical respectively. The sign convention for the pitch angle and the roll angle are as shown in Fig. 4. The conical probes were manufactured with a permanent roll angle of 5^{o}, so the surface pressure orifices a,b,c and d were at circumferential angles 5, 275, 185 and 95 degrees respectively.

i. Computational Calibration of the Conical Probes

The calibration of conical probes has traditionally required an exhaustive amount of experimental data taken with the probe at different pitch and roll angles, over a range of Mach numbers. In the present study the conical probe calibration curves were generated using a computational solution. These solutions were obtained using a Navier-Stokes solver developed by Marconi.[19] This code uses a computational algorithm based on Beam and Warming's approximate factorization[20] in conjunction with Roe's flux difference splitting.[21] The solution of the equations is accomplished using an upwind alternate direction implicit technique similar to that of Thomas.[22] In the present study it was found that for the Reynolds numbers considered, the solutions obtained by running the code as an Euler solver agreed well with the Navier-Stokes solutions. Thus all the data presented here was obtained from inviscid computations.

The process of numerically generating a full set of calibration curves for a conical probe with specified half angle is as follows. Firstly, a conical grid must be generated to match the probe geometry. For the current work the 81 x 63 grid used was sheared to the leeward side to capture all shocks. Computational runs can then be completed for each combination of Mach number and pitch angle in the range of interest. Note that

each run calculates the complete flow past the probe, so that the full circumferential pressure distribution can be extracted from a single run. For the current work the Mach number range of interest was between Mach 1.75 and 2.5, and the maximum pitch angle was 20^{o}. These values represent the anticipated Mach numbers and maximum flow angularity in the core region of supersonic wing tip vortices. Calibration curves were generated for M = 1.75, 2.0, 2.25 and 2.5 at pitch angle increments of 5 degrees. A typical calibration curve for Mach 2.5 is shown in Fig. 5. After Centolanzi,[23] the surface pressure data at each θ and ϕ is plotted versus $C_{p\eta} = (P_d - P_b)/q_\infty$ and $C_{p\xi} = (P_a - P_c)/q_\infty$. It is generally found[23,24] that when experimental 5-hole probe data is plotted in this way, little variation with Mach number occurs. This was also the case for the numerically generated data used in the current work. The pointed cone assumption made in the numerical model means that no calculation of the pitot pressure is performed in the numerical solution at different pitch angles and Mach numbers. Results of both Centolanzi[23] and Naughton et al[24] showed that between Mach 1.5 and 4, the pitot pressure measured by a 5-hole conical probe corresponds well with the theoretical stagnation pressure behind a normal shock for pitch angles up to 20^{o}. Hence the Raleigh pitot formula is used in the current work to complete the data needed for a full conical probe calibration. Figure 6 shows a graph of P_{av}/P_2 (where $P_{av} = (P_a+P_b+P_c+P_d)/4$) versus Mach number calculated using the numerical method and the Raleigh pitot formula.

The iterative procedure for determining the Mach number, total pressure and flow angularity from the pitot and surface pressures measured by a 5-hole probe is fully described in references 23 and 24. In short, the flow Mach number is estimated from the ratio P_{av}/P_2, and then combined with the measured cone surface pressures to calculate $C_{p\eta}$ and $C_{p\xi}$. The two Euler angles θ and ϕ can then be determined from calibration maps such as Fig. 5. In general, iteration is required because P_{av}/P_2 varies with θ, hence after a first estimate of Mach number and flow angularity has been made, the Mach number must be adjusted for this variation. It is usually found[23,24] that only one or two iterations are required. A plot of the ratio P_{av}/P_2 versus calculated by the numerical scheme at Mach 2.5 is shown in Fig. 7. Negligible variation of P_{av}/P_2 is observed, which was the case for all the Mach numbers included in the calibration, hence no iteration of the Mach number is required. Determination of the flow properties in the current work was therefore reduced to a one step procedure. In summary, the determination of flow properties using the numerically generated calibration curves is identical to the conventional procedure, except that no iteration is required.

ii. Experimental Results

Cone probe surveys were conducted for the wing tip vortices generated by the half-wing at α = 5.7 and 10.4 degrees. In this work, the vortex generated by the half-wing at α= 5.7 degrees will be called the weak vortex, and that generated by the half-wing at α= 10.4 degrees will be called the strong vortex. The survey of each tip vortex was conducted 2.25 half-wing chords downstream of its trailing edge in a spanwise (vertical) line through the axis of each vortex. The lateral position of the vortex axes is de-

fined as the position at which the pitot pressure was observed to be a minimum. The downwash of each vortex is then the lateral distance from the trailing edge of the half-wing to the position of minimum pitot pressure. The downwash for the weak and strong vortices was measured to be 2.0 mm and 2.5 mm respectively. Spanwise pitot pressure surveys through the axis of each vortex are shown in Fig. 8. The spanwise position of the vortex axes is defined as the position of minimum pitot pressure once again, and the inwash of each vortex is then the spanwise distance between the half-wing tip and the vortex axis. Noting that the wing tip is 165 mm above the base of the test section, the inwash of the weak and strong vortices are 3.4 mm and 4.3 mm respectively. As can be seen from Fig. 8, significant pitot pressure deficit relative to the freestream is observed for both tip vortex strengths. For the weak vortex, the pitot pressure ratio dips to a minimum of $P_2/P_0 = 0.187$ and approaches the freestream value of $P_2/P_0 = 0.503$ approximately 9 mm outboard of the half-wing tip. Some effect of the wake may be seen at the lower limit of the survey where the pitot pressure ratio continues to decrease below its freestream value. For the strong vortex the pitot pressure ratio is seen to reach a minimum of $P_2/P_0 = 0.101$ and approaches the freestream value 15 mm outboard of the half-wing. Some evidence of a wake is also observed in a similar fashion to the weak vortex. In general, the magnitude and spatial scale of the pitot pressure deficit increases with half-wing angle of attack.

Figures 9(a)-9(c) show the spanwise Mach number distribution for both vortices. A single step procedure based on that by Centolanzi[23] was used to calculate these values from the raw pressure data. Since significant variation in the pitot pressure occurs over lengths of the order of the diametral distance between opposite surface pressure taps (2.0 mm), the pitot value used to calculate the flow properties was averaged over a 2 mm length centered on the conical probe tip. Figure 9(a) shows the distribution of lateral Mach number (M_x) for both vortices. For the geometry of the current experiments, M_x may be interpreted as the swirl component of the Mach number. The distributions show a similarity to the classic Burgers swirl velocity profile with an inner linear swirl distribution, surrounded by a region with swirl similar to an irrotational vortex. The point of zero swirl was found to correspond closely with the point of minimum pitot pressure (Fig. 8) for both vortices. It is noted however that the profiles are not symmetric, but show a larger swirl and core radius outboard of the half-wing. This asymmetry is typical of wing tip vortices. The average core diameter for the weak and strong vortices was observed to be 4.0 mm and 5.5 mm respectively. Figure 9(b) shows the distribution of spanwise Mach number (M_y) for both vortices. The magnitude of the inwash indicated in Figure 9(b) increased with half-wing angle of attack, and peaked close to the vortex axes for both cases. Figure 9(c) shows the distribution of streamwise Mach number (M_z) for both vortices. Significant Mach number deficit is observed to occur for both vortices in a small region near their respective axes. Outside this region, which is of the same spatial scale as the vortex core, M_z is close to M_∞. The wake-like M_z profiles reach a minimum of $M_z = 1.77$ and 1.64 for the weak and strong vortices respectively. Streamwise Mach number deficits of this magnitude have not been previously reported

for supersonic wing tip vortices and have significant implications for vortex interaction studies.

The spanwise total pressure (P_1) distributions for the weak and strong vortices are shown in Fig. 10. As expected, significant total pressure deficits occur in the core regions, the minimum total pressure ratios being $P_1/P_0 = 0.21$ and 0.12 respectively for the weak and strong vortices. Also of note is the absence of any effect of the shock-expansion wave structure generated by the half-wing, which indicates that the survey position 2.25 chords downstream of the half-wing trailing edge is within the 'test diamond' in the current experiments. In summary, the supersonic wing tip vortices exhibited many characteristics commonly found in low speed wing tip vortices, including an asymmetric 'Burger like' swirl distribution and significant total pressure deficits. To the author's knowledge the substantial streamwise Mach number deficit observed in the vortex core regions have not been previously reported for supersonic wing tip vortices. The spatial scale and the strength of the vortices was observed to increase with half-wing angle of attack.

V. OBLIQUE SHOCK WAVE/VORTEX INTERACTION

A generic illustration of the experimental arrangement for the oblique shock wave/vortex interaction experiments is shown in Fig. 11. The wedge had variable angle of attack capability from 0 to 10 degrees which enabled generation of flow deflections between 20 and 30 degrees. The shock-generator section was equipped with a 6 x 3 grid of 18 equally spaced pressure ports in which miniature high frequency pressure transducers were mounted. The six rows spanning the wedge were equally spaced between x/l = 0.17 and x/l = 0.75, (where x is the chord-wise distance along the wedge surface from the leading edge). The three rows in the chord-wise direction were located at y/l = 0.12, y/l = 0.0, and y/l = -0.12 (where y = 0.0 is the lateral location of the half-wing). For these experiments the wedge was placed 15.2 cm (6 in; 3 vortex generator chords) downstream of the half-wing trailing edge, with its leading edge 25.4 mm (1.0 in) below the half-wing tip. The dimensions and relative orientation of the half-wing and the wedge section were chosen so that the interaction took place well within the 'test diamond' of nearly uniform flow formed by the shock-expansion wave structure emanating from the half-wing.

Wedge calibration experiments were performed to establish the base-line pressure distribution on the wedge. The time averaged chord-wise pressure distributions for θ = 22, 25 and 29 degrees are shown in Fig. 12. These results compare favorably with two-dimensional theory, except for the downstream portion of the $\theta = 29^{\circ}$ case. The pressure relief observed in this instance is a consequence of the fact that the shock generating wedge does not span the entire width of the test section, giving rise to some three-dimensional effects at the edges.

i. Weak Interaction Results

Figures 13(a) and 13(b) illustrate a typical shadowgraph of the flowfield in the absence

of the vortex and during the interaction of the weak vortex respectively. The particular case shown in Fig. 13(b) involves the shock wave generated by a flow deflection of $\theta = 25^{o}$. The shadowgraph clearly indicates a concentrated tip vortex convecting downstream and intersecting the oblique shock wave, creating a classical oblique shock wave/vortex interaction. There appears to be no appreciable alteration to the vortex upon intersecting the oblique shock front, but a slight distortion of the shock wave in the interaction zone is noticeable. The above shadowgraph indicates that the presence of the weak vortex has moved the shock wave slightly upstream of its undisturbed position, a movement consistent with a Mach number and stagnation pressure deficit in the vortex. Flow behind the shock wave appears to be smooth, but the view of the vortex is obscured by waves from the wedge edge effects. This flow structure is typical of the weak interactions observed in this study. Variation of the shock wave intensity did not produce any substantial changes to the flow structure and multiple shadowgraphs taken during typical three second runs showed no changes with time.

Time averaged wedge surface pressure distributions for the weak interaction are shown in Figs. 14(a), (b) and (c), for $\theta = 22$, 25 and 29 degrees respectively. The dashed lines in the Figs. correspond to the base-line data for each flow deflection angle, and the solid lines represent the chord-wise pressure distributions at the three span-wise positions of $y/l = 0.12$, 0.0 and -0.12. Examining Fig. 14(b) ($\theta = 25^{o}$) indicates that the chord-wise variation of pressure is similar at each span-wise position. The pressure is constant up to approximately $x/l = 0.4$, followed by a dip which reaches a minimum at $x/l = 0.52$ and finally a return towards the base-line wedge pressure at $x/l = 0.63$. Pressures at $y/l = 0.12$ are the highest, $y/l = -0.12$ are the lowest and pressures at $y/l = 0.0$ are in between. This description of the pressure distribution in Fig. 14(b) is also applicable to Figs. 14(a) and (c) for the 22^{o} and 29^{o} flow deflections, except that the streamwise position at which the constant chord-wise pressure is disrupted moves to $x/l = 0.5$ and 0.25 respectively. The disrupted region, consisting of a dip to a minimum pressure approximately 7% below the base-line followed by a return towards the base-line pressure, is of a similar magnitude and chord-wise scale for all three shock wave strengths. It is noted that the time accurate pressure measurements showed no large amplitude fluctuations during typical three second test periods.

The time averaged pressure measurements show some interesting features of the oblique shock wave/vortex interaction. The span-wise pressure variation on the wedge is believed to be due to the fact that the component of velocity normal to the oblique shock is not uniform in the vortex. In the present geometry, the vortex swirl velocity adds to the freestream velocity component normal to the shock for positive y/l and subtracts from the freestream velocity component for negative y/l. This leads to a locally stronger shock for positive y/l (creating a higher pressure on the wedge) and a locally weaker shock for negative y/l (creating a suction on the wedge). Superimposed on this is the fact that there is a pressure deficit in the vortex with respect to the freestream, hence the wedge pressure at $y/l = 0.0$ is also lower than the base-line.

The localized low pressure region observed for all three flow deflection angles on the mid-chord portions of the wedge is thought to be due to waves emanating from the

interaction zone. The incoming stream-wise vortex consists of a region of stagnation pressure and axial Mach number deficit, combined with a swirl. As the shock distorts due to passage of the vortex, waves are generated in the supersonic flow behind the shock which propagate towards the wedge. It is postulated that these waves are the cause of the low pressure region, and therefore must be expansion waves. Evidence to support this postulation can be obtained by calculating the point at which waves from the interaction zone would be expected to reach the wedge. A simple first order estimate of the expected point of minimum pressure can be obtained by assuming that shock distortion and variations in the local Mach angle behind the shock are small. Using the geometry shown in Fig. 15, the wave emanating from the point of intersection of the vortex axis and the oblique shock wave reaches the wedge at x/l = 0.64, 0.59 and 0.45 for flow deflection angles of 22, 25 and 29 degrees respectively. These values correspond reasonably well with the observed positions of minimum pressure in each case.

In summary, the weak interaction showed slight distortion of the oblique shock wave for all three flow deflection angles. Small spanwise pressure variation was observed to occur due to vortex swirl, together with a localized low pressure region at the mid-chord location. The chord-wise position of this low pressure region moved forward with increased shock wave intensity, while its magnitude and chord-wise scale did not vary with shock wave strength.

ii. Strong Interaction Results

The strong interaction results exhibit many characteristics similar to the weak interaction, however the increased swirl causes some more dramatic features to become apparent. Figure 16(a), (b) and (c) show spark shadowgraphs of the strong interaction for θ = 22, 25 and 29 degrees respectively. Figure 16(b) ($\theta = 25^{O}$) indicates that a tip vortex convects downstream from the half-wing to form a classic oblique shock wave/vortex interaction, which in this case precipitates a dramatic change in the structure of the shock wave and a considerable disruption to the vortex. The shadowgraph depicts the formation of a local three dimensional shock structure well upstream of the position of the undisturbed oblique shock wave, which surrounds an expanding vortex core in much the same manner as a shock wave forms about a blunted body. It appears that the Mach number and stagnation pressure deficits which occur in the viscous core of the vortex are of such a magnitude that an oblique or slightly deformed shock wave cannot be sustained in the core region, producing a local separation of the shock. It is noted that multiple spark shadowgraphs taken during typical three second runs showed no change in the scale or shape of this structure, so it appears that the conditions which force the shock wave to separate locally are equilibrated by the formation of the structure shown in the shadowgraph. The separated shock wave is normal to the freestream in the core region of the vortex, locally forming a normal shock wave/vortex interaction. After passing through this normal shock wave the vortex core is seen to expand considerably. Away from the vortex core the observed separated shock structure appears to be simply a response of the surrounding free stream to the expansion of the vortex core.

This shock structure is similar to that reported for the head-on interaction of a streamwise vortex with a wedge leading edge reported in reference 14, except for the fact that the head-on interaction was found to be inherently unsteady. Although the flow structure leading to vortex distortion as a result of oblique shock wave/vortex interaction is similar to that observed during a head-on collision of a vortex with a wedge leading edge, a fundamental difference between the two encounters exists. In the vortex wedge interaction problem of Ref. 14, a stagnation point is forced in the flow while in the present study the flow is not forced to stagnate. This difference is particularly important since existence of a stagnation point is universally accepted as a characteristic feature of the vortex breakdown. Despite the fact that certain features known to occur in subsonic vortex breakdown cannot be verified in this study (for example, presence of reversed flow region and formation of a stagnation point), the above picture indicates a strong visual resemblance of the distorted vortex structure to the low-speed vortex-breakdown reported in the literature. These observations clearly demonstrate that destruction of a vortex as a result of an oblique shock wave/vortex interaction is possible; a behavior not reported in the two numerical studies of the problem.[15,17] Corpening and Anderson[15] for example, suggested that the absence of vortex breakdown in these interactions may be due to the supersonic flow downstream of the shock wave while in contrast, the results of the present investigation indicate a local region of subsonic flow in the vicinity of vortex viscous core.

Another interesting feature of the strong interaction shown in Fig. 16(b) and to the author's knowledge not previously reported, is the continuation of the separated shock through the plane of the undisturbed oblique shock wave to impinge on the wedge surface. The lower portion of the shock is clearly seen to strike the wedge at approximately x/l = 0.3 in this case, and forms a three dimensional shock wave-boundary layer interaction on the wedge surface. The details of the region where the lower portion of the separated shock structure crosses the original oblique shock wave is obscured in the shadowgraph, but the two appear to interact as independent shock waves of different families, with the local downstream angle of both dictated by the need to match flow angle and static pressure.

The effect of shock wave intensity on the strong interaction is clearly shown by comparing Figs. 16(a), (b) and (c). In Fig. 16(a) ($\theta = 22^{O}$) the separated shock structure appears to be just on the verge of formation. The oblique shock wave shows significant deformation in the interaction region, but no separate structure is apparent. In Fig. 16(b) ($\theta = 25^{O}$), the separated shock structure is fully formed with the leading portion located 6.7 mm (0.26 in.) upstream of the undisturbed oblique shock wave. Finally, Fig. 16(c) ($\theta = 29^{O}$) shows a separated shock wave with the leading portion located 13 mm (0.53 in.) upstream of the undisturbed oblique shock wave, the largest of the three cases examined. It appears that the effect of increased oblique shock wave intensity on the strong interaction is an increase in the scale of separated shock structure. The position at which the lower portion of the separated shock impinges on the wedge surface also varies with the shock wave intensity. For the 22^{O} flow deflection case no shock wave

was observed to impinge on the wedge surface. As already stated, the lower portion of the separated shock is observed to strike the wedge surface at x/l = 0.3 for the 25^{O} flow deflection. Increase of the flow deflection to 29^{O} removed the impinging shock wave. This is thought to be due to the fact that no downstream solution which includes a continuation of the separated shock wave through the oblique shock is possible for the $\theta = 29^{O}$ case. In general it may be stated that the overall structure of the strong interaction is observed to be quite sensitive to the strength of the original oblique shock wave.

Time averaged surface pressure distributions for the strong interactions are shown in Figs. 17(a), (b) and (c) for θ = 22, 25 and 29 degrees respectively. As for the weak interactions, the time accurate pressure measurements showed no large amplitude fluctuations in typical three second test periods. Examining Fig. 17(b)($\theta = 25^{O}$) indicates that some features of the pressure distribution are similar to the weak interaction. Spanwise pressure variation due to the non-uniform velocity component normal to the undisturbed oblique shock wave occurs once again, but with a greater magnitude due to the increased vortex strength. The chord-wise pressure distributions are similar once again for each span-wise position on the wedge, but include a feature not apparent in the weak interactions. Figure 17(b) shows constant pressure up to x/l = 0.25, followed by a significant peak at x/l = 0.4, a substantial drop to a minimum at x/l = 0.55 and finally a return towards the base-line pressure at x/l = 0.8. The peak experienced at all span-wise locations at x/l = 0.4 was not observed for the weak interactions, and appears to be in response to the separated shock wave shown in the shadowgraph (Fig. 16(b)) to impinge on the wedge at approximately x/l = 0.3. The full pressure rise across the impinging shock may not be shown in these results due to the coarseness of the pressure port grid on the wedge. Downstream of the peak a significant suction is experienced on the wedge in a similar fashion to the weak interaction, but of significantly larger magnitude. The minimum pressure measured on the wedge for this case is approximately 24% below the base-line. The description above is applicable to the form of the pressure distributions for all strong interactions examined.

Variation of shock wave intensity has a two fold effect on the wedge surface pressure for the strong interaction. Comparison of Figs. 17(a), (b) and (c) indicates that increasing shock wave strength moves the disrupted region (peak, trough and return towards base-line) upstream, and increases the relative magnitudes (compared to the base-line) of the pressure extremes experienced by the wedge. The magnitude of the maximum suction for the three flow deflections 22, 25 and 29 degrees is 10%, 24% and 31% of the base-line pressure respectively. The scale of the disrupted pressure region does not vary with shock wave strength and is greater for the strong interaction than for the weak encounter. It is expected that the low pressure region observed at the wedge is generated by waves emanating from the interaction zone, in a similar fashion to that suggested for the weak interaction, however the presence of the separated shock structure in the strong interaction makes analysis of the expected position of the low pressure region far more difficult than for the weak interaction.

In summary, the strong interaction precipitates a significant distortion of the

oblique shock wave which takes the form of a steady three dimensional separated shock structure well upstream of the undisturbed oblique shock front. The scale of the structure increases significantly with increase in the oblique shock wave intensity and a portion of the separated shock was observed to impinge on the wedge surface for some oblique shock wave strengths. The pressure distributions on the wedge exhibits a similar form and position to the corresponding weak interaction results, except for a local pressure peak in the vicinity of the observed shock wave impingement on the wedge. The magnitude of the pressure changes with respect to the base-line were significantly larger than for the corresponding weak interaction.

VI. PLANAR LASER SHEET VISUALIZATION DURING THE OBLIQUE SHOCK WAVE/VORTEX INTERACTION

In order to gain better understanding of the vortex structure during the oblique shock wave/vortex interaction, planar visualization of the flowfield were made using a Ruby laser with a pulse duration on the order of 30 ns. A thin (on the order of 2 mm) laser sheet illuminates the segment of interest in the test section to provide planar visualization of the flowfield. Schematic of the laser sheet visualization set-up is shown in Fig. 18. The flow was seeded using a mixture of water and alcohol (2/3 water and 1/3 alcohol by volume) in the settling chamber prior to the tunnel start. These planar visualizations were performed at 10 different locations along the shock generating surface extending from the wedge leading to its trailing edge.

For this study, the vortex generator wing was placed at an angle of attack of 10.4^{o} and the wedge was set to produce a flow deflection of $29,^{o}$ which creates nearly the strongest attached oblique shock at Mach 2.49. This case was selected since the oblique shock wave/vortex interaction experiments discussed earlier revealed the most pronounced effect for this configuration. a shadowgraph of the flow taken during the interaction was shown in Fig.16(c) which clearly indicates a concentrated tip vortex convecting downstream and interacting with the oblique shock wave. A bulged-forward conical shock wave may be seen as a result of the encounter, which surrounds a subsonic region composed of the vortex core. The bulged-forward shock wave is seen to be normal to the free stream at the vortex axis, creating a subsonic flow of limited extent downstream of the shock wave. This indicates that the oblique shock wave/vortex interaction degenerates locally into a normal shock wave/vortex interaction. The aforementioned picture however, does not provide detailed information concerning the extent of the subsonic region at distances further downstream, as the view is obscured by the integrated effect of the shadowgraph technique.

A planar visualization of the flowfield with the laser sheet at the wedge leading edge is shown in Fig. 19(a) in which the vortex core is clearly visible above the wedge surface. This picture corresponds to a planar view just upstream of the bulged-forward shock structure representing the undisturbed vortex structure. As is evident from the shadowgraph of Fig. 16(c), the vortex core expands drastically upon entering the interaction zone, a behavior similar to the incompressible vortex breakdown. Planar visuali-

zations of the flow illustrating this behavior are shown in Figs. 19(b)-19(f). The aforementioned figures represent planar visualizations at several streamwise distances along the wedge surface. The above pictures illustrate the vortex growth, and some evidence of vortex generator wake may be observed to impinge on the wedge surface. These planar laser sheet pictures also indicate a nearly constant vortex diameter along with a diffused structure at distances downstream of the x = 12.7 mm. Of particular interest is the laser-induced light sheet taken at the streamwise distance of 66.6 mm downstream of the wedge leading edge shown in Fig. 19(f). The above picture clearly indicates that the vortical structure is still visible but is highly diffused.

Tracking of the vortex center at distances downstream of the wedge leading edge was possible by measuring the height of the vortex center above the wedge surface. Figure 20 shows the results of such measurements indicating that the vortex center immediately downstream of the bulged-forward shock structure has the same height as that upstream of the shock wave. This result confirms that the vortex crosses the normal portion of the shock wave for which no deflection is expected (see also Fig. 16(c)). Downstream of the x=12.7 mm, the vortex center may be seen to deflect upward adjusting to the direction of the flow behind the undisturbed portion of the shock wave. Finally, downstream of the x=31 mm the vortex center travels essentially parallel to the wedge surface.

VII. CONCLUSIONS

In the current study the effect of shock wave strength on the interaction between wing tip vortices and oblique shock waves has been investigated. For the weak interaction, involving a vortex generated by the half-wing at 5.7^{o} angle of attack, the oblique shock wave was slightly distorted for the three shock strengths investigated and the vortex was seen to pass smoothly downstream. Small changes from the base-line surface pressure were experienced on the shock generating wedge. For the strong interaction, involving a vortex generated by the half-wing at 10.4^{o} angle of attack, a significant distortion of the oblique shock wave was observed in the interaction zone, which took the form of a steady separated shock structure upstream of the original oblique shock wave. The upstream stand-off distance and the scale of this structure increased with shock wave intensity. For some shock wave strengths a portion of the separated shock structure continued through the original oblique shock wave to strike the wedge and form a three dimensional shock wave-boundary layer interaction. Significant changes from the base-line pressure were experienced on the wedge, including a large suction at the mid-chord region of the wedge of up to 30 % of the base-line pressure for the strongest shock wave investigated. The magnitude of the surface pressure variations and their position on the wedge varied with shock wave strength.

Planar laser sheet visualizations of the flowfield generated by the oblique shock wave/vortex revealed an expansion of the vortex core in crossing a strong oblique shock front. The maximum vortex core diameter was seen to occur at a distance of 12.7 mm downstream of the wedge leading edge while at distances further downstream, the vortex

core diameter remained approximately constant. The vortical structure was observed to persist along the entire chord of the shock generating wedge but was seen to diffuse with distances downstream of the wedge leading edge. Measurements of the vortex center above the wedge surface indicated that immediately downstream of the normal portion of the bulged-forward shock wave the vortex center was parallel to the direction of the free stream flow. On the other hand, the vortex traveled parallel to the wedge surface at distances downstream of the wedge mid-chord position.

Conical probe surveys were conducted at Mach 2.5 for the wing tip vortices generated by a rectangular half-wing at 5.7 and 10.4 degrees angle of attack. The tip vortices exhibited many characteristics similar to their low speed counterparts, including asymmetric 'Burger like' swirl distributions and significant total pressure deficits. A wake-like streamwise Mach number distribution was observed for both cases, and the scale and strength of the vortices increased with half-wing angle of attack. Computational calibration of commercially available conical probes using an Euler solver was found to be satisfactory for pointed 4-hole probes. Extension of numerical calibration to 5-hole conical probes would require a treatment of the nose bluntness in the numerical model, which was not attempted here. The current investigation revealed that the use of computational fluid dynamics to calibrate conical probes is a viable alternative to conventional experimental calibration, particularly when wind-tunnel time is at a premium.

VIII. RECOMMENDATIONS FOR FUTURE WORK

All of the data generated and analyzed in the present investigation point to the fact that more detailed study of the interaction problem is required in order to gain a better understanding of the complex flowfield. Detailed measurements of flow properties in the vortex core and interaction region are needed in order to more clearly characterize vortex-breakdown phenomenon in supersonic flows. Such measurements should be non-intrusive in nature without altering the natural environment of the flowfield. Although the results of present study indicate some similarities between incompressible 'B-breakdown' and supersonic vortex distortion, detail measurements in the breakdown region should be made in order to determine whether a reversed flow region and a stagnation point (both characteristics of incompressible vortex breakdown) are present.

Having developed some understanding of vortex behavior during oblique shock wave/vortex interaction, focus should be placed on investigating behavior of vortices and their influence on flow characteristics in an inlet type configuration having mixed oblique and normal shock waves. Such an study is a natural extension of the problem considered during the present investigation and will be of practical importance from a performance point of view in the operational environment of supersonic inlets.

IX. REFERENCES

1. Werle, H.,"Sur l'eclatement des tourbillons d'apex d'une aile delta aux faibles vitesses", *La Recherche Aeronautiique,* No. 74, Jan-Feb. 1960, pp. 23-30.

2. Lambourne, N. C., and Bryer, D. W.,"The Bursting of Leading-Edge Vortices - Some

Observations and Discussion of the Phenomenon", Aeronautical Research Council Report 3282, London, April 1961.
3. Harvey, J.K., "Some Observations of Vortex Breakdown Phenomenon", *Journal of Fluid Mechanics,* Vol. 14, (1962), pp. 585-592.
4. Benjamin, T.B., "Theory of the Vortex Breakdown Phenomenon," *Journal of Fluid Mechanics,* Vol. 14, (1962), pp. 593-629.
5. Sarpaka,T., "Effect of the Adverse Pressure Gradient on Vortex Breakdown", *AIAA Journal,* Vol. 12, No. 5, 1974, pp. 602-607.
6. Hall, M.G., "Vortex Breakdown", *Annual Review of Fluid Mechanics,* Vol. 4, 1972, pp. 195-218.
7. Leibovich, S., "Vortex Stability and Breakdown: Survey and Extension," *AIAA Journal,* Vol. 22, No. 9, Sept. 1983, pp. 1192-1206.
8. Delery, J.M, "Aspects of Vortex Breakdown", *Progress in Aerospace Sciences,* Vol. 30, No. 1., Jan. 1994, pp. 1-59.
9. Delery, J., Horowitz, E., Leuchter, O., and Solignac, J.L., "Fundamental Studies on Vortex Flows," *LaRecherche Aerospatiale* (English Edition), (ISSN 0379-380X), No. 2, 1984.
10. Metwally, O., Settles, G., and Horstman, C., "An Experimental Study of Shock Wave/Vortex Interaction," AIAA Paper 89-0082, January 1989.
11. Zatoloka, V., Ivanyushkin, A.K., and Nikolayev, A.V., "Interference of Vortexes with Shocks in Airscoops. Dissipation of Vortexes," *Fluid Mechanics, Soviet Research,* Vol. 7, No. 4, July-August 1978, pp. 153-158.
12. Hayes, W.D., "The Vorticity Jump across a Gasdynamic Discontinuity," *Journal of Fluid Mechanics,* Vol. 2, (1957) pp. 595-600.
13. Cattafesta, L.N., and Settles, G.S., "Experiments on Shock/Vortex Interaction," AIAA Paper 92-0315, January 1992.
14. Kalkhoran, I.M., "Vortex Distortion During Vortex-Surface Interaction in a Mach 3 Stream," *AIAA Journal,* Vol. 32, No. 1, 1994, pp. 123-129.
15. Corpening, G., and Anderson, J., "Numerical Solutions to Three-Dimensional Shock Wave/Vortex Interaction at Hypersonic Speeds," AIAA paper 89-0674, January 1989.
16. Kalkhoran, I.M., and Sforza, P.M., "Airfoil Pressure Measurements During Oblique Shock Wave-Vortex Interaction in a Mach 3 Stream," *AIAA Journal,* Vol. 32, No. 4, 1994, pp. 783-788.
17. Rizzetta, D.P., "Numerical Simulation of Oblique Shock-wave/Vortex Interaction," AIAA Paper 94-2304, June 1994.
18. Kalkhoran, I.M., Cresci, R.J., and Sforza, P.M., "Development of Polytechnic University's Supersonic Wind Tunnel Facility," AIAA Paper 93-0798, January 1993.
19. Marconi, F., Private Communications.
20. Beam,R.M. and Warming,R.F., "An Implicit Factored Scheme for the Compressible Navier-Stokes Equations", *AIAA Journal,* Vol. 16, No. 4, 1978.
21. Roe,P.L., "Discrete Models for the Numerical Analysis of Time-Dependent Multidimensional Gas Dynamics", *Journal Comp. Phys.,* Vol. 63, pp 458-476, 1986.

22. Thomas,J.L. and Walters,R.W., "Upwind Relaxation Algorithms for the Navier-Stokes Equations", *AIAA Journal,* Vol. 25, No. 4, pp 527-534, 1987.
23. Centolanzi,F.,J, "Characteristics of a 40^{O} Cone for Measuring Mach Number, Total Pressure and Flow Angles a Supersonic Speeds", NACA-TN-3967, May 1957.
24. Naughton,J.W, Cattafesta, L.N, and Settles,G.S, "Miniature, Fast-Response 5-Hole Conical Probe for Supersonic Flowfield Measurement", *AIAA Journal,* Vol. 31, No. 3, March 1993.

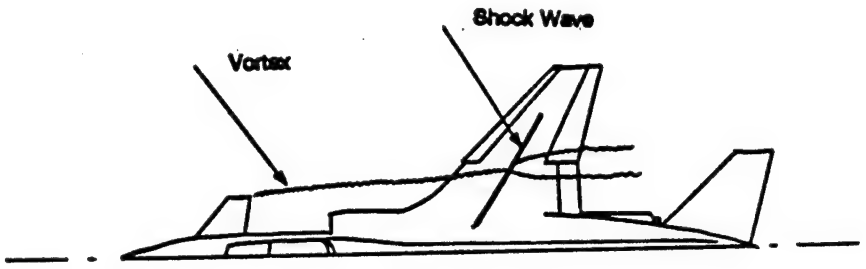

(a) Vortex-wing interaction.

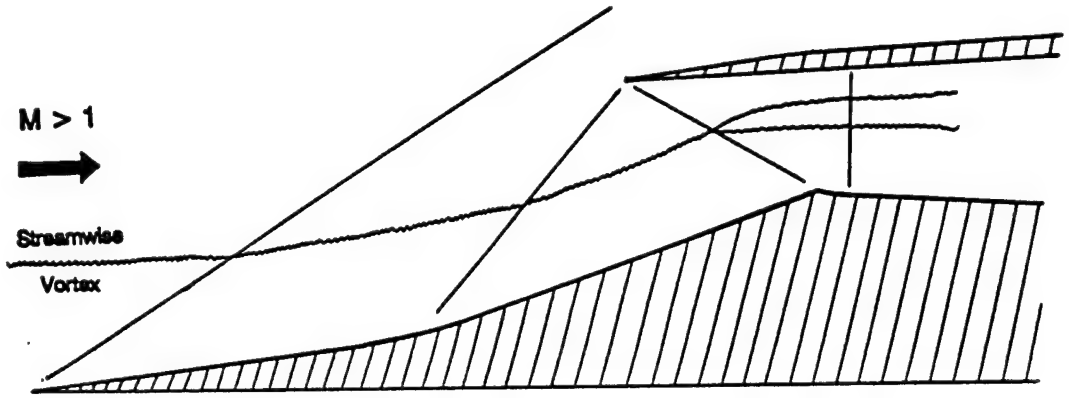

(b) Vortex-inlet interaction.

Figure 1. Examples of Shock Wave Vortex Interaction

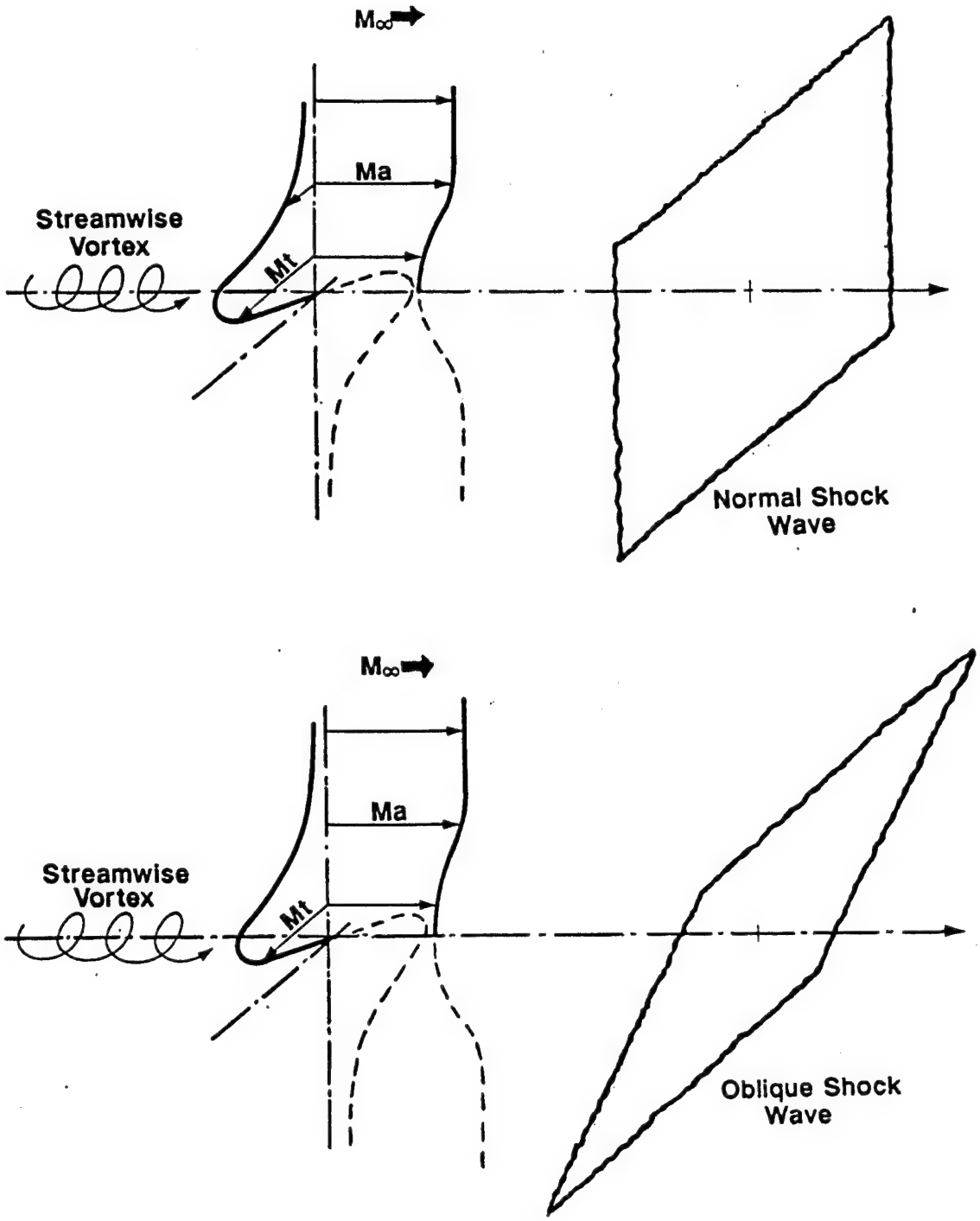

Figure 2. Normal and Oblique Shock Wave/Vortex Interactions

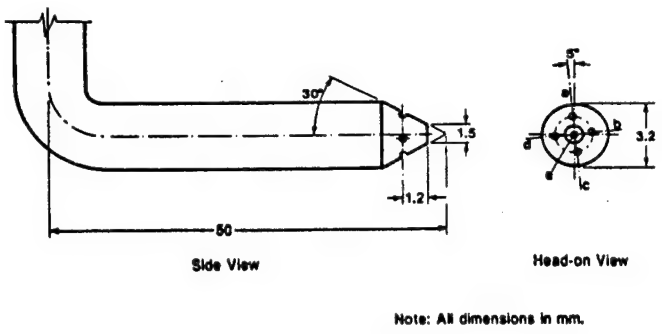

(a) 5-hole Probe

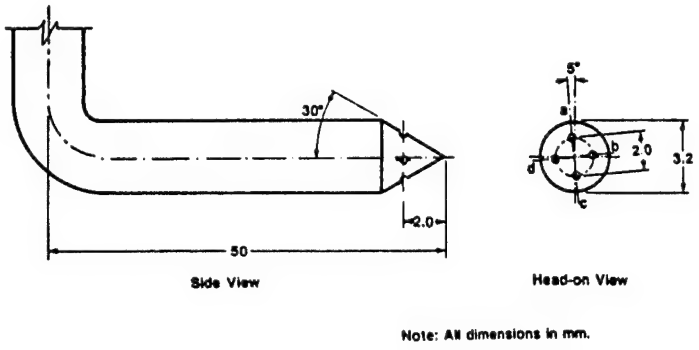

(b) 4-hole Probe

Figure 3. Schematic of the Conical Probes

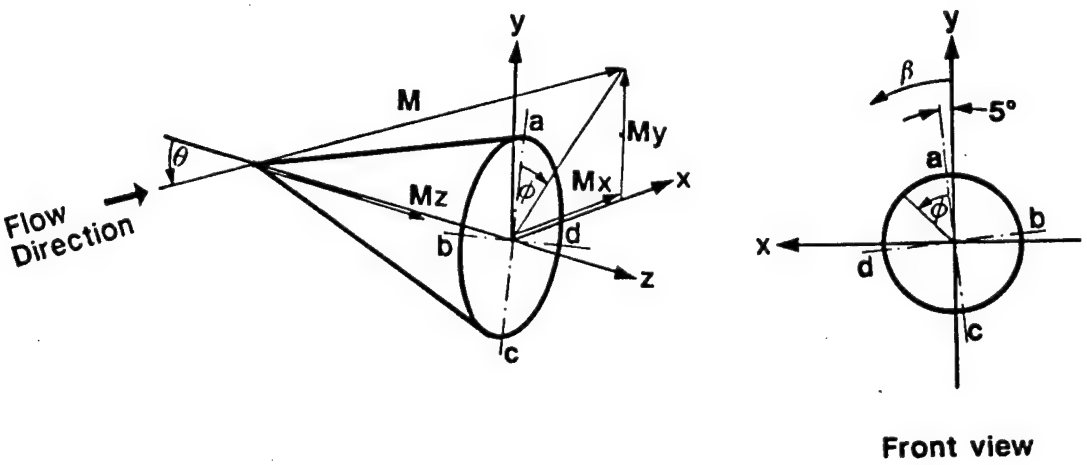

Figure 4. Spherical Coordinate System

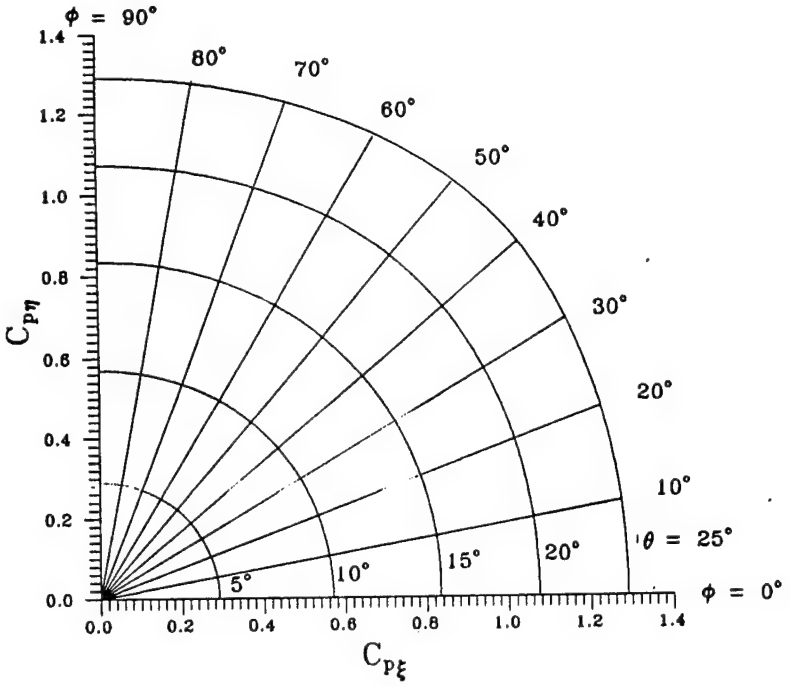

Figure 5. Numerically Generated Calibration Chart for M = 2.5

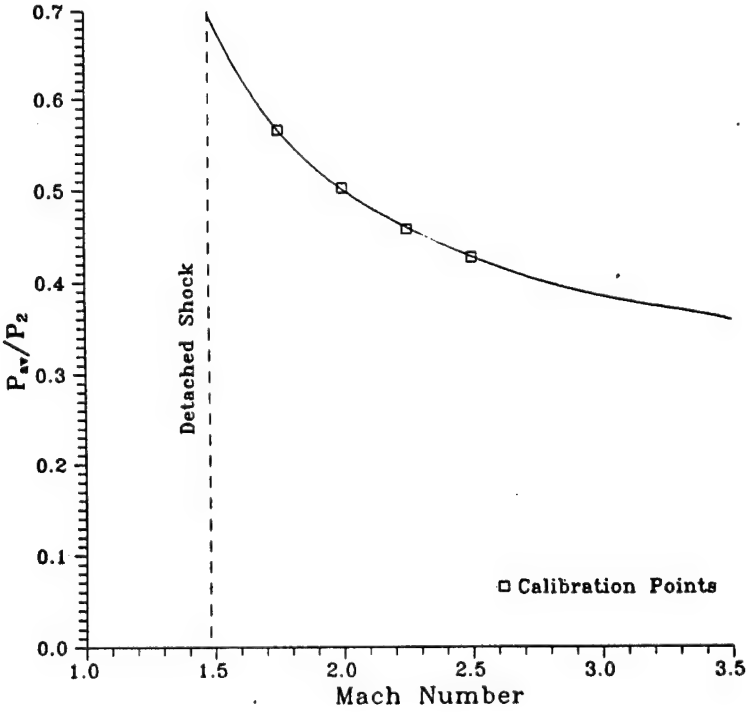

Figure 6. Variation of Average Cone Surface Pressure with Mach Number

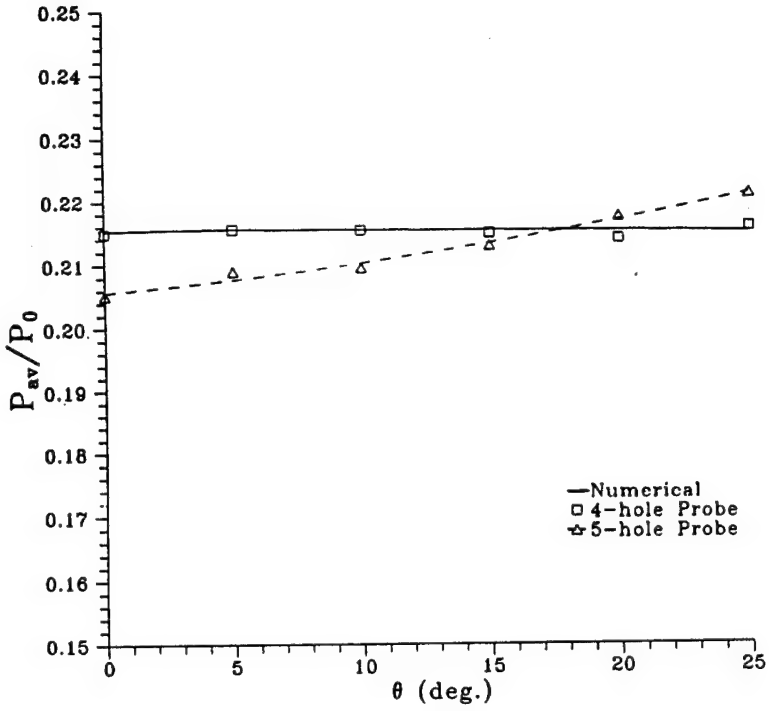

Figure 7. Variation of Average Cone Surface Pressure with θ at M = 2.49

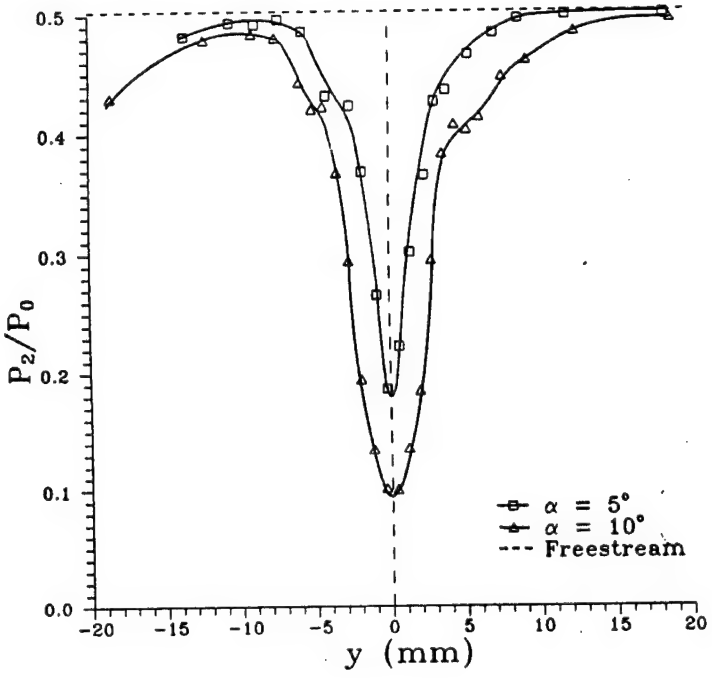

Figure 8. Pitot Pressure Distribution in the Vortex Cores

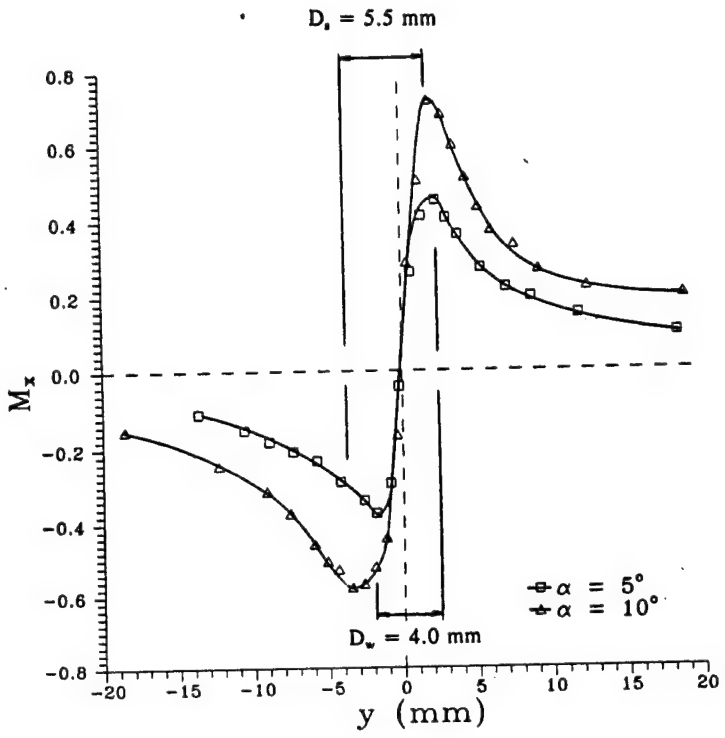

Figure 9(a). Swirl Mach Number Distribution in the Vortex Cores (M_x)

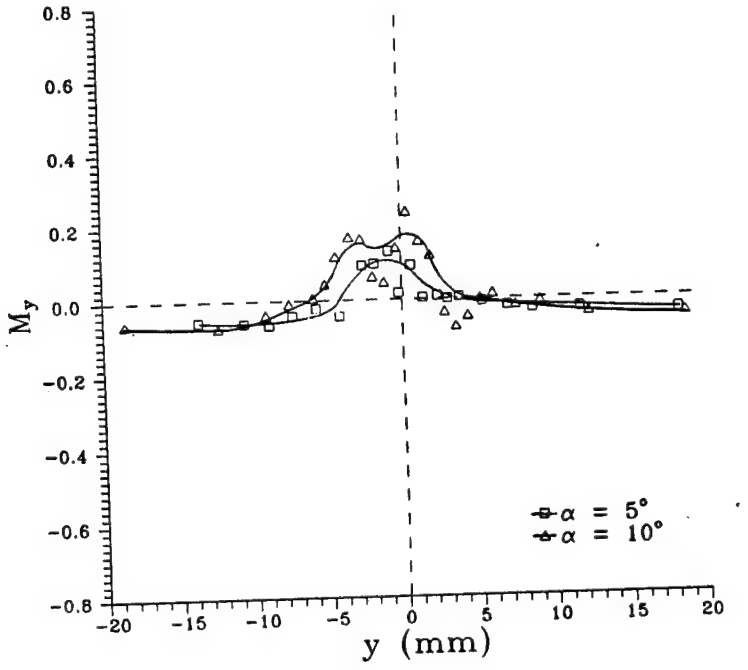

Figure 9(b). Spanwise Mach Number Distribution in the Vortex Cores (M_y)

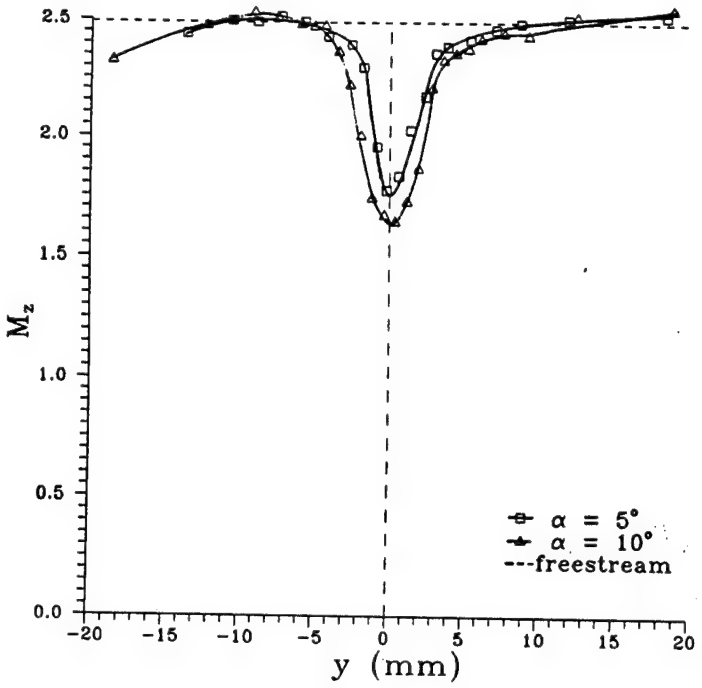

Figure 9(c). Streamwise Mach Number Distribution in the Vortex Cores (M_z)

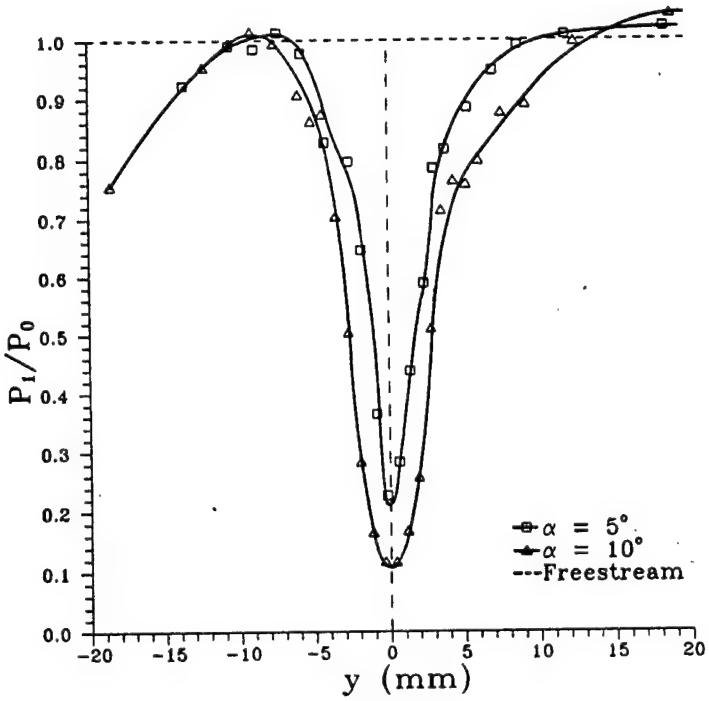

Figure 10. Total Pressure Distribution in the Vortex Cores

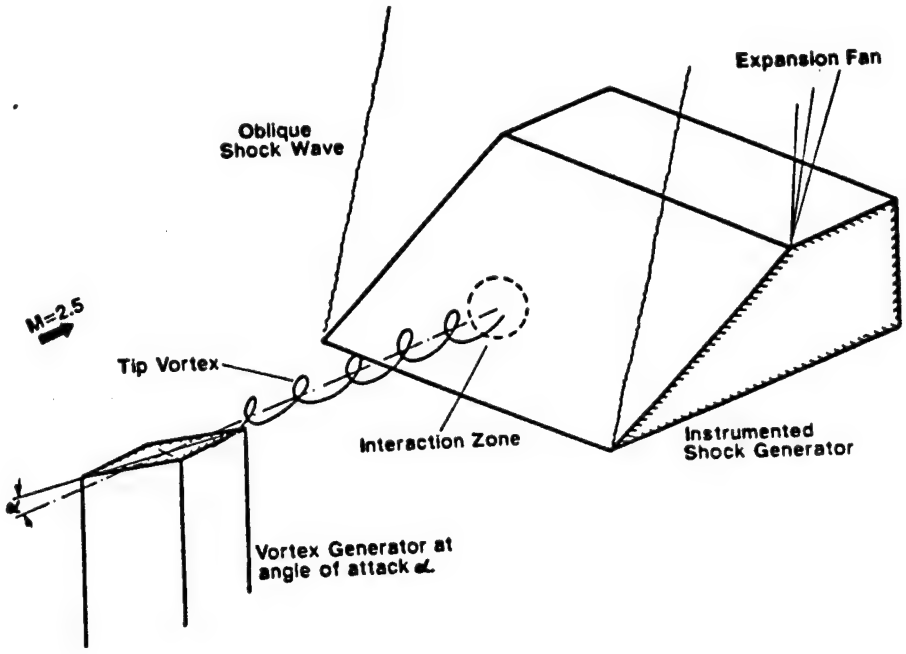

Figure 11. Schematic of the Experimental Arrangement for the Oblique Shock Wave/Vortex Interaction Experiments

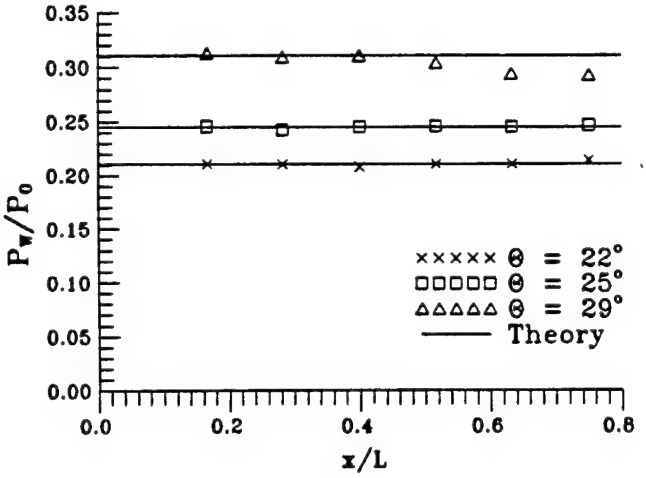

Figure 12. Base-Line Wedge Surface Pressure Distribution

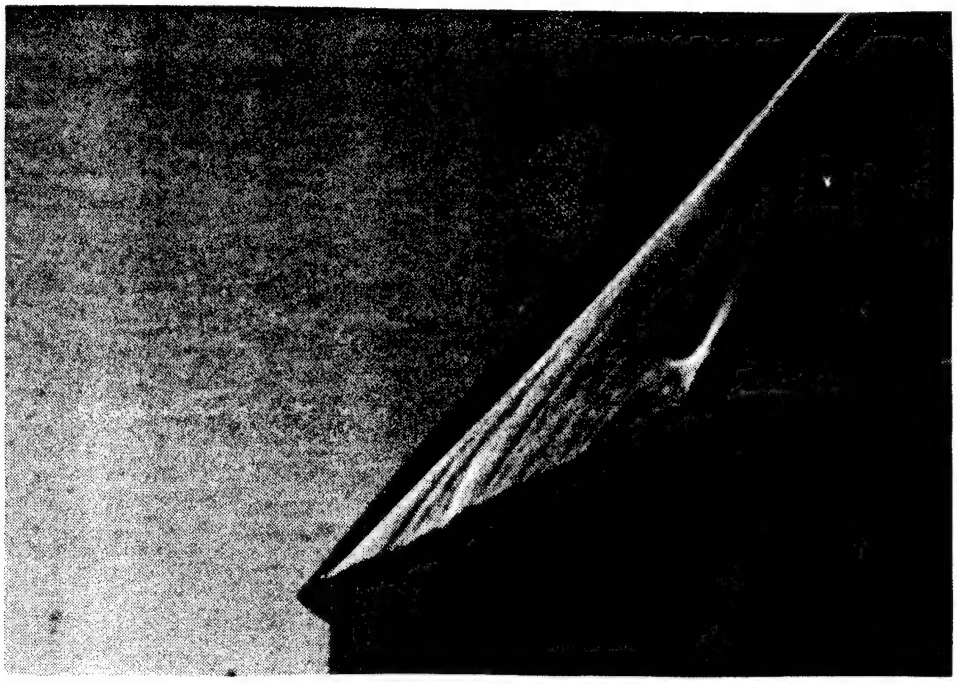

Figure 13(a). Shadowgraph of the Flow Over the 20^{O} Wedge at 5^{O} Angle of Attack

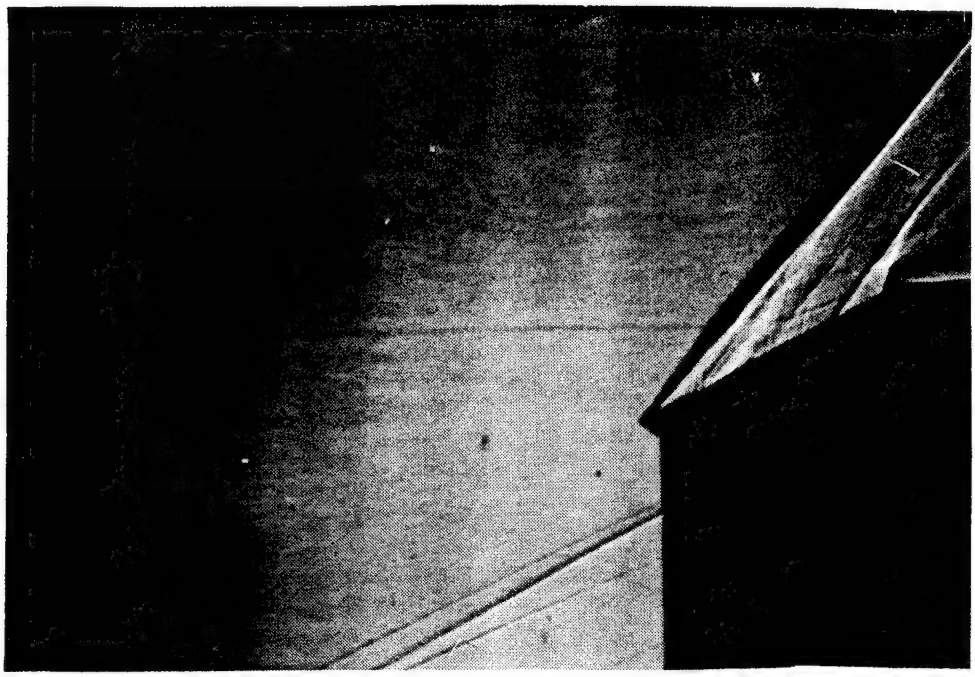

Figure 13(b). Shadowgraph of the Flow During the Weak Interaction

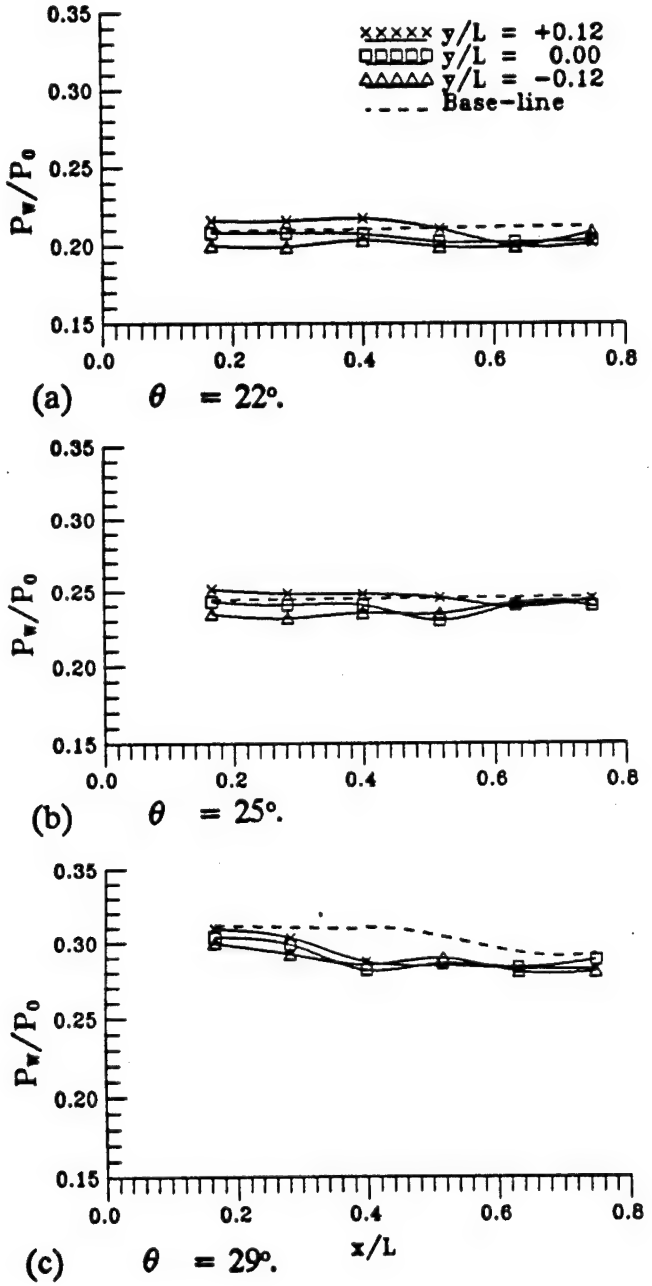

Figure 14. Wedge Surface Pressure Distribution During the Weak Interaction

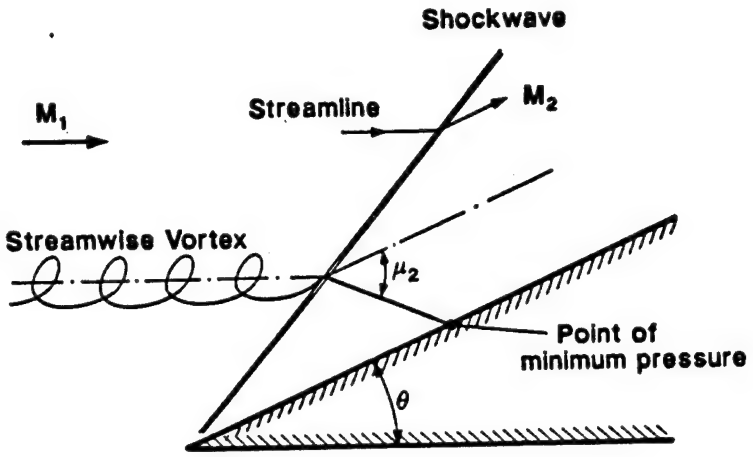

Figure 15. Wave Diagram for Flow Downstream of the Weak Interaction

Figure 16(a). Shadowgraph of the Flow During the Strong Interaction for $\theta = 22^{O}$

Figure 16(b). Shadowgraph of the Flow During the Strong Interaction for $\theta = 25^{O}$

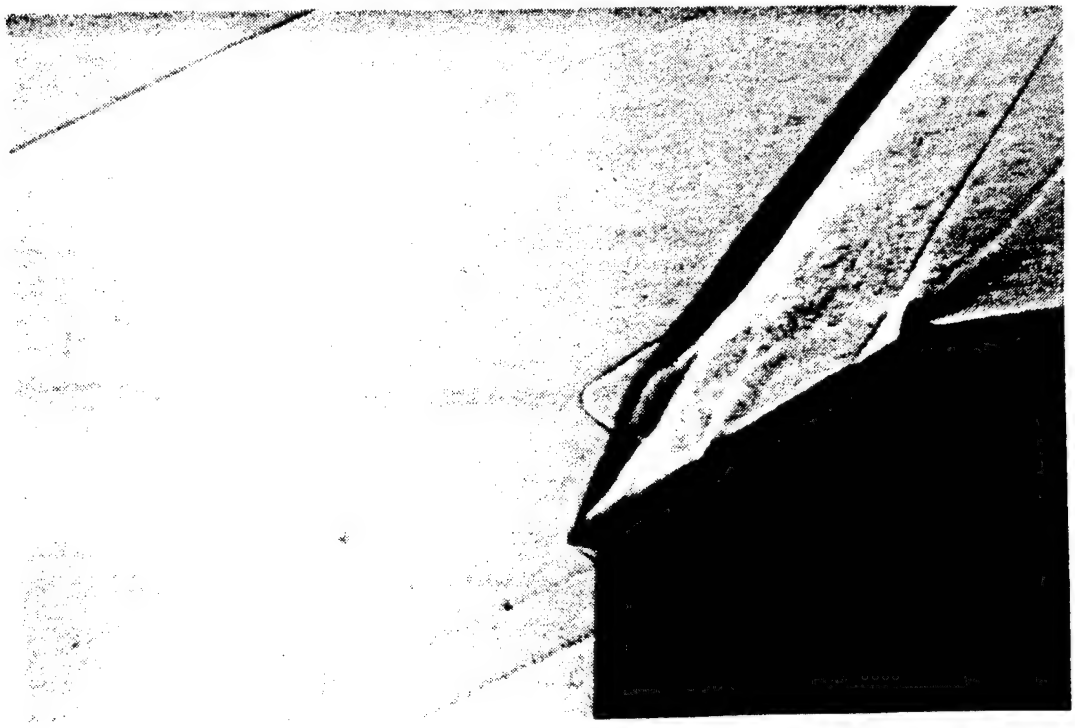

Figure 16(c). Shadowgraph of the Flow During the Strong Interaction for $\theta = 29^{O}$

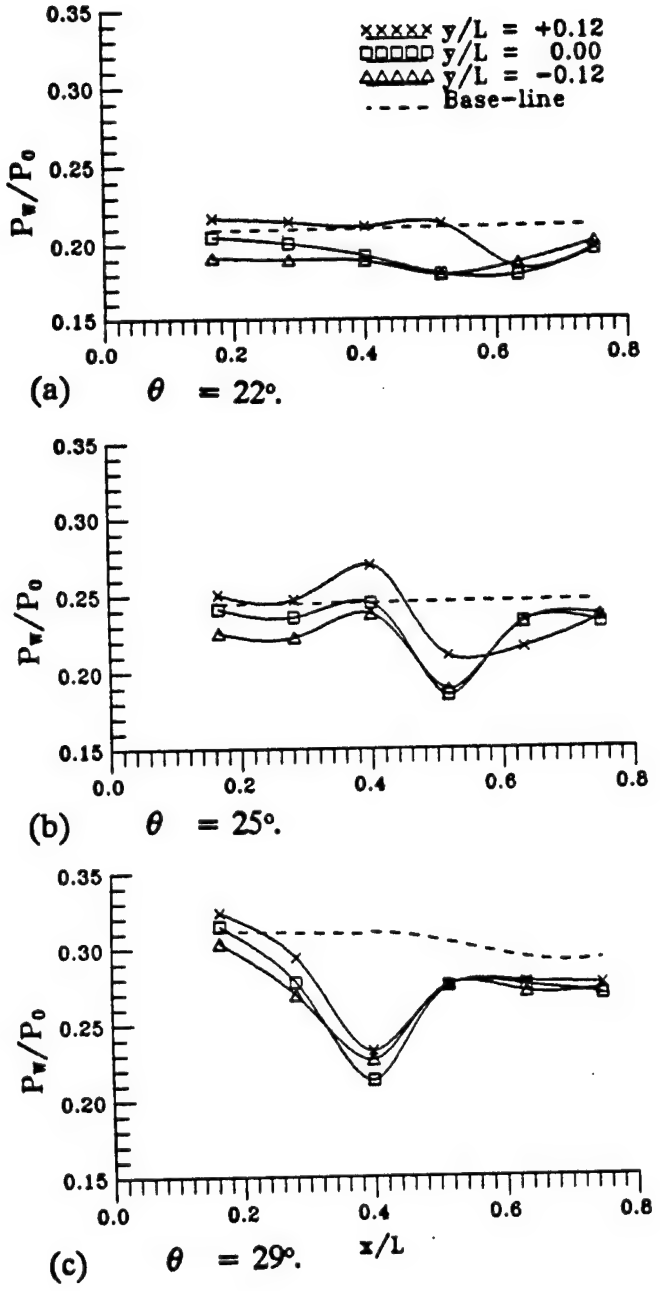

Figure 17. Wedge Surface Pressure Distribution During the Strong Interaction

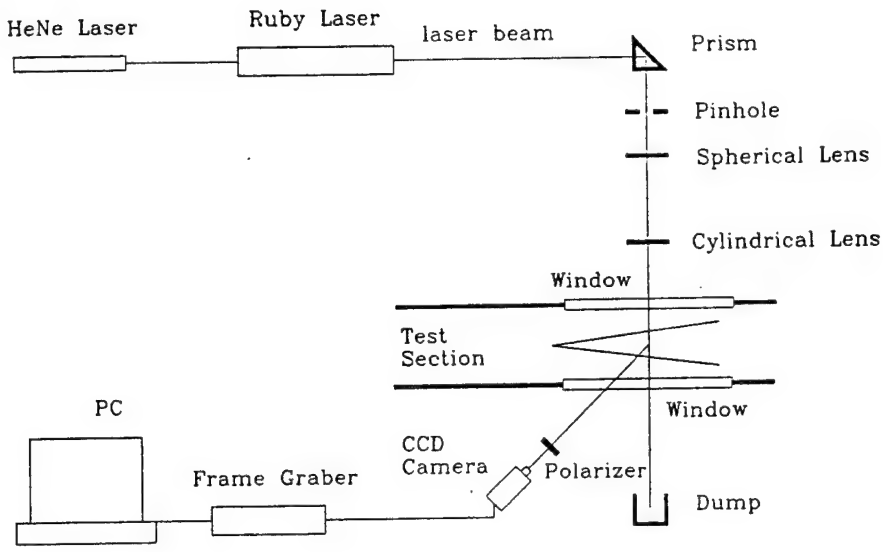

Figure 18. Schematic of the Laser Sheet Visualization Set-UP

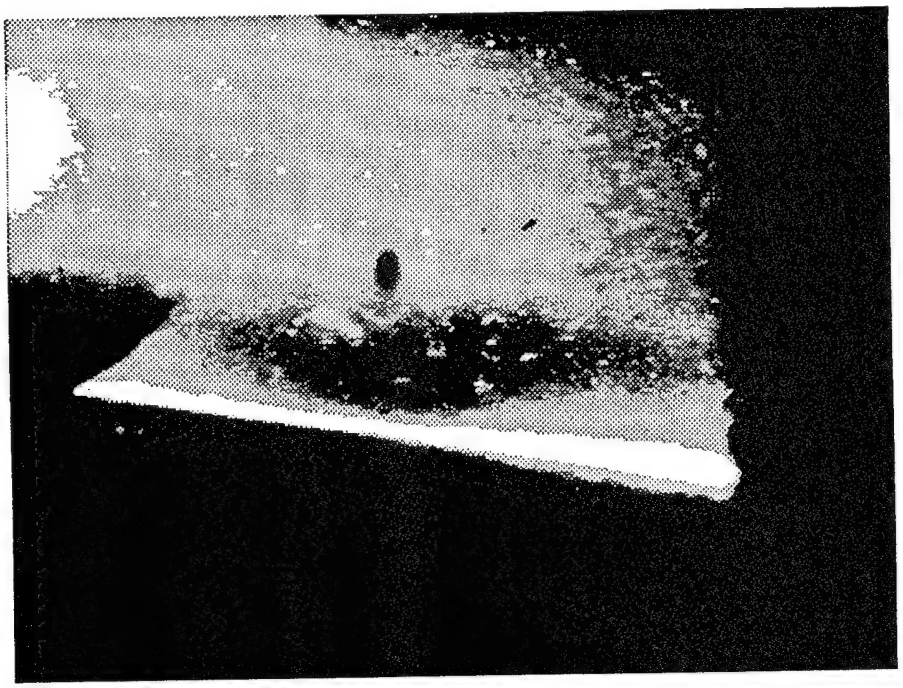

Figure 19(a). Planar Visualization During the Strong Interaction at x = 0 mm

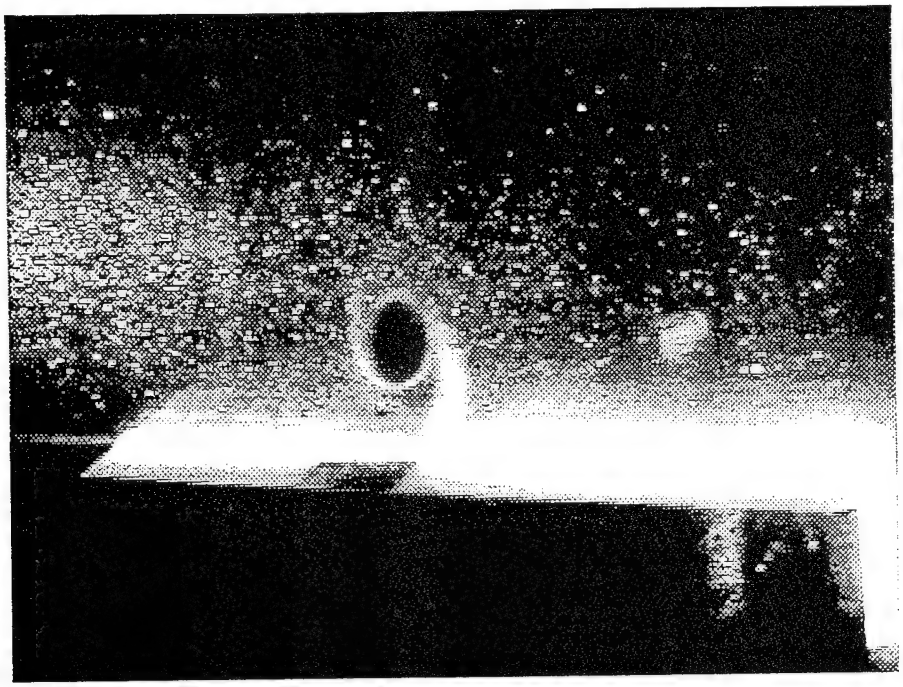

Figure 19(b). Planar Visualization During the Strong Interaction at x = 12.7 mm

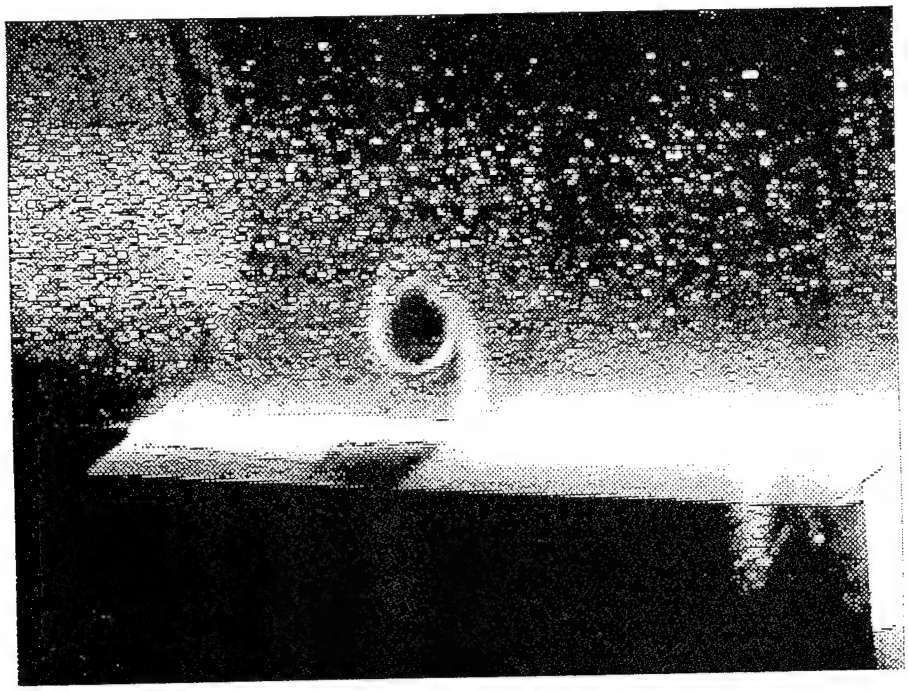

Figure 19(c). Planar Visualization During the Strong Interaction at x = 17.15 mm

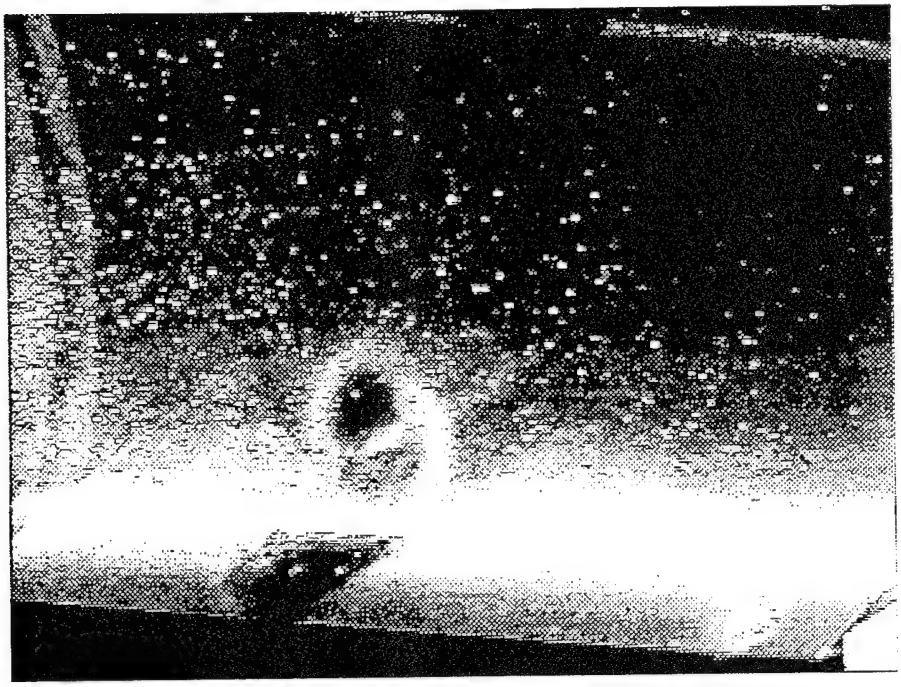

Figure 19(d). Planar Visualization During the Strong Interaction at x = 30.5 mm

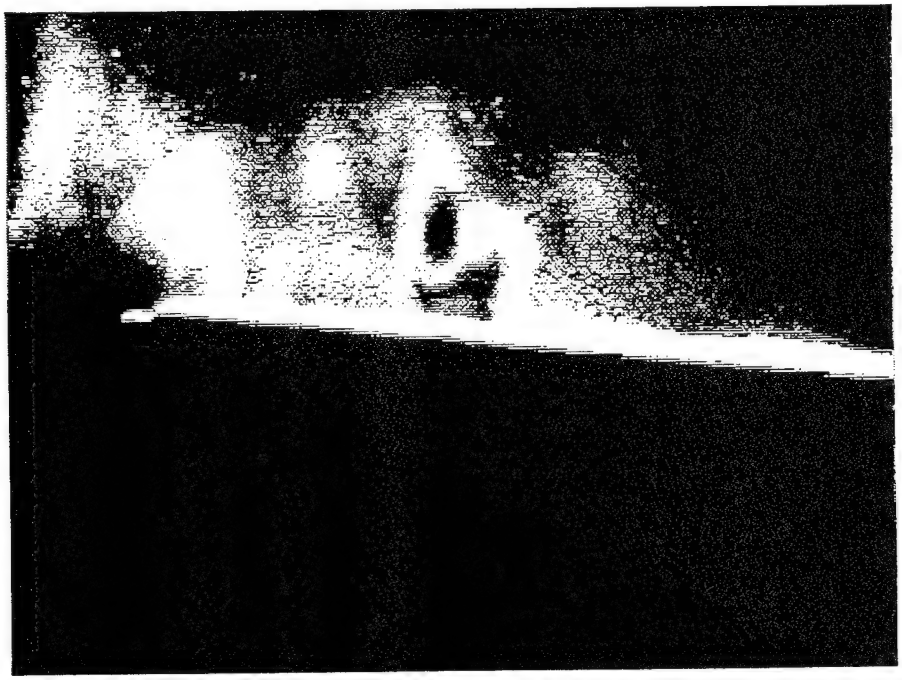

Figure 19(e). Planar Visualization During the Strong Interaction at x = 39.4 mm

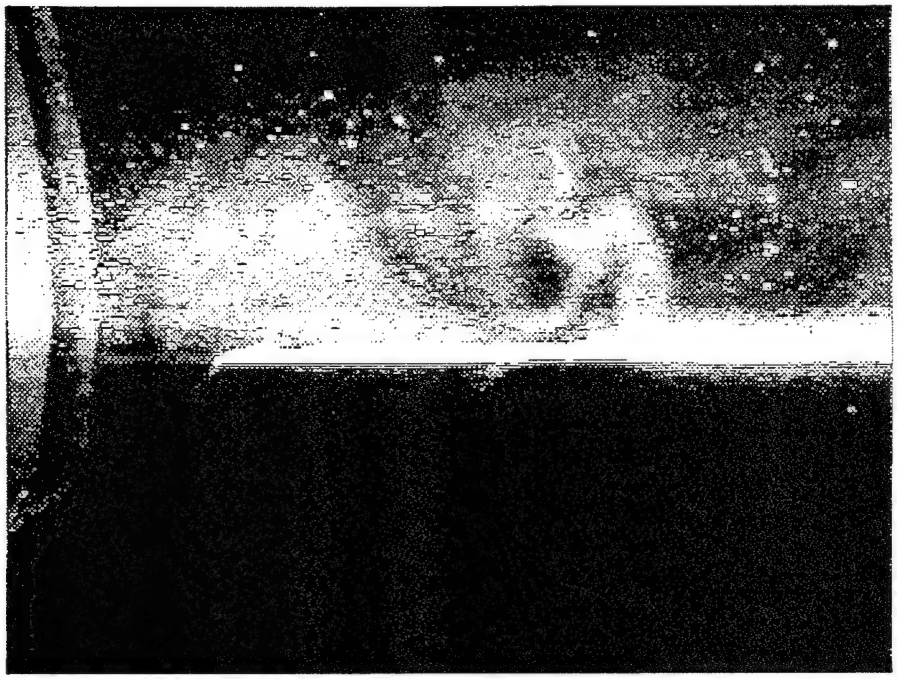

Figure 19(f). Planar Visualization During the Strong Interaction at x = 66.6 mm

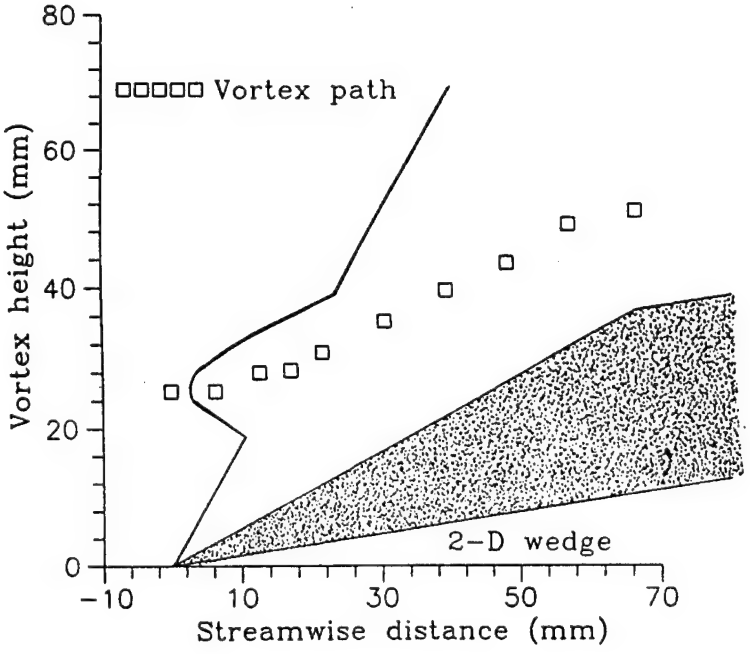

Figure 20. Measured Vortex Center Above the Wedge Surface

APPENDIX A. PERSONNEL SUPPORTED

The personnel supported during the funding period are as follows:

1. Dr. Iraj M. Kalkhoran, Assistant Professor, Department of Aerospace Engineering, Principal Investigator.

2. Dr. Sevetozar Popovic, Research Scientist, Weber Research Institute

3. Mr. Michael K. Smart, Ph.D. Candidate, Graduate Research Fellow, Department of Aerospace Engineering

APPENDIX B. CONFERENCE PAPERS

The list of paper presented at technical conferences during the funding period are as follows:

1. Smart, M. K., Kalkhoran, I. M., and Bentson, J., "Measurements of Supersonic Wing Tip Vortices," AIAA Paper 94-2576, June 1994.

2. Smart, M. K., and Kalkhoran, I. M., "The Effect of Shock Strength on Oblique Shock Wave Vortex Interaction,", AIAA Paper 95-0098, January 1995.

3. Kalkhoran, I. M., Smart, M. K., and Betti, A., "Interaction of Supersonic Wing-Tip Vortices with a Normal Shock," AIAA Paper 95-2283, June 1995.

Copies of these papers are shown in the following sections.

AIAA 94 - 2576
Measurements of Supersonic Wing Tip Vortices

M.K.Smart, I.M.Kalkhoran and J.Bentson,
Aerospace Engineering Department,
Polytechnic University,
Brooklyn, New York.

18th AIAA Aerospace Ground Testing Conference

June 20-23, 1994 / Colorado Springs, CO

MEASUREMENTS OF SUPERSONIC WING TIP VORTICES

Michael K. Smart*, Iraj M. Kalkhoran+ and James Bentson**
Aerospace Engineering Department,
Polytechnic University, Brooklyn, New York 11201

ABSTRACT

An experimental survey of supersonic wing tip vortices has been conducted at Mach 2.5 using small scale 4-hole and 5-hole cone probes. The survey was performed 2.25 chords downstream of a semi-span rectangular wing at angles of attack of 5 and 10 degrees. The main objective of the experiments was to determine the Mach number, flow angularity and total pressure distribution in the core region of supersonic wing tip vortices. A secondary aim was to demonstrate the feasibility of using cone probes calibrated with a numerical flow solver to measure flow characteristics at supersonic speeds. Results showed that the numerically generated calibration curves can be used for 4-hole cone probes, but were not sufficiently accurate for conventional 5-hole probes due to nose bluntness effects. Combination of 4-hole cone probe measurements with independent pitot pressure measurements indicated a significant Mach number and total pressure deficit in the core regions of supersonic wing tip vortices, combined with an asymmetric 'Burger like' swirl distribution.

Nomenclature

M	Mach number
P	Pressure
Cp	Pressure Coefficient
D	5-hole probe nose diameter
q	Dynamic Pressure
x,y,z	Cartesian coordinates
α	Vortex-generator angle of attack
θ	Pitch Angle
ϕ	Roll Angle
ξ	Cone half angle
ν	Uncertainty
τ	Swirl Angle = $\tan^{-1}(M_x/M_z)$
χ	Distance from probe tip

Subscripts

0	Settling Chamber
1	Total
2	Pitot
∞	Free Stream
av	Average

INTRODUCTION

Many fluid flow problems in aerodynamics and engineering are dominated by vortical structures. These vortical structures, or vortices for short, are the result of the separation and subsequent roll-up of boundary layers which have been forced to leave a surface. Study of the structure and dynamics of such vortex dominated flows is an active area of fluid mechanic research at the present time. Of particular interest to aerodynamicists are the vortices generated by the lifting surfaces of an aircraft. For example, the vortices shed by the wings of an aircraft play an integral part in the generation of lift, and an understanding of their development is important from a general performance standpoint. Also, the vortices shed by the forebody or canards of an aircraft flying at angle of attack can interact with downstream aerodynamic surfaces or be ingested by engine intakes, causing stability and control problems during particular flight manoeuvres. In an effort to expand the experimental data base on supersonic vortex dominated flows, various fundamental vortical interaction studies have been initiated at Polytechnic University[1,2]. These studies have primarily been concerned with the interaction of supersonic wing tip vortices with lifting surfaces and shock fronts. In order to thoroughly analyze the results of these experiments, a parallel program has been undertaken to develop the capability for accurate measurements of the Mach number, total pressure and flow angularity in these vortical flowfields.

Multi-hole cone probes have traditionally been the instrument of choice for measurements in three-dimensional supersonic flowfields. Pioneering work by Centolanzi[3], using a 20° half angle probe with a diameter of 9.5 mm (0.38 in), showed that 5-hole cone probes could be used to obtain accurate simultaneous measurements of Mach number, total pressure and flow

---

* Graduate Research Fellow, Student Member AIAA
+ Assistant Professor, Member AIAA
** Industry Professor

angularity in supersonic flow. The method he reported involved the experimental calibration of a 5-hole probe at numerous pitch and roll angles over a range of Mach numbers. This data was then cleverly cast into calibration curves so that the Mach number, total pressure and flow angularity could be obtained directly from the raw pressure data using an iterative procedure. This technique has become the standard, and numerous investigators[4,5] have reported successful calibration and use of their own cone probes with diameters as small as 1.5 mm (0.06 in).

The drawbacks of conventional cone probes are their relatively slow time response, of the order of 1 second, and the time consuming experimental calibration procedure. In an attempt to circumvent difficulties associated with slow response time, Naughton et al[5] reported the use of a miniature 5-hole probe incorporating fast response piezoelectric pressure transducers inside the wind-tunnel. This probe had a 30° half angle, a diameter of 1.5 mm (0.06 in) and was calibrated in the Mach number range 2-4. Their results indicated an improvement in time response of two orders of magnitude over conventional probes, and they used the probe to successfully measure supersonic streamwise vortices with a core size of approximately 4mm (0.16 in). The facet of conventional cone probe operation which limits their more widespread use is the experimental calibration procedure. To emphasize this point, a typical calibration of a 5-hole cone probe is summarized below. For a chosen Mach number, the probe is placed at a specified pitch angle, and then rotated about its axis in small increments, collecting the pitot pressure and the four surface pressures at each roll angle. This process is repeated at different pitch angles up to a maximum, and at a few Mach numbers in the range of interest. For typical roll increments of 10 degrees, with 5 different pitch angles and 3 Mach numbers, this amounts to 525 sets of data. This procedure must be performed for each probe of different geometry, and some cursory checking of the calibration should be performed for each similarly shaped probe that is fabricated. It is clear that the amount of wind-tunnel time needed to complete this process is prohibitive for many practical applications.

An alternative to this is the generation of probe calibration curves using a numerical flow solver. In recent years computational fluid dynamics has advanced to the point where the accurate prediction of supersonic flow past smooth pointed bodies is possible at moderate angles of attack. An example of this is reported in references 6 and 7, where a parabolized Navier-Stokes code was shown to accurately predict Mach 8 force and moment data for a 10° half angle conical body, at angles of attack up to 20°. With particular application to cone probes, it is expected that the flow past a sharp nosed 4-hole cone probe at moderate angles of attack can readily be solved using currently available inviscid conical flow solvers. The flow past a pitched 5-hole cone probe however, which includes a blunted nose for the pitot orifice, would need a full three-dimensional Navier-Stokes solver requiring a significant increase in computational time and effort. Use of numerical solutions to calibrate cone probes is clearly a viable alternative to experiment. Satisfactory calibration of 4-hole cone probes will require the least computational effort, followed by 5-hole probes with surface pressure orifices far from the nose. Calibration of 5-hole cone probes with pressure orifices close to the nose will be the most difficult to accomplish.

The main objective of the current investigation was to determine the Mach number, total pressure and swirl distributions in the core region of supersonic wing tip vortices. In order to accomplish this task, both a 4-hole cone probe and a 5-hole cone probe were commercially acquired. A half angle of $\xi = 30$ degrees was chosen for both probes and each had a diameter of 3.2 mm (0.125 in), which was the smallest available size. The calibration curves used for the cone probes were generated using computational solutions instead of the conventional experimental calibration. Cone probe surveys of the tip vortices generated by a rectangular half-wing at $\alpha = 5$ and 10 degrees angle of attack are presented in this report. The results of these surveys add to the scarce amount of experimental information on supersonic wing tip vortices currently available in the literature[8,9,10]. Such data is important to the increased understanding of supersonic vortical flows and for use as input to numerical computations. A discussion of the use of numerically generated calibration curves is also included in this work due to the original nature of this approach.

EXPERIMENTAL PROGRAM

Wind Tunnel and Test Conditions

The current investigation was conducted in Polytechnic University's 15 x 15 in^2 supersonic blowdown wind tunnel facility.[11] It is an intermittent blowdown wind tunnel with a square test section of 38.1 cm x 38.1 cm (15 in x 15 in) and is capable of producing unit Reynolds numbers in the range of 26 x 10^6 to 22 x 10^7 per meter (8 x 10^6 to 66 x 10^6 per foot) over a Mach number range from 1.75 to 4.0. The experimental studies reported here were conducted at a nominal test section Mach number of 2.5. The stagnation pressure and temperature for these experiments were 0.45 MPa (65 psia) and 290 K

respectively, resulting in a unit Reynolds number of 4.3 x 10^7 per meter (1.3 x 10^7 per foot). A typical test time for the experiments was three seconds.

Experimental Arrangement

A schematic of the experimental arrangement is shown in figure 1. The vortex generator was a rectangular half-wing with a diamond shaped cross section (8 degrees half angle), a chord length of 50.8 mm (2 in), and a span of 165 mm (6.5 in). The vortex generator was mounted vertically at the base of the test section with angle of attack capability between 0 and 10 degrees. The cone probes were mounted in a 25.4 mm (1.0 in) diameter tube which protruded vertically through the test section ceiling. The probes were situated with their tips approximately 108 mm (4.5 in) or 2.25 vortex generator chords downstream of the half-wing trailing edge, and were able to be traversed in the vertical direction. A wedge shaped fin with 18 degree included angle was installed at the leading edge of the support tube for structural support of the cone probes and to isolate the probes from any upstream influence of the support tube bow shock.

Cone Probes

Two small scale cone probes were used in for the current study, dimensioned sketches of which are shown in figure 2. Each probe had a diameter of 3.2 mm (0.125 in) and a half angle ξ = 30 degrees. The 5-hole cone probe included four equally spaced static pressure orifices on the cone surface (denoted a, b, c and d), together with a total pressure orifice placed centrally on a blunted nose (denoted e). The 4-hole cone probe included four equally spaced static pressure orifices on the cone surface but had negligible nose bluntness. The probes had a 90° elbow 50.8 mm (2.0 in) behind the tip in order to reduce the line length between the pressure orifices and the transducers to 36 cm (14 in). The pressure lines in the probe tips and the pressure orifices on the probes were 0.38 mm (0.015 in) in diameter. A line length of 36 cm (14 in) at this diameter was expected to degrade probe response time to an unacceptable level for typical test times of 3 seconds. To circumvent this problem, the internal diameter of the pressure lines was increased to 0.64 mm (0.025 in) approximately 25 mm (1 in) behind the elbow. Benchtop tests indicated that the time response of the cone probes to instantaneous pressure changes of the order of 1 atmosphere was approximately 0.5 seconds. The spherical co-ordinate system shown in figure 3 is used for the current work. The z direction is parallel with the free stream and the probe axis, while the x and y directions are horizontal and vertical respectively. The sign convention for the pitch angle θ and the roll angle ϕ are as shown in figure 3. The cone probes were manufactured with a permanent roll angle of $\phi = 5^o$, so the surface pressure orifices a,b,c and d were at circumferential angles 5, 275, 185 and 95 degrees respectively.

Instrumentation and Data Acquisition System

Five Kulite pressure transducers (model ITQ-1000-50A) were used in the experiments. These had a range from 0-345 kPa (0-50 psia) and a natural frequency response of 12 KHz. Output from the transducers was first amplified by Honeywell Accudata 122 DC amplifiers and then digitised using a Metrabyte das-16, 12-bit analog-to-digital converter board at a rate of 500 hz per channel for a period of three seconds. The experimental error associated with typical cone surface and pitot pressures reported in this paper is ν_p = ± 0.25 psia, and a conventional uncertainty analysis indicated that the uncertainty in test section Mach number and cone surface pressure coefficient are ν_M = ±0.018 and ν_{Cp} = ±0.03 respectively. Shadowgraphs were taken of the flow using a spark light source which provided micro-second range exposure times. Multiple spark shadowgraphs of the flowfield were possible at a rate of two per second.

COMPUTATIONAL CALIBRATION OF THE CONE PROBES

As already described, the calibration of cone probes has traditionally required an exhaustive amount of experimental data taken with the probe at different pitch and roll angles, over a range of Mach numbers. In the present study the cone probe calibration curves were generated using a computational solution. These solutions were obtained using a Navier-Stokes solver obtained from F.Marconi of Grumman Aerospace. This code uses a computational algorithm based on Beam and Warming's approximate factorization[12] in conjunction with Roe's flux difference splitting[13]. The solution of the equations is accomplished using an upwind alternate direction implicit technique similar to that of Thomas[14]. In the present study it was found that for the Reynolds numbers considered, the solutions obtained by running the code as an Euler solver agreed well with the Navier-Stokes solutions. Thus all the data presented here was obtained from inviscid computations.

The process of numerically generating a full set of calibration curves for a cone probe with specified half angle is as follows. Firstly, a conical grid must be

generated to match the probe geometry. For the current work the 81 x 63 grid used was sheared to the leeward side to capture all shocks. Computational runs can then be completed for each combination of Mach number and pitch angle in the range of interest. Note that each run calculates the complete flow past the probe, so that the full circumferential pressure distribution can be extracted from a single run. The 525 sets of cone surfaces pressures required for the typical experimental calibration described above can be obtained with 15 runs. For the current work the Mach number range of interest was between Mach 1.75 and 2.5, and the maximum pitch angle was 20°. These values represent the anticipated Mach numbers and maximum flow angularity in the core region of supersonic wing tip vortices. Calibration curves were generated for M = 1.75, 2.0, 2.25 and 2.5 at pitch angle increments of 5 degrees. A typical calibration curve for Mach 2.5 is shown in figure 4. After Centolanzi[3], the surface pressure data at each θ and ϕ is plotted versus $C_{p\eta} = (P_d - P_b)/q_\infty$ and $C_{p\xi} = (P_a - P_c)/q_\infty$. It is generally found[3,5] that when experimental 5-hole probe data is plotted in this way, little variation with Mach number occurs. This was also the case for the numerically generated data used in the current work. The pointed cone assumption made in the numerical model means that no calculation of the pitot pressure is performed in the numerical solution at different pitch angles and Mach numbers. Results of both Centolanzi[3] and Naughton et al[5] showed that between Mach 1.5 and 4, the pitot pressure measured by a 5-hole cone probe corresponds well with the theoretical stagnation pressure behind a normal shock for pitch angles up to 20°. Hence the Raleigh pitot formula is used in the current work to complete the data needed for a full cone probe calibration. Figure 5 shows a graph of P_{av}/P_2 (where $P_{av} = (P_a + P_b + P_c + P_d)/4$) versus Mach number calculated using the numerical method and the Raleigh pitot formula.

The iterative procedure for determining the Mach number, total pressure and flow angularity from the pitot and surface pressures measured by a 5-hole probe is fully described in references 3 and 5. In short, the flow Mach number is estimated from the ratio P_{av}/P_2, and then combined with the measured cone surface pressures to calculate $C_{p\eta}$ and $C_{p\xi}$. The two Euler angles, ϕ and θ, can then be determined from calibration maps such as figure 4. In general, iteration is required because P_{av}/P_2 varies with θ, hence after a first estimate of Mach number and flow angularity has been made, the Mach number must be adjusted for this variation. It is usually found[3,5] that only one or two iterations are required. A plot of the ratio P_{av}/P_2 versus θ calculated by the numerical scheme at Mach 2.5 is shown in figure 6. Negligible variation of P_{av}/P_2 is observed, which was the case for all the Mach numbers included in the calibration, hence no iteration of the Mach number is required. Determination of the flow properties in the current work was therefore reduced to a one step procedure. In summary, the determination of flow properties using the numerically generated calibration curves is identical to the conventional procedure, except that no iteration is required.

EXPERIMENTAL RESULTS AND DISCUSSION

Initial Test Results

The initial phase of the experimental program was concerned with establishing the accuracy and time response characteristics of the cone probes. Figure 7 shows the normalized pressure versus time traces for the 4-hole probe with nominal test section Mach number of 2.5 and θ = 20°. The pressure recorded at all orifices are observed to reach a steady state value after approximately 0.75 seconds. This result was typical of both the 4-hole and 5-hole probes, indicating that the time response of the probes are acceptable for use in short duration blowdown tunnels. In general, the initial one second of a typical three second run was discarded during data processing. Satisfactory use of the 4-hole and 5-hole cone probes depends entirely on the accuracy with which the numerical solution predicts their surface pressure distribution. A comparison between the numerical and experimental results at Mach 2.5 is shown in figure 8, with the probes at θ = 0, 5, 10, 15 and 20 degrees. It can be seen that except for a slight under prediction of the peak pressure on the windward side of the probe, the numerical scheme predicts the 4-hole cone probe surface pressure with high accuracy. The surface pressures measured on the 5-hole probe however, differed from both the 4-hole probe and numerical results, particularly on the leeward side where a significantly greater suction was observed. The generally lower surface pressures observed for the 5-hole cone probe at small pitch angles are consistent with those reported in the literature where a blunted nose has been found to cause an over-expansion in the region local to the nose, followed by an asymptotic approach to the pointed cone results. Krasnov[15] supplied a universal curve for predicting the scale of the over-expanded region on blunted cones at zero angle of attack. For a flat nosed cone with ξ = 30° at Mach 2.5, this curve predicts that the pressure coefficient on the cone surface approaches 99 % of the pointed cone result at χ/D = 3.22 (where χ is the downstream distance measured from the flat nose).

The pressure orifices on the 5-hole probe used in this study are at $\chi/D = 0.83$, which is well within the region expected to be affected by nose bluntness. The effect of nose bluntness on cones at angle of attack is not as easy to quantify, but it is not surprising that the 5-hole probe shows significant over-expansion due to its blunt nose, particularly on the leeward side. Based on these results, it is expected that calibration curves generated by the conical Euler solver can be used with confidence for the sharp nosed 4-hole cone probe. However, numerically generated calibration for the blunted 5-hole probe would require a fully three-dimensional numerical scheme and a significant increase in computational time and effort.

Limitation of the current work to the 4-hole cone probe introduces an additional complexity to the determination of the Mach number, total pressure and flow angularity. That is, the pitot pressure must be measured independent of the cone surface pressures. In order to fully determine the properties at a point, two measurements are required; a 4-hole probe measurement (supplying the cone surfaces pressures) and a separate pitot pressure measurement. This doubles the number of runs needed to complete a survey and also introduces the geometrical complexity of making sure both measurements are taken at the same position in the flow. For the surveys presented here, the 5-hole probe was used simply as a pitot probe. The use of the conical Euler solver to generate cone probe calibration curves has required a doubling of the number of runs in return for significant economy gains in the probe calibration. This difficulty may be overcome by using a three-dimensional computational scheme which properly treats the nose bluntness.

A shadowgraph of the flow taken during a typical cone probe survey of the tip vortex generated by the half-wing at $\alpha = 10^\circ$ is shown in figure 9(a). Flow is from left to right and the vortex core can be clearly seen convecting downstream from the tip of the half-wing towards the cone probe. Figure 9(b) shows a shadowgraph of the same flow but with the leading edge fin removed from the probe support tube. Here the intersection of the vortex with the detached bow shock on the support tube is believed to generate the observed large scale vortex distortion which renders the cone probe useless. Similar vortex distortions were reported in reference 1 for the head-on interaction of vortices with wedge leading edges. This figure vividly illustrates one of the difficulties which can be encountered during intrusive measurements of vortical flows. The vortex distortion was removed by addition of a leading edge fin (18° included angle) which generates a significantly weaker shock than the support tube, while still supplying the required structural support. An image of the $\alpha = 10^\circ$ tip vortex generated by a laser light sheet technique is shown in figure 10. The sheet was projected normal to the flow direction approximately 3 chords downstream of the half-wing. The vortex core can be clearly seen in the image surrounded by an asymmetric swirling structure which joins up with the half-wing wake in the lower portion of the image.

Vortex Surveys

Cone probe surveys were conducted for the wing tip vortices generated by the half-wing at $\alpha = 5$ and 10 degrees. In this work, the vortex generated by the half-wing at $\alpha = 5$ degrees will be called the weak vortex, and that generated by the half-wing at $\alpha = 10$ degrees will be called the strong vortex. The survey of each tip vortex was conducted 2.25 half-wing chords downstream of its trailing edge in a spanwise (vertical) line through the axis of each vortex. The lateral position of the vortex axes is defined as the position at which the pitot pressure was observed to be a minimum. The upwash of each vortex is then the lateral distance from the trailing edge of the half-wing to the position of minimum pitot pressure. The upwash for the weak and strong vortices was measured to be 3.1 mm (0.12 in) and 3.3 mm (0.13 in) respectively. Spanwise pitot pressure surveys through the axis of each vortex are shown in figure 11. The spanwise position of the vortex axes is defined as the position of minimum pitot pressure once again, and the inwash of each vortex is then the spanwise distance between the half-wing tip and the vortex axis. Noting that the wing tip is 165 mm (6.5 in) above the base of the test section, the inwash of the weak and strong vortices are 1.3 mm (0.05 in) and 3.5 mm (0.14 in) respectively. As can be seen from figure 11, significant pitot pressure deficit relative to the freestream is observed for both tip vortex strengths. For the weak vortex, the pitot pressure ratio dips to a minimum of $P_2/P_0 = 0.27$ and approaches the freestream value of $P_2/P_0 = 0.503$ approximately 9.7 mm (0.38 in) above the half-wing tip. Some effect of the wake may be seen at the lower limit of the survey where the pitot pressure ratio continues to decrease below its freestream value. For the strong vortex the pitot pressure ratio is seen to reach a minimum of $P_2/P_0 = 0.175$ and approaches the freestream value 19 mm (0.75 in) above the half-wing tip. Some evidence of a wake is also observed in a similar fashion to the weak vortex. In general, the magnitude and spatial scale of the pitot pressure deficit increases with half-wing angle of attack.

Figures 12(a), (b) and (c) show the spanwise Mach number distributions for both vortex strengths.

A single step procedure based on that by Centolanzi[3] was used to calculate these values from the raw pressure data. Since significant variation in the pitot pressure occurs over lengths of the order of the cone probe diameter (3.2 mm), the pitot value used to calculate the flow properties was averaged over a 2 mm (0.08 in) length centered on the cone probe tip. Figure 12(a) shows the distribution of lateral Mach number (M_x) for both vortices. For the geometry of the current experiments, M_x may be interpreted as the swirl component of the Mach number. The distributions show a similarity to the classic Burgers swirl velocity profile with an inner linear swirl distribution, surrounded by a region with swirl similar to an irrotational vortex. The point of zero swirl was found to correspond closely with the point of minimum pitot pressure (figure 11) for both vortices. It is noted however that the profiles are not symmetric, but show a larger swirl and core radius outboard of the half-wing (see also figure 10). This asymmetry is typical of wing tip vortices. The average core diameter for the weak and strong vortices was observed to be 6.7 mm (0.26 in) and 8.0 mm (0.32 in) respectively. Figure 12(b) shows the distribution of spanwise Mach number (M_y) for both vortices. These distributions indicate that the vortex cores were not travelling parallel with the freestream at the survey position, but were being washed inwards. Further evidence of this may be obtained by close examination of figure 9(a), where the tip vortex core can be clearly seen to be washed inwards from the half-wing tip. The magnitude of the inwash indicated in Figure 12(b) increased with half-wing angle of attack, and peaked close to the vortex axes for both cases. Figure 12(c) shows the distribution of streamwise Mach number (M_z) for both vortices. Significant Mach number deficit is observed to occur for both vortices in a small region near their respective axes. Outside this region, which is of the same spatial scale as the vortex core, M_z is close to M_∞. The wake-like M_z profiles reach a minimum of M_z = 1.70 and 1.53 for the weak and strong vortices respectively. Streamwise Mach number deficits of this magnitude have not been previously reported for supersonic wing tip vortices and have significant implications for vortex interaction studies.

Based on the results presented in Figures 12(a) and (c), the magnitude of the swirl angle τ in the vortices is plotted in figure 13. As noted earlier, the vortices are not axi-symmetric and the peak swirl angle occurred outboard of the half-wing tip. The maximum swirl angles are $\tau = 7.4^\circ$ and 8.7° for the weak and strong vortices respectively. The spanwise total pressure (P_1) distributions for the weak and strong vortices are shown in figure 14. As expected, significant total pressure deficits occur in the core regions, the minimum total pressure ratios being P_1/P_o = 0.33 and 0.19 respectively for the weak and strong vortices. Also of note is the absence of any effect of the shock-expansion wave structure generated by the half-wing, which indicates that the survey position 2.25 chords downstream of the half-wing trailing edge is within the 'test diamond' in the current experiments. In summary, the supersonic wing tip vortices exhibited many characteristics commonly found in low speed wing tip vortices, including an asymmetric 'Burger like' swirl distribution and significant total pressure deficits. To the authors' knowledge the substantial streamwise Mach number deficit observed in the vortex core regions have not been previously reported for supersonic wing tip vortices. The spatial scale and the strength of the vortices was observed to increase with half-wing angle of attack.

CONCLUSIONS

Cone probe surveys were conducted at Mach 2.5 for the wing tip vortices generated by a rectangular half-wing at 5 and 10 degrees angle of attack. The tip vortices exhibited many characteristics similar to their low speed counterparts, including asymmetric 'Burger like' swirl distributions and significant total pressure deficits. A wake-like streamwise Mach number distribution was observed for both cases, and the scale and strength of the vortices increased with half-wing angle of attack. These results add to the small amount of experimental supersonic tip vortex data available in the literature. Computational calibration of commercially available cone probes using an Euler solver was found to be satisfactory for pointed 4-hole probes. Extension of numerical calibration to 5-hole cone probes would require a treatment of the nose bluntness in the numerical model, which was not attempted here. The current use of computational fluid dynamics to calibrate cone probes is a viable alternative to conventional experimental calibration, particularly when wind-tunnel time is at a premium.

Acknowledgements

This work was supported by the Air Force Office of Scientific Research under Grant F49620-93-1-0009 and by NASA Lewis Research Center under Grant NAG3-1378. Computing resources for the work presented here was provided by the Pittsburgh Supercomputing Center. The authors are grateful to Frank Marconi for many useful discussions and for providing the computer code used to generate the calibration curves. The assistance of Mr Lester Orlick,

Mr Kuo-Kuang Liu and Mr Joe Zammit was greatly appreciated during the work.

REFERENCES

1. Kalkhoran,I.M., "Vortex Distortion During Vortex-Surface Interaction in a Mach 3 Stream", AIAA Journal, Vol 32, No. 1, January 1994.

2. Kalkhoran, I.M., and Sforza, P.M., "Airfoil Pressure Measurements During Oblique Shock Wave-Vortex Interaction in a Mach 3 Stream," AIAA Journal, Vol. 32, No. 4, April 1994.

3. Centolanzi,F.,J, "Characteristics of a 40° Cone for Measuring Mach Number, Total Pressure and Flow Angles a Supersonic Speeds", NACA-TN-3967, May 1957.

4. Andrews,D.R, and Sawyer,W.G, "The Calibration of a 60° Cone to Measure Mach Number, Total Pressure, and Flow Angles at Supersonic Speeds", Aeronautical Research Council CP-628, London, 1962.

5. Naughton,J.W,Cattafesta, L.N, and Settles,G.S, "Miniature, Fast-Response 5-Hole Conical Probe for Supersonic Flowfield Measurement", AIAA Journal, Vol. 31, No. 3, March 1993.

6. Oberkampf,W.L, and Aeschliman,D.P, "Joint Computational/Experimental Aerodynamics Research on a Hypersonic Vehicle, Part 1: Experimental Results, AIAA Journal, Vol. 30, No. 8, August 1992.

7. McWherter Walker,M., and Oberkampf,W.L, "Joint Computational/Experimental Aerodynamics Research on a Hypersonic Vehicle, Part 2: Computational Results, AIAA Journal, Vol. 30, No. 8, August 1992.

8. Davis,T., "The Measurement of Downwash and Sidewash Behind a Rectangular Wing at Mach 1.6", Journal of Aeronautical Science, May 1952, p329.

9. Adamson,D. and Boatright,W.B., "Investigation of Downwash, Sidewash and Mach number Distribution Behind a Rectangular Wing at Mach 2.41", NACA TR 1340, 1950.

10. Wang,F.Y., and Sforza,P.M., "An Experimental Investigation of Tip Vortices at Mach 2.5", AIAA paper 93-3448, 1993.

11. Kalkhoran, I.M., Cresci, R.J., and Sforza, P.M., "Development of Polytechnic University's Supersonic Wind Tunnel Facility," AIAA Paper 93-0798, January 1993.

12. Beam,R.M. and Warming,R.F., "An Implicit Factored Scheme for the Compressible Navier-Stokes Equations", AIAA Journal, Vol. 16, No. 4, 1978.

13. Roe,P.L., "Discrete Models for the Numerical Analysis of Time-Dependent Multi-dimensional Gas Dynamics", J. Comp. Phys., Vol. 63, pp 458-476, 1986.

14. Thomas,J.L. and Walters,R.W., "Upwind Relaxation Algorithms for the Navier-Stokes Equations", AIAA Journal, Vol. 25, No. 4, pp 527-534, 1987.

15. Krasnov, N.F, "Aerodynamics of Bodies of Revolution", American Elsevier Publishing Company, New York, 1970.

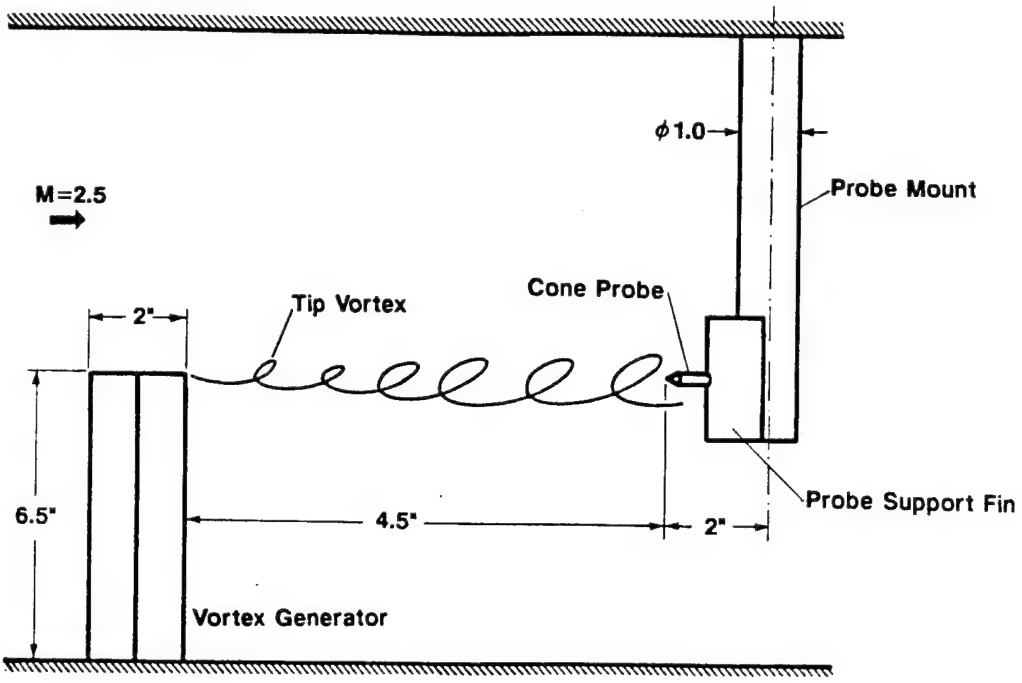

Figure 1 - Schematic of Experimental Arrangement.

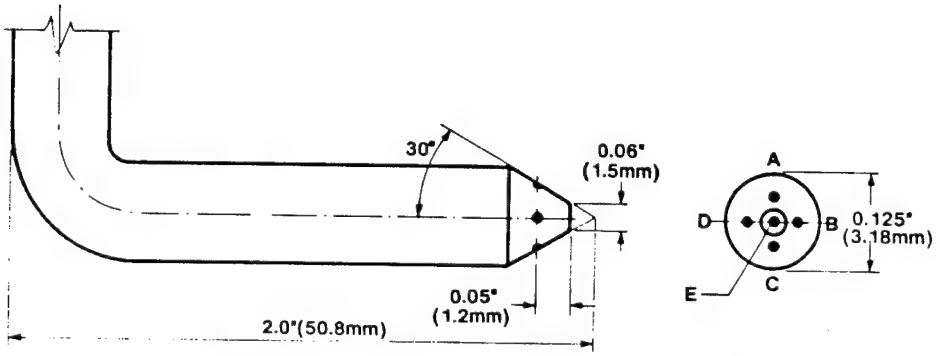

(a) 5 Hole Probe

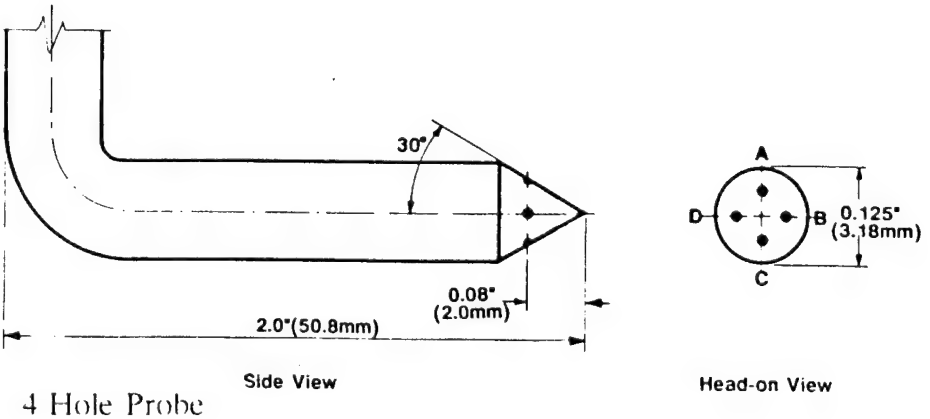

(b) 4 Hole Probe

Figure 2 - Cone Probes

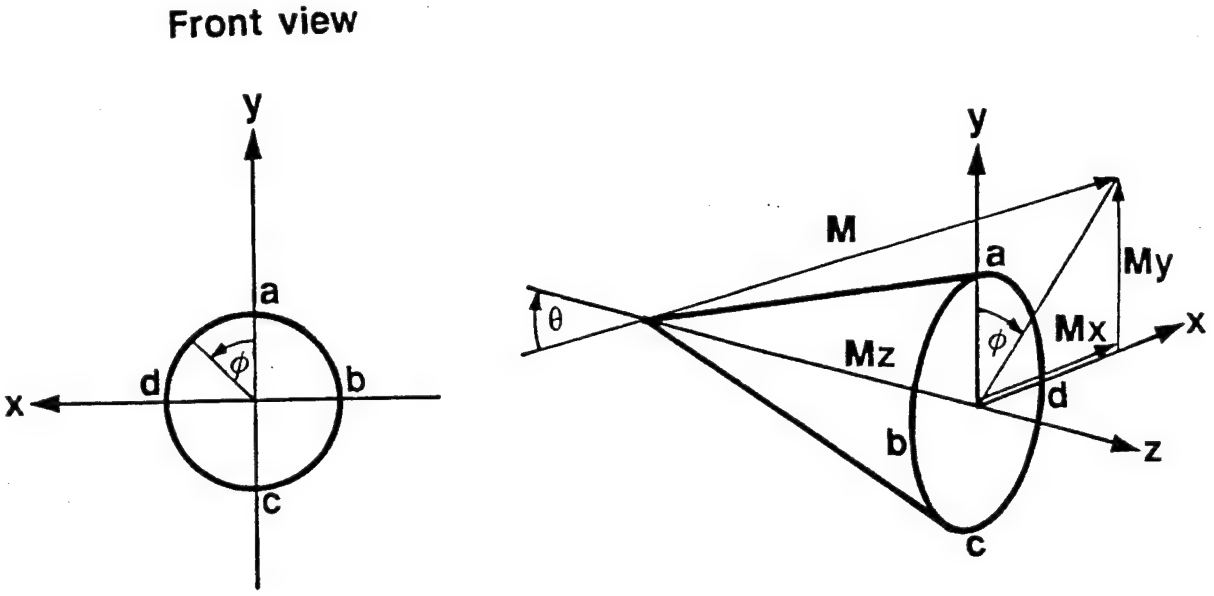

Figure 3 - Spherical Co-ordinate System.

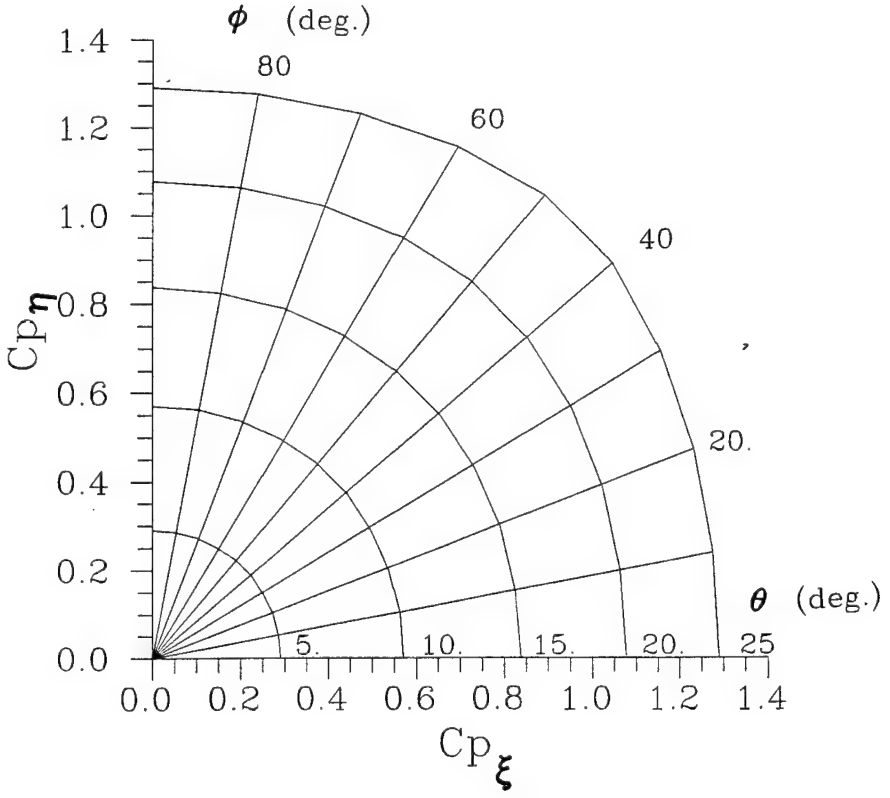

Figure 4 - Calibration Map for M = 2.5.

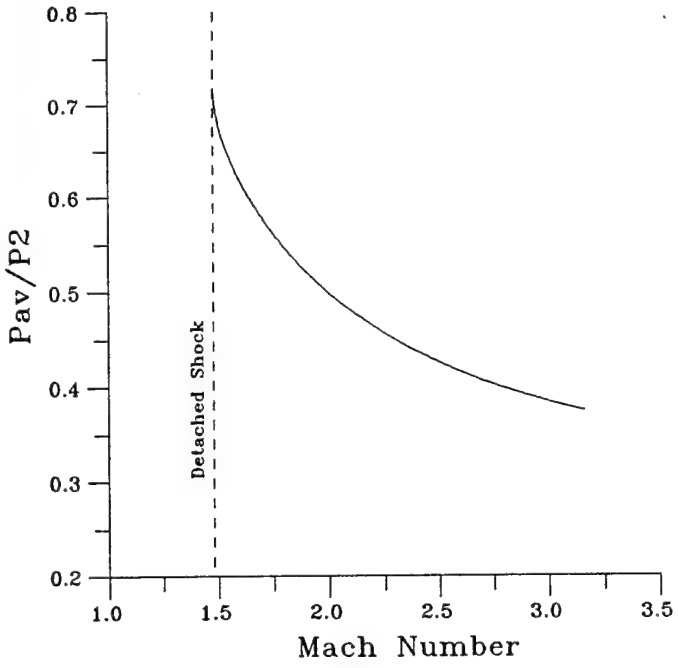

Figure 5 - P_{av}/P_2 versus Mach Number.

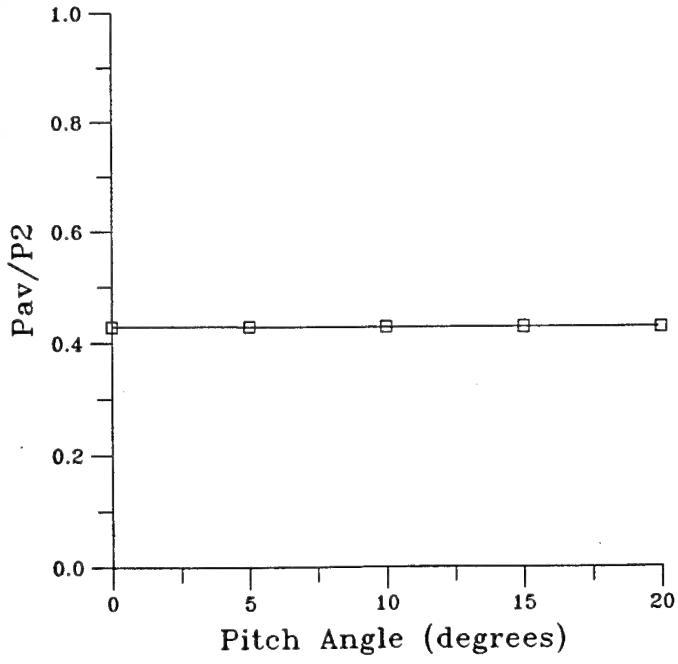

Figure 6 - P_{av}/P_2 versus pitch angle at M = 2.5.

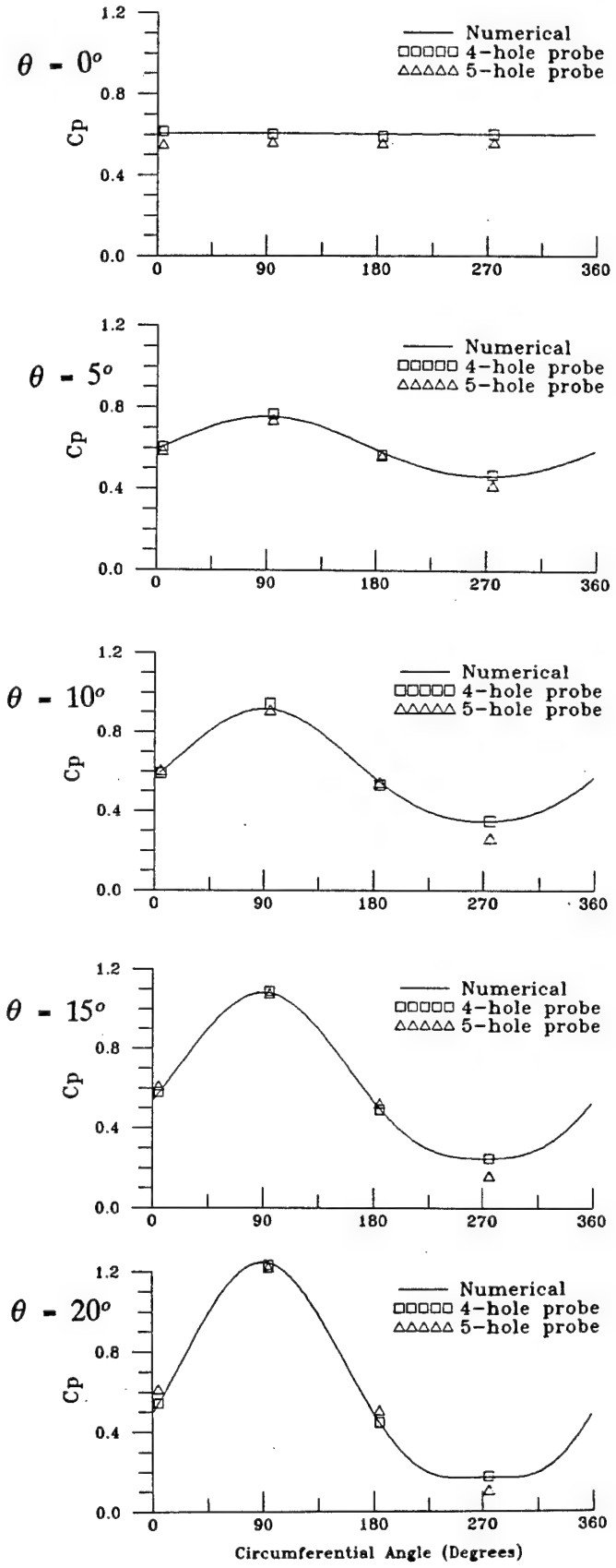

Figure 8 - Circumferential Cp Distributions at M = 2.5.

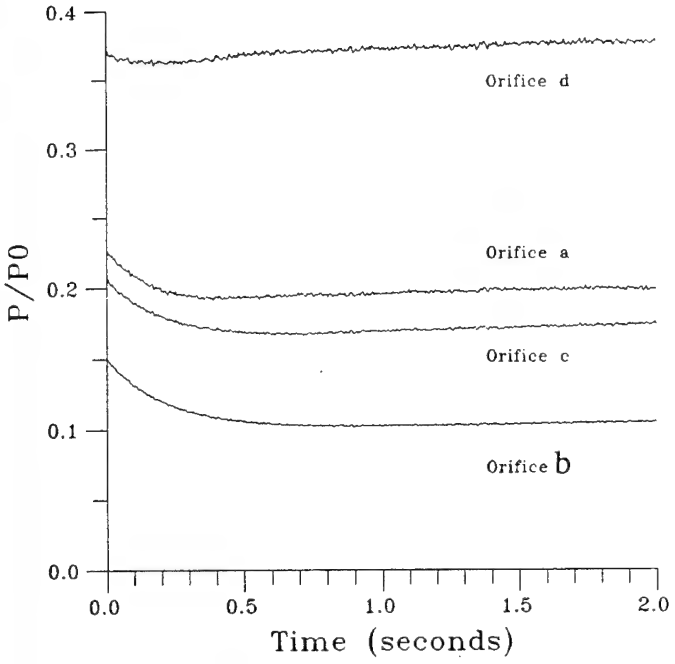

Figure 7 - Pressure versus time for a typical run.

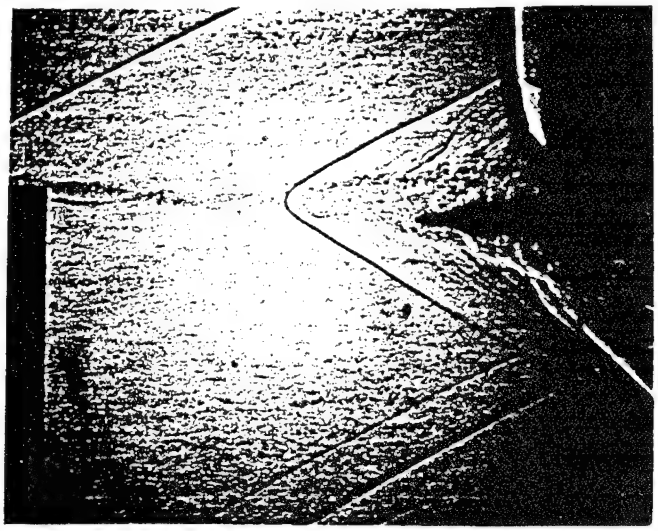

Figure 9(b) - Shadowgraph of typical 5-hole probe survey with leading edge fin removed.

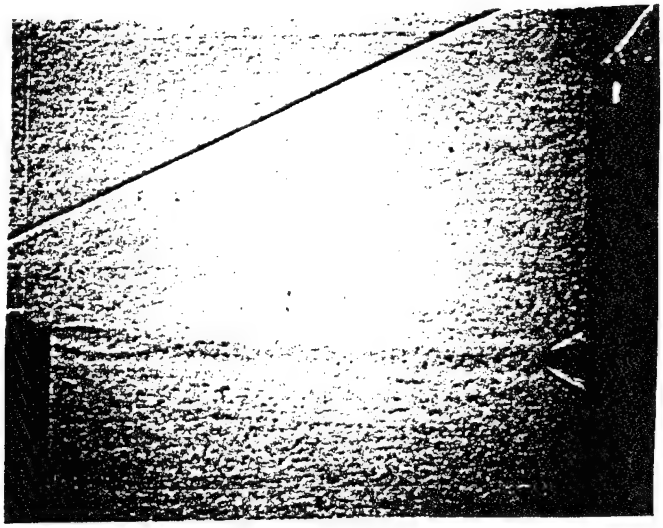

Figure 9(a) - Shadowgraph of typical 5-hole probe survey.

Figure 10 - Laser light sheet image of α = 10° vortex.

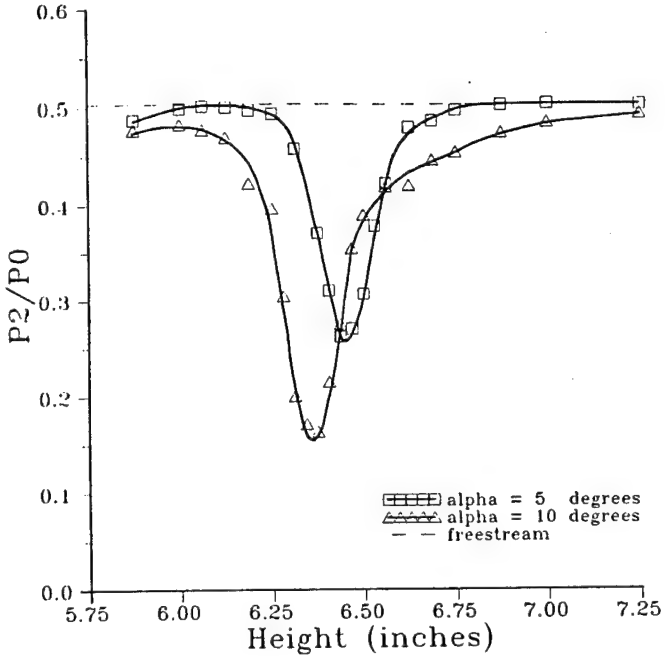

Figure 11 - Pitot Pressure Distribution

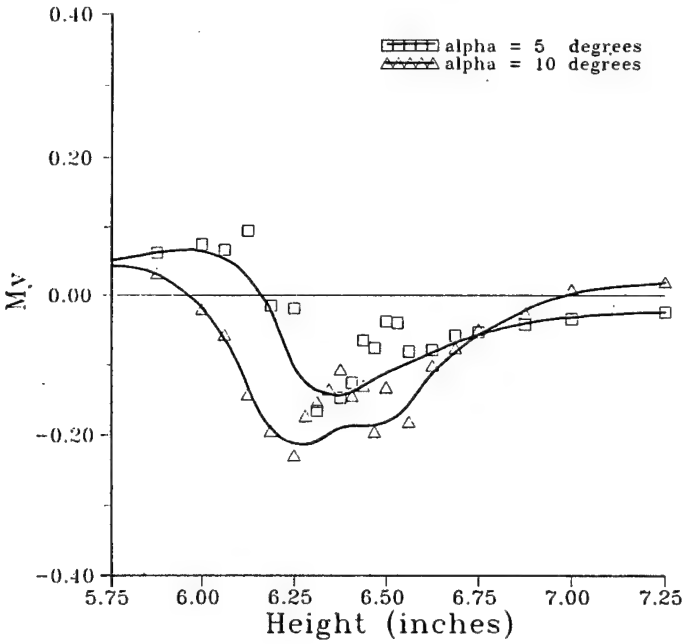

Figure 12(b) - M_y Distribution

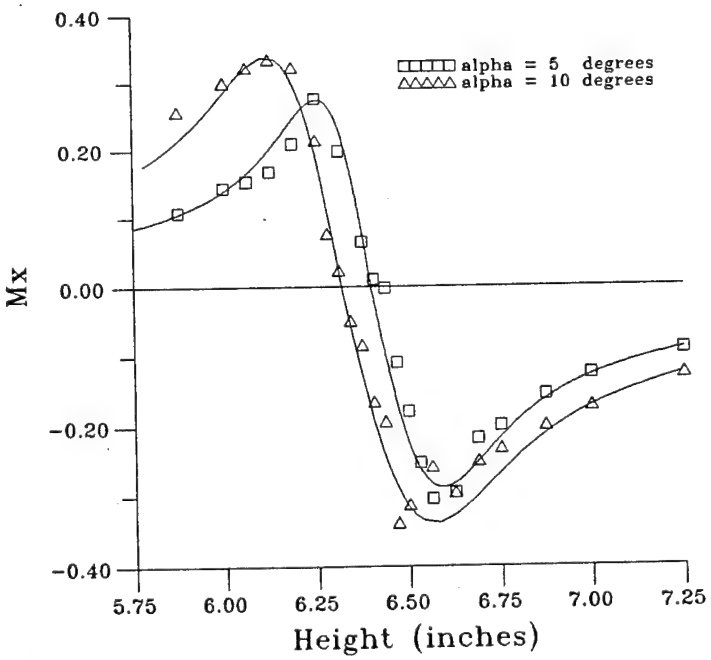

Figure 12(a) - M_x Distribution

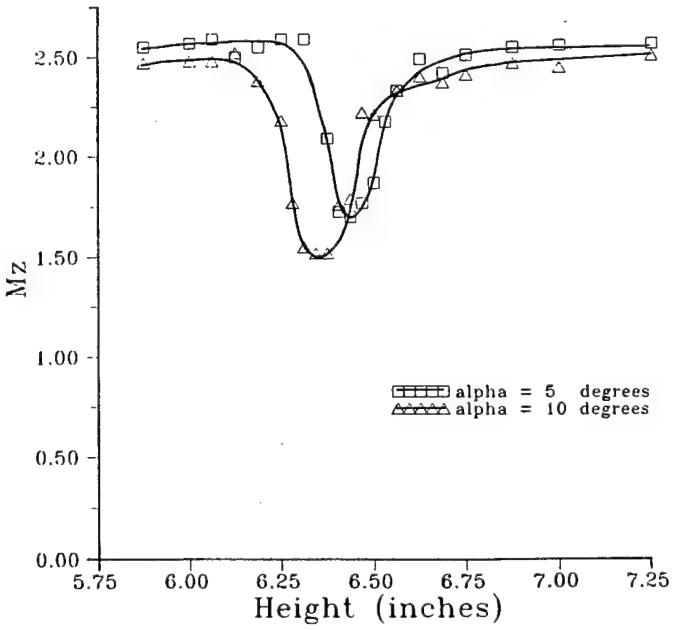

Figure 12(c) - M_z Distribution

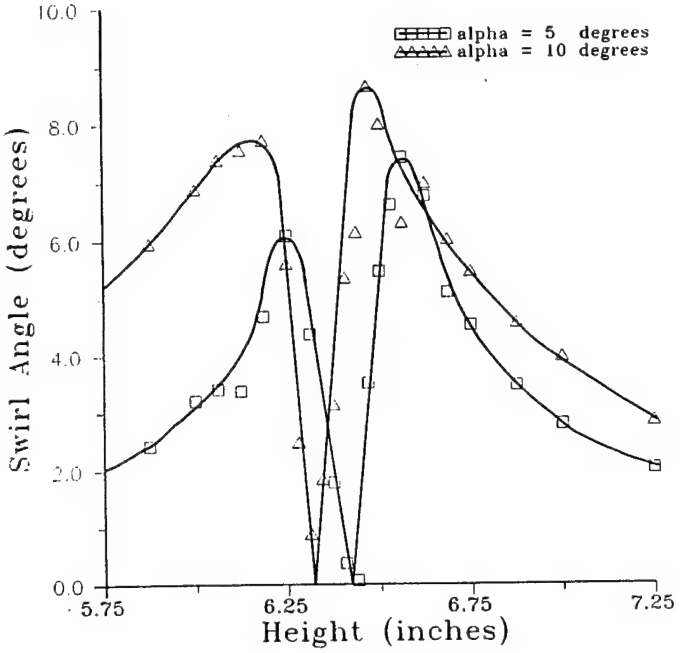

Figure 13 - Swirl Angle Distribution

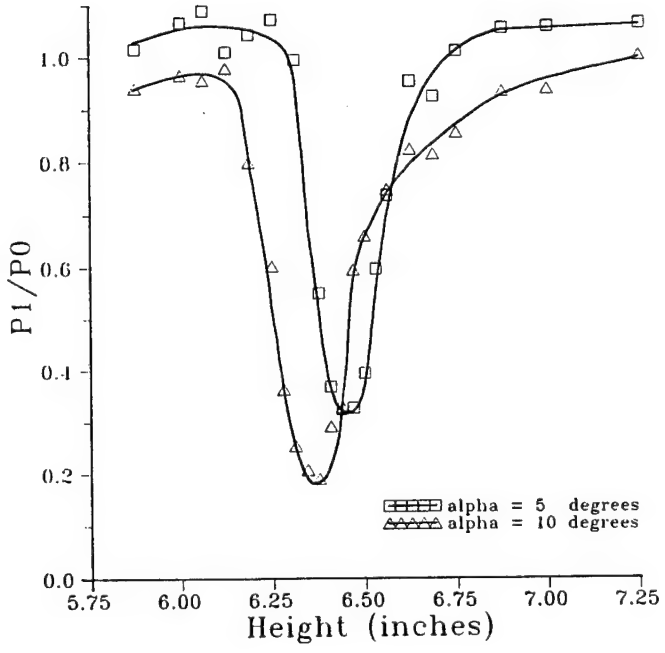

Figure 14 - Total Pressure Distribution

AIAA 95 - 0098

THE EFFECT OF SHOCK STRENGTH ON OBLIQUE SHOCK WAVE-VORTEX INTERACTION

M.K.Smart and I.M.Kalkhoran,
Aerospace Engineering Department,
Polytechnic University,
Brooklyn, New York.

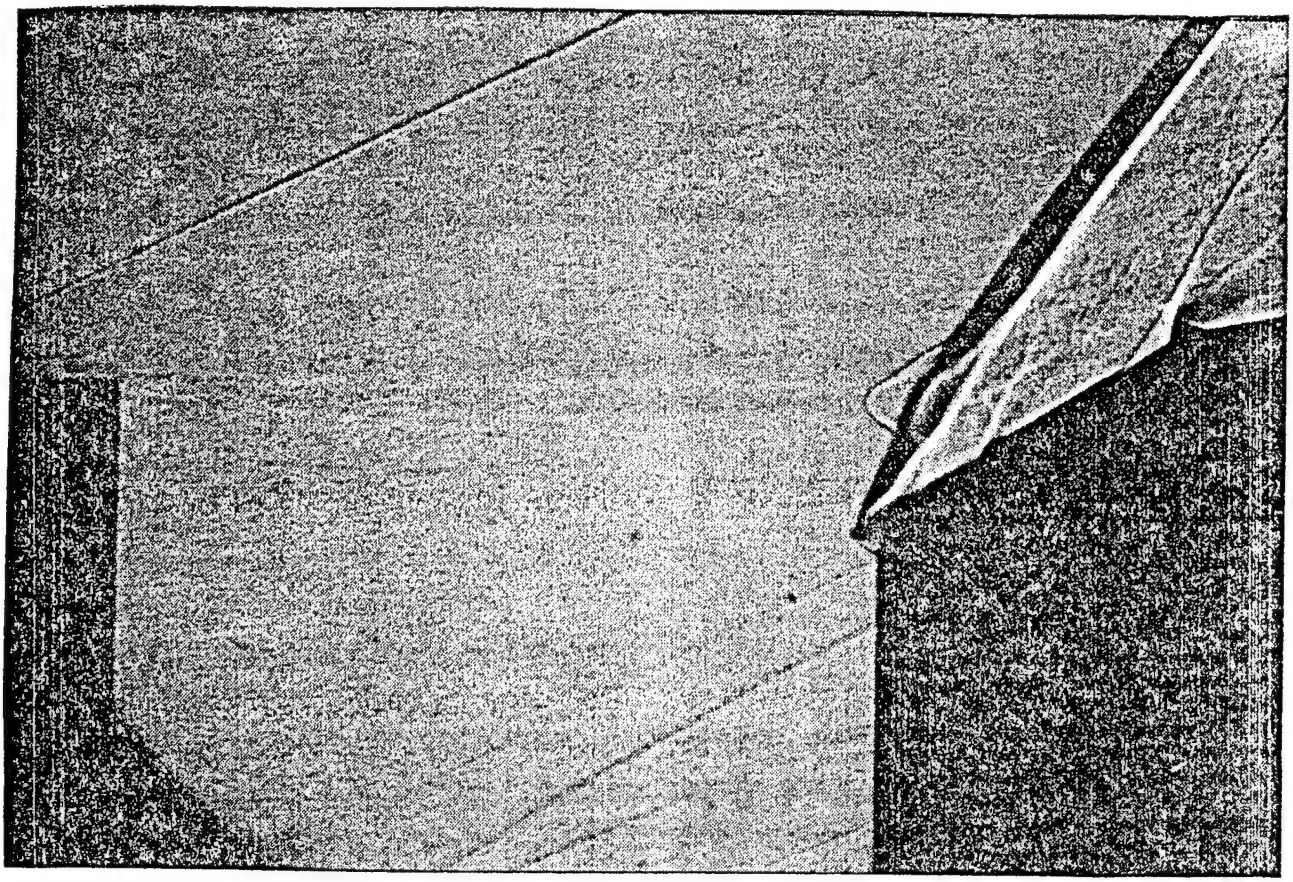

33rd Aerospace Sciences Meeting and Exhibit
January 9-12, 1995 / Reno, NV

THE EFFECT OF SHOCK STRENGTH ON OBLIQUE SHOCK WAVE-VORTEX INTERACTION

Michael K. Smart* and Iraj M. Kalkhoran+
Aerospace Engineering Department,
Polytechnic University, Brooklyn, New York 11201

ABSTRACT

An experimental study of the interaction between streamwise vortices and two-dimensional oblique shock waves has been conducted at Mach 2.5. The experiments involved positioning an instrumented two-dimensional wedge downstream of a semi-span wing so that the trailing tip vortex from the wing interacted with the oblique shock wave formed over the wedge surface. The experiments were designed to simulate interaction of streamwise vortices with shock waves formed over aerodynamic surfaces or in supersonic inlets. The influence of oblique shock wave intensity on this inherently three-dimensional interaction was examined for vortices of variable strength. Results indicated that the interaction of a moderate strength vortex with an oblique shock wave can lead to the formation of a steady separated shock structure upstream of the oblique shock front. The scale of the structure increased with shock wave intensity and showed a close resemblance to the unsteady vortex distortion observed during the head-on interaction of streamwise vortices with a wedge leading edge reported in previous studies. In some instances the separated shock structure was observed to continue through the oblique shock front to strike the shock generating wedge forming a three-dimensional shock wave-boundary layer interaction.

Nomenclature

M	Mach number
P	Pressure
V	Velocity
l	Length of wedge surface
d	Characteristic length
x,y,z	Cartesian coordinates
α	Vortex-generator angle of attack
Γ	Circulation
β	Shock angle
ρ	Density
ξ	Vorticity
ν	Uncertainty

Subscripts

1	Condition ahead of shock
2	Condition behind shock
w	Wedge
o	Chamber
M	Mach number
∞	Free Stream
n	Normal
t	Tangential
a	Axial

---

* Graduate Research Fellow, Student Member AIAA
+ Assistant Professor, Member AIAA

INTRODUCTION

Concentrated streamwise vortices occur in many aeronautical applications such as the flow past wings and slender bodies at angle of incidence. They are formed by the separation and subsequent roll up of the thin viscous sheet near a surface which once away from the surface then convects downstream with the surrounding flow. This concentrated rotational region contained in a generally irrotational flow may then interact with other components of an aircraft or body of interest. For example, the vortices shed by the forebody or canards of a high speed aircraft flying at angle of attack may pass over or strike its wings and aft control surfaces leading to loss of lift, increased drag or changes in the pitching moment characteristics of the aircraft (figure 1(a)). Another deleterious possibility is the ingestion of streamwise vortices by the air intake systems resulting in decreased engine performance or blockage of the engine intake (figure 1(b)). The flow fields generated by such encounters are in general three-dimensional and at supersonic speeds exhibit strong compressibility effects due to the presence of shock waves.

The strength of streamwise vortices steadily increases with the angle of incidence of the wing or body until a drastic disruption to its structure occurs, commonly called 'vortex breakdown'[1-4]. This phenomenon is characterized by a sudden increase in the size of the vortex, the appearance of reversed flow and a stagnation point on its axis, and the presence of large scale unsteadiness. It is well known that in low speed flows vortex breakdown may also be precipitated in a streamwise vortex by the application of a sufficiently strong adverse pressure gradient[5]. A considerable number of investigations have been reported in this area including several review articles by Hall[6], Liebovitch[7] and most recently by Delery[8]. In supersonic flows it has been experimentally demonstrated that vortex breakdown can result from the interaction of sufficiently strong streamwise vortices with normal shock waves[9-11]. The interaction of vortices with shock waves and in particular supersonic vortex breakdown has been investigated by a few authors, but has only recently attracted serious attention.

Shock wave-vortex interactions are generally separated into two distinct classifications; normal shock wave-

vortex interactions and oblique shock wave-vortex interactions (figure 2). Interaction of a vortex with a normal shock wave always results in a change from supersonic flow (a supercritical region incapable of admitting upstream wave propagation) to subsonic flow (a subcritical region that allows upstream propagating waves). The interaction of a vortex with an oblique shock wave does not necessarily involve a supercritical to subcritical transition, as in most cases the flow remains supersonic behind the shock wave. A simple examination of the shock wave-vortex interaction problem indicates that the governing simulation parameters are the free stream Mach number and Reynolds number, a vortex intensity parameter defined by $\Gamma/V_\infty d$ (where d is an appropriate characteristic length), and a shock strength parameter such as the density ratio across the shock (ρ_2/ρ_1). For the oblique shock wave-vortex interaction the shock wave inclination angle (β) is also an important parameter, since for these encounters the downstream flow properties depend on the component of Mach number normal to the shock.

Introduction of a streamwise vortex upstream of an otherwise planar shock wave will in general lead to curvature of the shock front due to gradients of Mach number and total pressure in the vortex. Examining the geometry of the normal shock wave-vortex interaction (figure 2(a)), if the shock wave remained normal to the freestream during the interaction, the vortex swirl would be at all times tangent to the shock wave and therefore have no effect upon it. However as the shock wave deforms in response to axial Mach number and total pressure gradients in the vortex core, the swirl will contribute to the shock curvature in a non-uniform manner depending on the local component of swirl Mach number (M_t) normal to the shock front. It is clear therefore that the interaction of a streamwise vortex with a normal shock wave will in general lead to a three-dimensional curvature of the shock front. For the special case of an axi-symmetric streamwise vortex, in which the Mach number and total pressure vary in an axi-symmetric manner, the curved shock front will degenerate to an axi-symmetric form. Examining the geometry of the oblique shock wave-vortex interaction (figure 2(b)), the fact that the undisturbed shock front is not normal to the free stream introduces an extra 'non-symmetric' element to the shock wave curvature produced by a given stream-wise vortex. A three-dimensional curvature of the shock front will always occur in this case, even if the incoming vortex is axi-symmetric. In summary, all shock wave-vortex interactions include a three-dimensional curvature of the shock wave, which for the special case of the interaction between an axi-symmetric streamwise vortex and a normal shock wave degenerates to an axi-symmetric form.

A first step in the analysis of any shock wave-vortex interaction is the determination of the three-dimensional curved shock front. Given that this non-trivial task has been accomplished, the changes in the vortex properties across the shock wave are of interest, in particular the change in its vorticity. Fundamental studies by Hays[12] demonstrated that the vorticity jump ($\delta\xi$) across a general three-dimensional steady curved shock is given by:

$$\delta\xi_n = 0 \qquad \text{- (1)}$$

$$\delta\xi_t = \bar{n} \times [\nabla_t(\rho_1 V_{1n})/\delta\rho - \bar{V}_{1t} \cdot \nabla_t \bar{V}_{1t}\, \delta\rho \,/\, (\rho_1 V_{1n})] \qquad \text{- (2)}$$

In equations 1 and 2 above the subscripts n and t indicate components normal and tangential to the shock surface and $\bar{n}$ is its local unit normal. It is clear from these equations that there is no vorticity jump normal to the shock surface and that the vorticity jump tangent to the shock surface depends only on the density jump across the shock ($\delta\rho$) and the upstream properties. Due to the shock wave curvature inherent in all shock wave-vortex interactions, a streamwise vortex will undergo a change in its vorticity for both normal and oblique shock wave-vortex interactions alike.

Previous experimental and numerical studies relevant to the interaction problem have concentrated on the interaction of streamwise vortices with normal shock waves. Delery et al[9] carried out a wind tunnel study of the interaction between streamwise vortices with constant axial Mach number and normal shock waves, reporting some shock-induced modifications to both the structure and trajectory of the vortices. Their results indicated that interactions which precipitated vortex breakdown showed negative axial velocity at the vortex axis, a considerable reduction in maximum tangential velocity, and an increase in the radius of the vortex core. Based on these experiments they established a vortex breakdown limit as a function of vortex swirl rate and shock wave intensity. A companion numerical study was reported with the experiments[9] using the steady axi-symmetric Euler equations and a prescribed Burgers' vortex with constant axial Mach number. A breakdown limit similar to the experiments was predicted, but the numerical simulation was not able to accurately calculate flow structure downstream of the breakdown.

Interaction of normal shock waves with vortices generated by a swirling vane injector was studied experimentally by Metwally et al[10], and Cattafesta and Settles[11]. Cone probe measurements[10,11] showed that the vortices used in these experiments exibited a 'wake-like' axial Mach number in combination with a strong swirl. Both studies reported a strong influence of vortex swirl rate and Mach number on the interaction, a vortex breakdown, and an oscillating upstream shock propagation. Based on their experiments, Metwally et al[10] suggested a hypothetical supersonic vortex breakdown model consisting of a region of reversed flow as well as a stagnation point downstream of a bulged-forward shock wave. The interaction of supersonic wing tip vortices with normal shock waves in an inlet type configuration was experimentally investigated by Zatoloka et al.[13] They reported development of a stagnation zone as a result of the encounter and also showed some distorted shock patterns. Experiments involving the head-on interaction of wing tip vortices with the leading edge of a shock generating wedge were reported by Kalkhoran.[14] This interaction is different from the studies mentioned above as a stagnation point is forced to occur in the flow at the wedge leading edge.

It was observed during these experiments that the encounter resulted in formation of an unsteady detached shock front far upstream of the wedge leading edge. This structure was reported to instantaneously form a conical slip surface separating an internal subsonic flow from a surrounding supersonic region. No free standing stagnation point or flow recirculation was reported. It was not clear from these experiments whether the detected unsteadiness was due to an observed unsteady inwash of the incoming tip vortex or whether it was a feature of the head-on interaction.

The aforementioned studies all involved interaction of concentrated streamwise vortices of different types with normal shock waves. Previous studies of the oblique shock wave-vortex interaction problem include numerical work by Copening and Anderson[15], in which the steady 3-D Euler equations were used to study interaction of constant axial Mach number Burger vortices with oblique shock waves at Mach 2.28 and 5.0. They observed no vortex breakdown or appreciable alteration of vortex strength as a result of interactions, but did report a deformation of the planar shock into a three-dimensional convex-concave shock shape. An experimental study of the interaction between wing tip vortices and oblique shock waves was reported by Kalkhoran and Sforza[16]. In this study a tip vortex from a rectangular wing encountered an oblique shock wave generated by a 27° two-dimensional wedge in a Mach 3 stream. Vortex strength and separation distance between the vortex and the wedge leading edge were varied while the shock strength remained constant. An unsteady interaction was observed and time averaged wedge surface pressure measurements showed significant suction on the forward portions of the wedge. An unsteady inwash of the incoming tip vortex was observed in a similar fashion to reference 14. Rizzetta[17] conducted a numerical study of these experiments incorporating both the time dependent 3-D Euler and mass averaged Navier-Stokes equations. This study differed from previous numerical work on the interaction problem[9,15] in that the vortex generation was included in the numerical model. The results showed wedge surface pressure distributions similar to the experiments for some of the cases examined. However in contrast to the experiments, no vortex distortion or breakdown was predicted and no flow unsteadiness was observed.

The oblique shock wave-vortex interaction study reported here was conducted at Mach 2.5 with a similar experimental configuration to that used in reference 16. The experiments involved positioning an instrumented two-dimensional wedge downstream of a semi-span wing so that the trailing tip vortex from the wing interacted with the oblique shock wave formed over the wedge surface. Use of a wing tip vortex for the current work was prompted by a desire to generate an interaction which closely resembles that which occurs in flight. The essential aim of the study was to examine the effect of shock strength on oblique shock wave-vortex interaction, a facet of the shock wave-vortex interaction problem not previously addressed. Furthermore, the study was designed to investigate vortex distortion phenomenon during oblique shock wave-vortex interaction, in lieu of the fact that numerical solutions of the problem[15,17] have not indicated any vortex distortion or breakdown. Modifications to the experimental configuration of reference 16 include a simpler vortex generator wing geometry, a variable angle shock generating wedge, and the installation of miniature high frequency pressure transducers at the wedge surface. In addition, the study has been conducted in a Mach 2.5 wind tunnel[18] of larger size than the Mach 3 facility used for the previous studies[14,16].

EXPERIMENTAL PROGRAM

Wind Tunnel and Test Conditions

The current investigation was conducted in Polytechnic University's 15 x 15 in^2 supersonic wind tunnel facility.[18] It is an intermittent blowdown wind tunnel with a square test section of 38.1 cm x 38.1 cm (15 in x 15 in) and is capable of producing unit Reynolds numbers in the range of 26 x 10^6 to 22 x 10^7 per meter (8 x 10^6 to 66 x 10^6 per foot) over a Mach number range from 1.75 to 4.0. The interaction studies reported here were conducted at a nominal test section Mach number of 2.49. The stagnation pressure and temperature for these experiments were 0.45 MPa (65 psia) and 290 K respectively, resulting in a unit Reynolds number of 4.3 x 10^7 per meter (1.3 x 10^7 per foot). A typical test time for the experiments was three seconds.

Experimental Arrangement

The experimental arrangement for this study was similar to that used in earlier work in a Mach 3 wind tunnel.[16] A generic illustration of the experimental arrangement is shown in figure 3, followed by a dimensioned drawing in figure 4. The vortex generator was a rectangular half-wing with a diamond shaped cross section (8 degree half angle), a chord length of 50.8mm (2 in), a span of 165.1 mm (6.5 in) and angle of attack capability from 0 to 10 degrees. The shock wave generator was a two-dimensional wedge section with an included angle of 20°, a wedge surface length of 76.2 mm (3.0 in) and a span of 177.8 mm (7.0 in). The wedge had variable angle of attack capability from 0 to 10 degrees which enabled generation of flow deflections between 20 and 30 degrees. The shock generator section was equipped with a 6 x 3 grid of 18 equally spaced pressure ports in which miniature high frequency pressure transducers were mounted. The six rows spanning the wedge were equally spaced between $x/l = 0.17$ and $x/l = 0.75$, (where x is the distance along the wedge surface from the leading edge). The three streamwise rows were located at $y/l = 0.12$, $y/l = 0.0$, and $y/l = -0.12$ (where $y = 0.0$ is the lateral location of the half-wing). For these experiments the wedge was placed 15.2cm (6 in; 3 vortex generator chords) downstream of the half-wing trailing edge, with its leading edge 25.4 mm (1.0 in) below the half-wing tip. The dimensions and relative orientation of the half-wing and the wedge section were chosen so that the interaction took place well within the 'test diamond' of nearly uniform flow formed by the shock-expansion wave structure emanating from the half-wing.

Instrumentation and Data Acquisition System

Miniature Kulite high frequency pressure transducers (model XCQ-062-50A) with protective screens were used in the experiments. These had a range from 0-345 kPa (0-50 psia), an outer diameter of 1.6 mm (0.063 in) and a natural frequency response of 50 kHz. Transducers outputs were first amplified by Honeywell Accudata 122 DC amplifiers and then digitized using a Metrabyte das-16, 12-bit analog-to-digital converter board at a rate of 500 hz per channel for a period of three seconds. The error associated with typical wedge surface pressure measurements reported in this work was $\nu_p = \pm 0.25$ psia, and a conventional uncertainty analysis indicates that the uncertainty in test section Mach number was $\nu_M = \pm 0.018$. Shadowgraphs were taken of the flow using a spark light source which provided micro-second range exposure times. Multiple spark shadowgraphs of the flowfield were possible at a rate of two per second.

Test Program

Experiments were carried out to systematically investigate the effect of shock wave strength on the interaction of wing tip vortices with two-dimensional oblique shock fronts. Tests were performed for flow deflection angles of $\theta = 22$, 25 and 29 degrees. For each flow deflection angle a base-line run was conducted with the half-wing removed, followed by runs with the half wing at $\alpha = 5$ and 10 degrees. For each combination of flow deflection angle and half-wing angle of attack, time accurate pressure measurements were recorded at the 18 grid positions on the wedge, together with multiple spark shadowgraphs. Throughout the entire test program approximately 30 % of the runs were repeated to check for consistency. It was found that the results were repeatable to well within the calculated accuracy of the instrumentation. For the purposes of this study, the tip vortex generated by the half-wing when placed at 5° angle of attack will be referred to as the weak vortex, and interactions involving it will be called weak interactions. Correspondingly the tip vortex generated by the half-wing when placed at 10° angle of attack will be referred to as the strong vortex and interactions involving it will be called strong interactions.

EXPERIMENTAL RESULTS AND DISCUSSION

Wedge Calibration and Tip Vortex Characterization

Wedge calibration experiments were performed to establish the base-line pressure distribution on the wedge. The time averaged streamwise pressure distributions for $\theta =$ 22, 25 and 29 degrees are shown in figure 5. These results compare favorably with two-dimensional theory, except for the downstream portion of the $\theta = 29°$ case. The pressure relief observed in this case is a consequence of the fact that the shock generating wedge does not span the entire width of the test section, giving rise to some three-dimensional effects at the edges. Figure 6 shows a typical shadowgraph of the base-line flowfield for the particular case of $\theta = 25°$. The oblique shock wave shown is close to the angle predicted by two-dimensional theory ($\beta = 50.5°$). The disturbances appearing in the shadowgraph downstream of the oblique shock are generated at the wedge supports and are far removed from the interaction zone.

Measurements of the tip vortices using a conical probe located 2.25 chords downstream of the half-wing trailing edge were reported in reference 19. The inwash (measured from tip of the wing) and the upwash (measured from the trailing edge) of the weak tip vortex were 1.3 mm (0.05 in.) and 3.1 mm (0.12 in.) respectively. The inwash and upwash of the strong tip vortex were 3.5 mm (0.14 in.) and 3.3 mm (0.13 in.) respectively. The vertical position of the wedge leading edge changes slightly with deflection angle. For the $\theta = 25°$ case the weak vortex enters the interaction zone approximately 27 mm (1.05 in.) above the wedge leading edge and at y/l = 0.01 (figure 4). For the same wedge position the strong vortex enters the interaction zone approximately 24 mm (0.95 in.) above the wedge leading edge and at y/l = 0.05. The conical probe measurements[19] indicated that the tip vortices consist of a region of total pressure deficit in combination with a 'wake-like' axial Mach number and a significant swirl. Figure 7, which is extracted from reference 19, illustrates the relative magnitude of the swirl and core size of the weak and strong vortices. The figure shows a plot of the pressure difference across the cone probe measured during a vertical (spanwise with respect to the half-wing) survey through the axes of the vortices. The viscous core of the weak and strong vortices was observed to have an average diameter of 6.7 mm (0.26 in.) and 8.0 mm (0.32 in.) respectively[19]. Outside the viscous core the cone surface pressures approach the freestream value in the test section, indicating a return towards the freestream Mach number and no influence of the shock-expansion wave structure generated by the half-wing.

Weak Interaction Results

Figure 8 illustrates a typical shadowgraph of the flowfield resulting from the interaction of the weak vortex with a two-dimensional oblique shock wave; ie a weak interaction. The particular case shown in the figure involves the shock wave generated by a flow deflection of $\theta = 25°$. Flow is from left to right with the half-wing in the lower left hand corner and the wedge section on the right. The shadowgraph clearly indicates a concentrated tip vortex convecting downstream and intersecting with the oblique shock wave, creating a classical oblique shock wave-vortex interaction. There appears to be no appreciable alteration to the vortex upon intersecting the oblique shock front, but a slight distortion of the shock wave in the interaction zone is noticeable. Comparison with figure 6 indicates that the presence of the weak vortex has moved the shock wave slightly upstream of its undisturbed position, a movement consistent with a 'wake-like' axial Mach number in the vortex. Flow behind the shock wave appears to be smooth, but the view of the vortex is obscured by waves from the wedge edge effects. This flow structure is typical of the weak interactions observed in this study. Variation of the shock wave intensity

did not produce any substantial changes to the flow structure and multiple shadowgraphs taken during typical three second runs showed no changes with time.

Time averaged wedge surface pressure distributions for the weak interaction are shown in figures 9(a), (b) and (c), for θ = 22, 25 and 29 degrees respectively. The dashed lines in the figures correspond to the base-line data for each flow deflection angle, and the solid lines represent the streamwise pressure distributions at the three spanwise positions of y/l = 0.12, 0.0 and -0.12. Examination of figure 9(b) (θ = 25°) indicates that the streamwise variation of pressure is similar at each spanwise position. The pressure is constant up to approximately x/l = 0.4, followed by a dip which reaches a minimum at x/l = 0.52 and finally a return towards the base-line wedge pressure at x/l = 0.63. Pressures at y/l = 0.12 are the highest, y/l = -0.12 are the lowest and pressures at y/l = 0.0 are in between. This description of the pressure distribution in figure 9(b) is also applicable to figures 9(a) and (c) for the 22° and 29° flow deflections, except that the streamwise position at which the constant pressure is disrupted moves to x/l = 0.5 and 0.25 respectively. The disrupted region, consisting of a dip to a minimum pressure approximately 7% below the base-line followed by a return towards the base-line pressure, is of a similar magnitude and streamwise scale for all three shock wave strengths. It is noted that the time accurate pressure measurements showed no large amplitude fluctuations during typical three second test periods.

The time averaged pressure measurements show some interesting features of the oblique shock wave-vortex interaction. The spanwise pressure variation on the wedge is believed to be due to the fact that the component of velocity normal to the oblique shock is not uniform in the vortex. In the present geometry, the vortex swirl velocity adds to the freestream velocity component normal to the shock for positive y, and subtracts from the freestream velocity component for negative y. This leads to a locally stronger shock for positive y (creating a higher pressure on the wedge) and a locally weaker shock for negative y (creating a suction on the wedge). Superimposed on this is the fact that there is a pressure deficit in the vortex with respect to the freestream, hence the wedge pressure at y/l = 0.0 is also lower than the base-line value.

The localized low pressure region observed for all three flow deflection angles on the mid-chord portions of the wedge is thought to be due to waves emanating from the interaction zone. The incoming wing tip vortex consists of a region of total pressure and axial Mach number deficit, combined with a swirl. As the shock distorts due to passage of the vortex, waves are generated in the supersonic flow behind the shock which propagate towards the wedge. It is postulated that these waves are the cause of the low pressure region, and therefore must be expansion waves. Evidence to support this postulation can be obtained by calculating the point at which waves from the interaction zone would be expected to reach the wedge. A simple first order estimate of the expected point of minimum pressure can be obtained by assuming that shock distortion and variations in the local Mach angle behind the shock are small. Using the geometry shown in figure 10, the wave emanating from the point of intersection of the vortex axis and the oblique shock wave reaches the wedge at x/l = 0.64, 0.59 and 0.45 for flow deflection angles of 22, 25 and 29 degrees respectively. These values correspond reasonably well with the observed positions of minimum pressure in each case.

In summary, the weak interaction tests showed slight distortion of the oblique shock wave for all three flow deflection angles. Small spanwise pressure variation was observed to occur due to vortex swirl, together with a localized low pressure region at the mid-chord region of the wedge. The streamwise position of this low pressure region moved forward with increased shock wave intensity, while its magnitude and streamwise scale did not vary with shock wave strength.

Strong Interaction Results

The strong interaction results exhibit many characteristics similar to the weak interaction, however the increased swirl causes some more dramatic features of the flowfield to become apparent. Figures 11(a), (b) and (c) show spark shadowgraphs of the strong interaction for θ = 22, 25 and 29 degrees respectively. The strong tip vortex can be seen in each of the shadowgraphs to convect smoothly downstream and enter a classical oblique shock wave-vortex interaction with the shock front generated by the wedge. Examination of figure 11(c) indicates that for θ = 29°, the strong interaction precipitates a dramatic change in the structure of the shock wave and a considerable disruption to the vortex. For this case the shadowgraph depicts the formation of a local three-dimensional shock structure well upstream of the position of the undisturbed oblique shock wave, which surrounds an expanding vortex core in much the same manner as a shock wave forms about a blunted body. It appears that the Mach number and total pressure deficits associated with the strong vortex are of such a magnitude that an oblique or slightly deformed shock wave cannot be sustained in its core region, producing a local separation of the shock. It is noted that multiple spark shadowgraphs taken during typical three second runs show no change in the scale or shape of this structure, so it appears that the conditions which force the shock wave to separate locally are equilibrated by the formation of this structure. The separated shock wave is normal to the freestream in the center of the vortex, locally forming a normal shock wave-vortex interaction and hence a local subsonic region downstream of the shock. After passing through this normal shock wave the vortex core is seen to expand considerably. Away from the vortex core the observed separated shock structure appears to be simply a response of the surrounding free stream to the expansion of the vortex core. This shock structure is similar to that reported for the head-on interaction of a wing tip vortex with a wedge leading edge reported in reference 14, except for the fact that the head-on interaction was found to be inherently unsteady.

Although the vortex distortion observed in the current study is similar to that exhibited during the head-on vortex-wedge interaction[14], a fundamental difference exists

between these two encounters. A stagnation point is forced to occur in the region of the wedge leading edge in the head-on interaction[14], whereas no such forced stagnation point exists in the interaction zone of the current encounter. This difference is particularly important since existence of a stagnation point is universally accepted as a characteristic feature of vortex breakdown. Despite the fact that certain features known to occur in subsonic vortex breakdown cannot be verified in this study (for example, the presence of reversed flow and formation of a stagnation point), figures 11(a)-(c) indicate a strong visual resemblance to the low-speed vortex-breakdown reported in the literature[1-3]. These observations clearly demonstrate that destruction of a vortex as a result of an oblique shock wave-vortex interaction is possible; a behavior not reported in the two numerical studies of the problem.[15,17] Copening and Anderson[15] suggested that the absence of breakdown in their numerical studies of oblique shock wave-vortex interaction may be due to the presence of supersonic flow downstream of the oblique shock wave; ie a supersonic downstream boundary condition. The current observations indicate that the supersonic downstream condition which occurs in most oblique shock wave-vortex interactions does not necessarily prohibit severe vortex distortion or possibly even vortex breakdown.

Another interesting feature of the strong interaction shown in figure 11(b) (θ = 25°), and to the authors' knowledge not previously reported, is the continuation of the separated shock through the plane of the undisturbed oblique shock wave to impinge on the wedge surface. The lower portion of the shock is clearly seen to strike the wedge at approximately x/l = 0.3 in this case, and forms a three-dimensional shock wave-boundary layer interaction on the wedge surface. The details of the region where the lower portion of the separated shock structure crosses the original oblique shock wave is obscured in the shadowgraph, but the two appear to interact as independent shock waves of different families, with the local downstream angle of both dictated by the need to match flow angle and static pressure.

The effect of shock wave intensity on the strong interaction is clearly shown by comparing figures 11(a), (b) and (c). In figure 11(a) (θ = 22°) the separated shock structure appears to be just on the verge of formation. The oblique shock wave shows significant deformation in the interaction region, but no separate structure is apparent. In figure 11(b) (θ = 25°) the separated shock structure is fully formed with the leading portion located 6.7 mm (0.26 in.) upstream of the undisturbed oblique shock wave. Finally, figure 11(c) (θ = 29°) shows a separated shock wave with the leading portion located 13 mm (0.53 in.) upstream of the undisturbed oblique shock wave, the largest of the three cases examined. It appears that the effect of increased oblique shock wave intensity on the strong interaction is an increase in the scale of separated shock structure. The position at which the lower portion of the separated shock impinges on the wedge surface also varies with the shock wave intensity. For θ = 22° no shock wave was observed to impinge on the wedge surface. As already stated, the lower portion of the separated shock is observed to strike the wedge surface at x/l = 0.3 for θ = 25°. Increase of the flow deflection to θ = 29° removes the impinging shock wave. This is thought to be due to the fact that no downstream solution which includes a continuation of the separated shock wave through the oblique shock is possible for the θ = 29° case. In general, it may be stated that the overall structure of the strong interaction is observed to be quite sensitive to the strength of the original oblique shock wave.

Time averaged surface pressure distributions for the strong interactions are shown in figures 12(a), (b) and (c) for θ = 22, 25 and 29 degrees respectively. As for the weak interactions, the time accurate pressure measurements showed no large amplitude fluctuations in typical three second test periods. Examination of figure 12(b)(θ = 25°) indicates that some features of the pressure distribution are similar to the weak interaction. Spanwise pressure variation due to the non-uniform velocity component normal to the undisturbed oblique shock wave occurs once again, but with a greater magnitude due to the increased vortex strength. The streamwise pressure distributions are similar once again for each spanwise position on the wedge, but include a feature not apparent in the weak interactions. Figure 12(b) shows constant pressure up to x/l = 0.25, followed by a significant peak at x/l = 0.4, a substantial drop to a minimum at x/l = 0.55 and finally a return towards the base-line pressure at x/l = 0.8. The peak experienced at all spanwise locations at x/l = 0.4 was not observed for the weak interactions, and appears to be in response to the separated shock wave shown in the shadowgraph (figure 11(b)) to impinge on the wedge at approximately x/l = 0.3. The full pressure rise across the impinging shock may not be shown in these results due to the coarseness of the pressure port grid on the wedge. Downstream of the peak a significant suction is experienced on the wedge in a similar fashion to the weak interaction, but of significantly larger magnitude. The minimum pressure measured on the wedge for this case is approximately 24% below the base-line. The description above is applicable to the form of the pressure distributions for all strong interactions examined.

Variation of shock wave intensity has a two fold effect on the wedge surface pressure for the strong interaction. Comparison of figures 12(a), (b) and (c) indicates that increasing shock wave strength moves the disrupted region (peak, trough and return towards base-line) upstream, and increases the relative magnitudes (compared to the base-line) of the pressure extremes experienced by the wedge. The magnitude of the maximum suction for θ = 22, 25 and 29 degrees is 10%, 24% and 31% of the base-line pressure respectively. The scale of the disrupted pressure region does not vary with shock wave strength but is greater for the strong interaction than for the weak encounter. It is expected that the low pressure region observed at the wedge is generated by waves emanating from the interaction zone in a similar fashion to that suggested for the weak interaction, however the presence of the separated shock structure in the strong interaction makes analysis of the expected position of the low pressure region far more difficult than for the weak interaction.

In summary, the strong interaction precipitates a local disruption of the oblique shock wave which takes the

form of a steady three-dimensional separated shock structure upstream of the undisturbed oblique shock front. This is accompanied by a significant expansion of the vortex core and a local subsonic region downstream of the separated shock. The scale of the structure increases significantly with increase in the oblique shock wave intensity, and a portion of the separated shock was observed to impinge on the wedge surface for some oblique shock wave strengths. The pressure distributions on the wedge exhibit a similar form and position to the corresponding weak interaction results, except for a local pressure peak in the vicinity of the observed shock wave impingement on the wedge. The magnitude of the pressure changes with respect to the base-line were significantly larger than the corresponding weak interaction.

CONCLUSIONS

The effect of shock wave strength on the interaction between wing tip vortices and oblique shock waves has been investigated at Mach 2.5 in the current study. For the weak interaction, involving a vortex generated by the half-wing at 5° angle of attack, the oblique shock wave was slightly distorted for the three shock strengths investigated and the vortex was seen to pass smoothly downstream. Small changes from the base-line surface pressure were experienced on the shock generating wedge. For the strong interaction, involving a vortex generated by the half-wing at 10° angle of attack, a local disruption of the oblique shock wave was observed in the interaction zone, which took the form of a steady separated shock structure upstream of the original oblique shock wave. This structure was accompanied by a significant expansion of the vortex core and a local subsonic region downstream of the separated shock. The upstream stand-off distance and the scale of this structure increased with shock wave intensity. For some shock wave strengths a portion of the separated shock structure continued through the original oblique shock wave to strike the wedge and form a three-dimensional shock wave-boundary layer interaction. Significant changes from the base-line pressure were experienced on the wedge, including a large suction at the mid-chord region of the wedge of up to 30 % of the base-line pressure for the strongest shock wave investigated. The magnitude of the surface pressure variations and their position on the wedge varied with shock wave strength. It was observed that significant distortion of supersonic streamwise vortices is not limited to normal shock waves, but can be precipitated by oblique shock fronts with supersonic downstream conditions. This exploratory study gives some insight into the nature of oblique shock wave-vortex interaction, and brings to light some interesting features of the problem which will require further study.

ACKNOWLEDGEMENTS

This work was supported by the Air Force Office of Scientific Research under Grant F49620-93-1-0009 and by NASA Lewis Research Center under Grant NAG3-1378. The assistance of Mr Lester Orlick and Mr Frank Wang was greatly appreciated during the work.

REFERENCES

1. Werle, H.,"Sur l'eclatement des tourbillons d'apex d'une aile delta aux faibles vitesses", La Recherche Aeronautiique, No. 74, Jan-Feb. 1960, pp. 23-30.

2. Lambourne, N.C., and Bryer, D.W.,"The Bursting of Leading-Edge Vortices - Some Observations and Discussion of the Phenomenon", Aeronautical Research Council Report 3282, London, April 1961.

3. Harvey, J.K., "Some Observations of Vortex Breakdown Phenomenon", Journal of Fluid Mechanics, Vol. 14, (1962), pp. 585-592.

4. Benjamin, T.B., "Theory of the Vortex Breakdown Phenomenon," Journal of Fluid Mechanics, Vol. 14, (1962), pp. 593-629.

5. Sarpaka,T., "The Effect of Adverse Pressure Gradient on Vortex Breakdown", AIAA Journal, Vol. 12, No. 5, 1974, pp. 602-607.

6. Hall, M.G., "Vortex Breakdown", Annual Review of Fluid Mechanics, Vol. 4, 1972, pp. 195-218.

7. Leibovich, S., "Vortex Stability and Breakdown: Survey and Extension," AIAA Journal, Vol. 22, No. 9, Sept. 1983, pp. 1192-1206.

8. Delery, J.M, "Aspects of Vortex Breakdown", Progress in Aerospace Sciences, , Vol. 30, No. 1., Jan. 1994, pp. 1-59.

9. Delery, J., Horowitz, E., Leuchter, O., and Solignac, J.L., "Fundamental Studies on Vortex Flows," LaRecherche Aerospatiale (English Edition), (ISSN 0379-380X), No. 2, 1984.

10. Metwally, O., Settles, G., and Horstman, C., "An Experimental Study of Shock Wave/Vortex Interaction," AIAA Paper 89-0082, January 1989.

11. Cattafesta, L.N., and Settles, G.S., "Experiments on Shock/Vortex Interaction," AIAA Paper 92-0315, January 1992.

12. Hayes, W.D., "The Vorticity Jump across a Gasdynamic Discontinuity," Journal of Fluid Mechanics, Vol. 2, (1957) pp. 595-600.

13. Zatoloka, V., Ivanyushkin, A.K., and Nikolayev, A.V., "Interference of Vortexes with Shocks in Airscoops. Dissipation of Vortexes," Fluid Mechanics, Soviet Research, Vol. 7, No. 4, July-August 1978, pp. 153-158.

14. Kalkhoran, I.M., "Vortex Distortion During Vortex-Surface Interaction in a Mach 3 Stream," AIAA Journal, Vol. 32, No. 1, 1994, pp. 123-129.

15. Copening, G., and Anderson, J., "Numerical Solutions to Three-Dimensional Shock Wave/Vortex Interaction at Hypersonic Speeds," AIAA paper 89-0674, January 1989.

16. Kalkhoran, I.M., and Sforza, P.M., "Airfoil Pressure Measurements During Oblique Shock Wave-Vortex Interaction in a Mach 3 Stream," AIAA Journal, Vol. 32, No. 4, 1994, pp. 783-788.

17. Rizzetta, D.P., "Numerical Simulation of Oblique Shock-wave/Vortex Interaction," AIAA Paper 94-2304, June 1994.

18. Kalkhoran, I.M., Cresci, R.J., and Sforza, P.M., "Development of Polytechnic University's Supersonic Wind Tunnel Facility," AIAA Paper 93-0798, January 1993.

19. Smart, M.K., Kalkhoran, I.M., and Bentson, J., "Measurements of Supersonic Wing Tip Vortices", AIAA Paper 94-2576, June 1994.

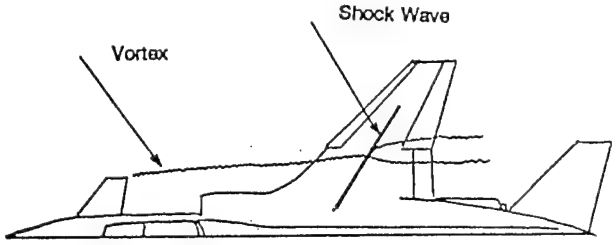

(a) Vortex-wing interaction.

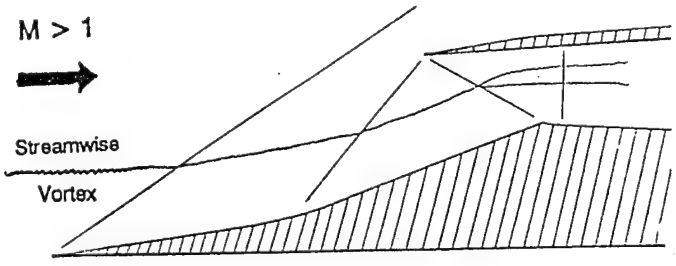

(b) Vortex-inlet interaction.

Figure 1 - Shock wave-vortex interactions in flight.

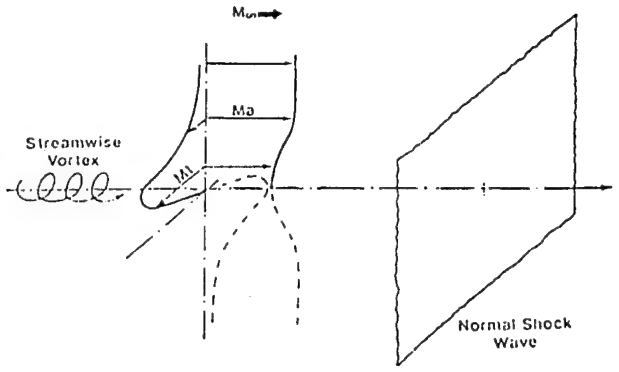

(a) Normal shock wave-vortex interaction.

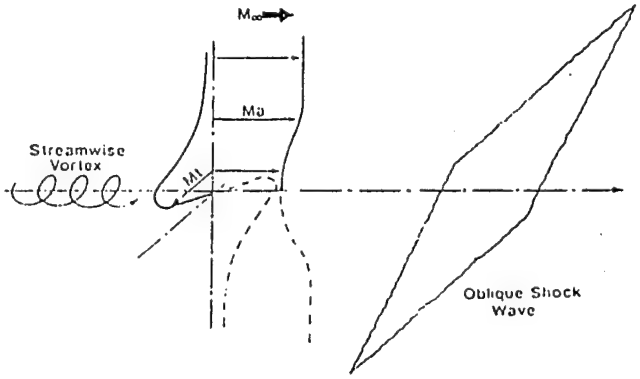

(b) Oblique shock wave-vortex interaction.

Figure 2 - Shock wave-vortex interaction classifications.

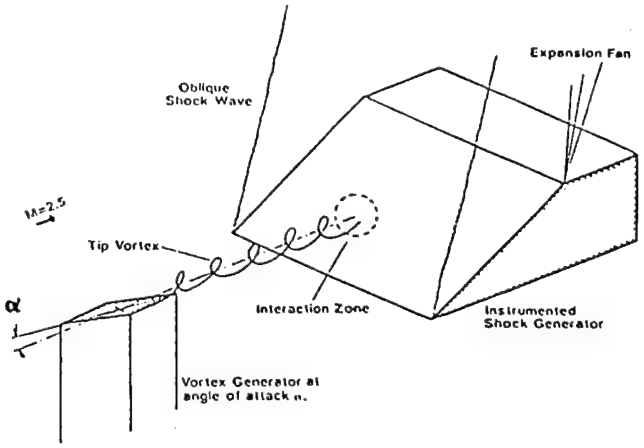

Figure 3 - Experimental Arrangement.

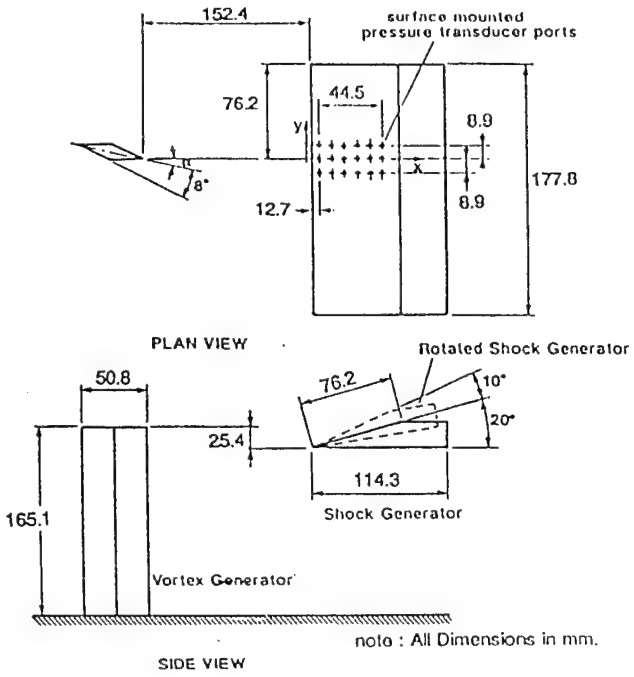

Figure 4 - Experimental Geometry.

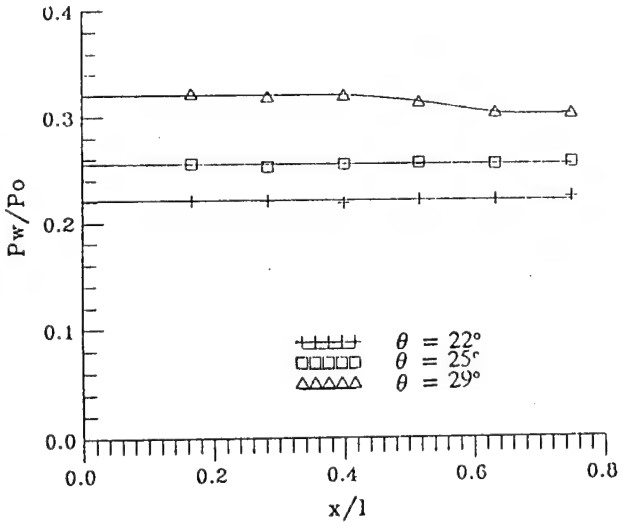

Figure 5 - Base-line wedge pressure distributions.

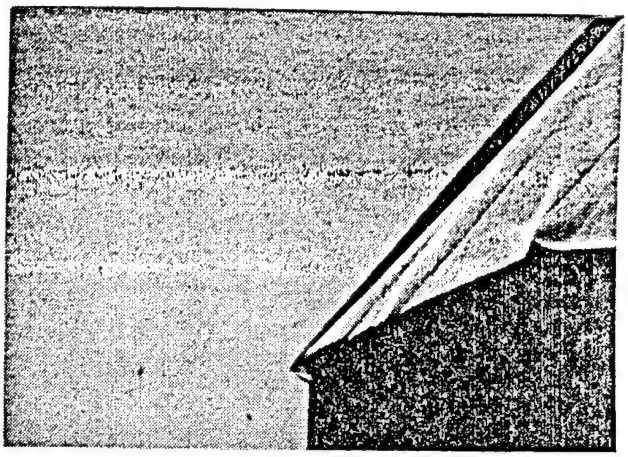

Figure 6 - Shadowgraph of base-line flowfield for $\theta = 25°$.

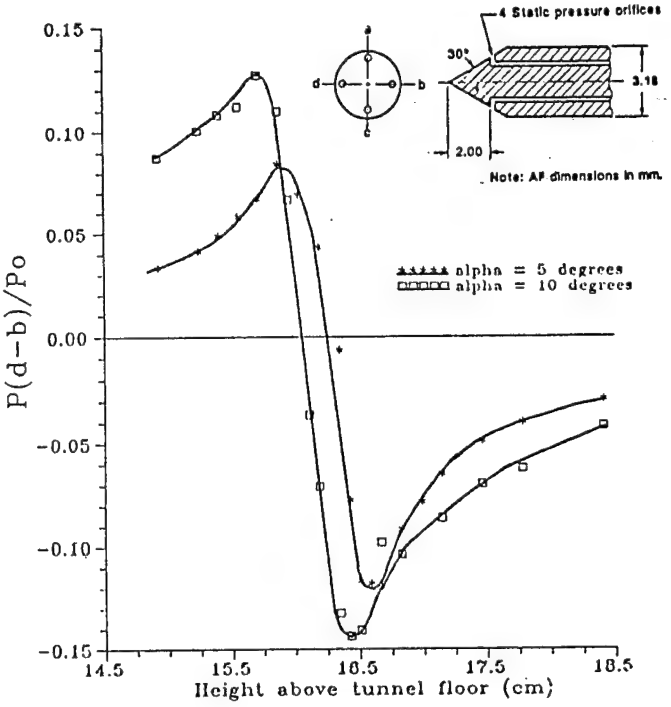

Figure 7 - Cone probe measurements of the wing tip vortices.

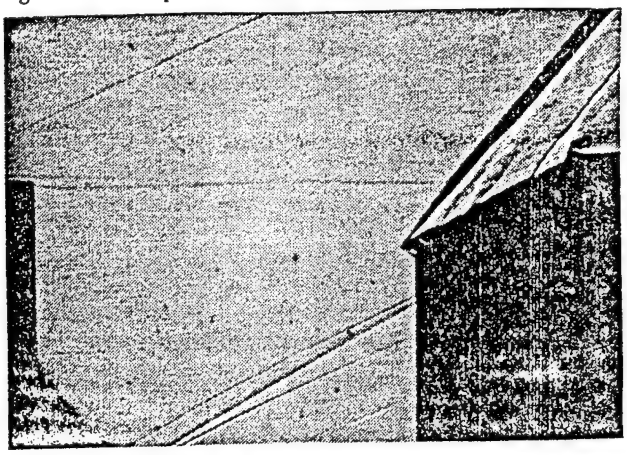

Figure 8 - Shadowgraph of the weak interaction flowfield for $\theta = 25°$.

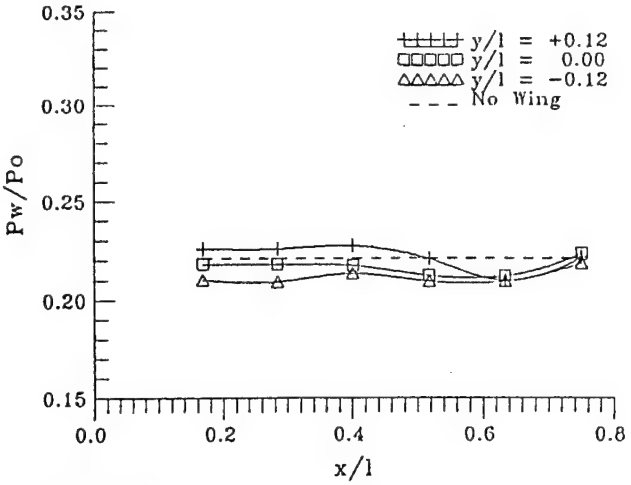

(a) $\theta = 22°$

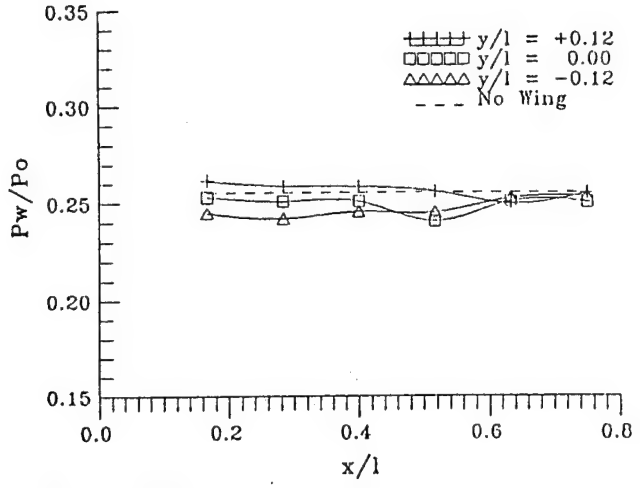

(b) $\theta = 25°$

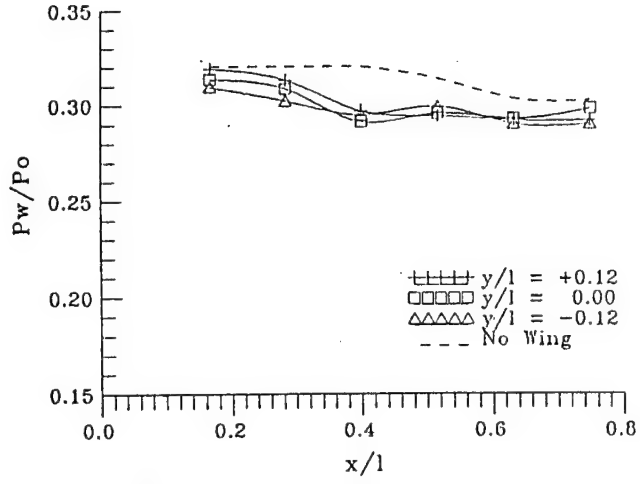

(c) $\theta = 29°$

Figure 9 - Wedge pressure distributions for the weak interaction.

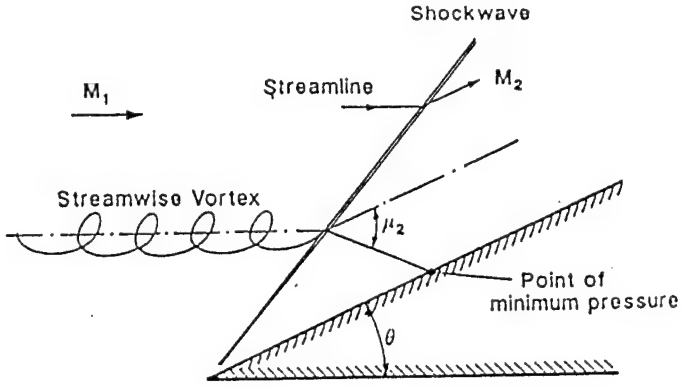

Figure 10 - Wave geometry for flow downstream of the weak interaction.

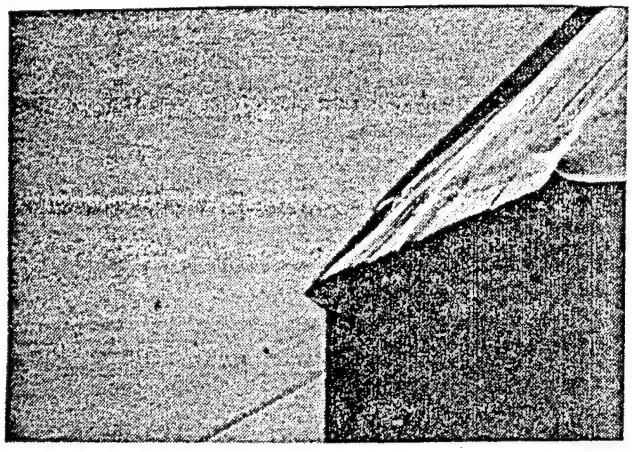

(a) θ = 22°

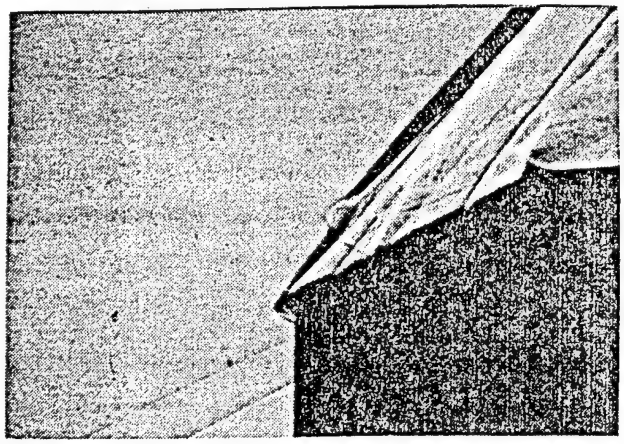

(b) θ = 25°

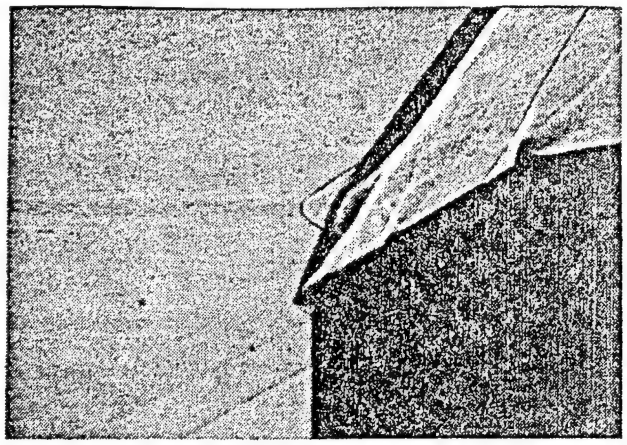

(c) θ = 29°

Figure 11 - Shadowgraphs of the strong interaction flowfield.

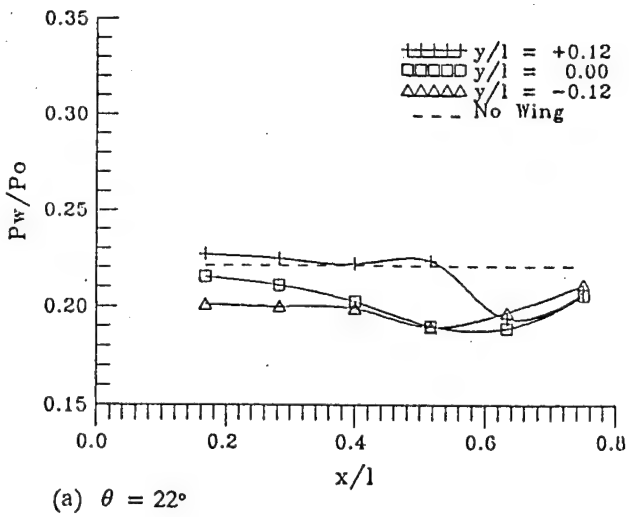

(a) θ = 22°

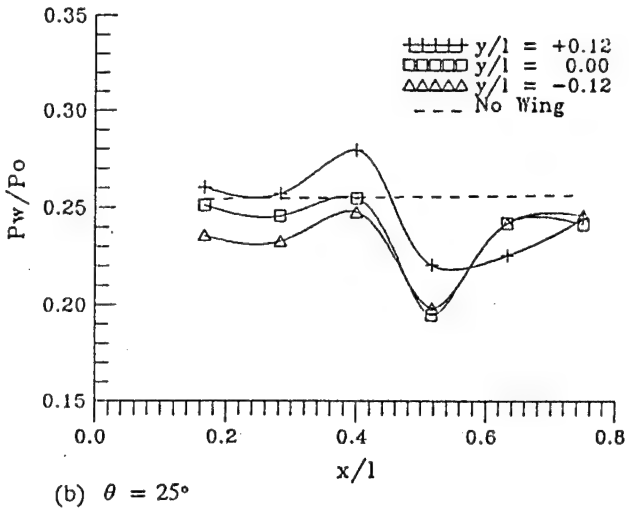

(b) θ = 25°

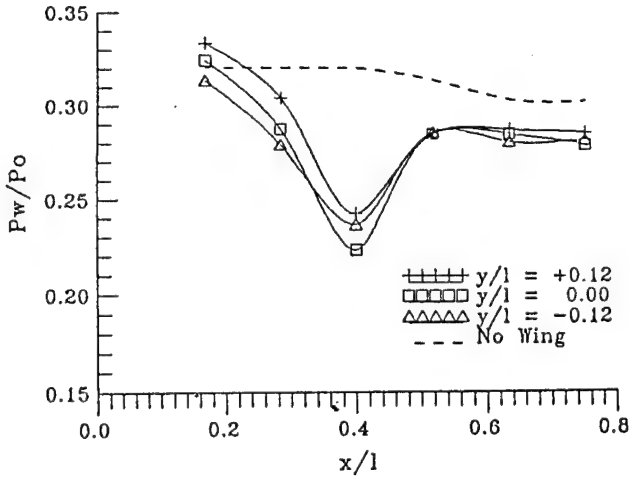

(c) θ = 29°

Figure 12 - Wedge pressure distributions for the strong interaction.

AIAA 95-2283

Interaction of Supersonic Wing Tip Vortices with a Normal Shock

I. M. Kalkhoran, M. K. Smart,
and A. Betti
Department of Aerospace Engineering
Polytechnic University
Brooklyn, New York

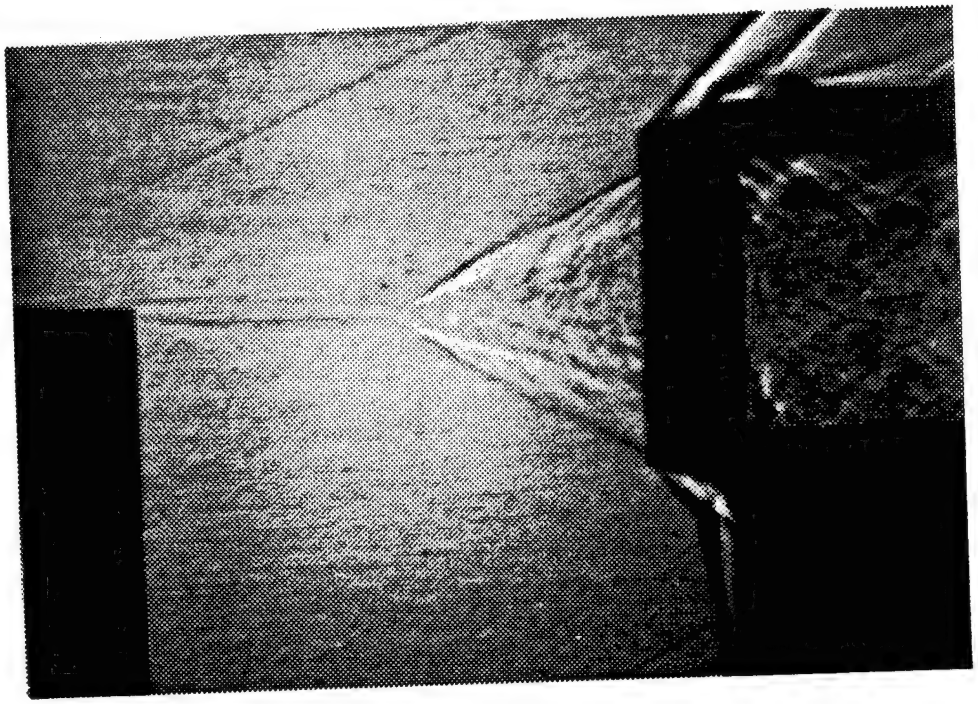

26th AIAA Fluid Dynamics Conference
June 19-22, 1995/San Diego, CA

AIAA 95-2283

INTERACTION OF SUPERSONIC WING TIP VORTICES WITH A NORMAL SHOCK

Iraj M. Kalkhoran,* Michael K. Smart,** and Alexander Betti+
Department of Aerospace Engineering
Polytechnic University, Brooklyn, New York 11201

Abstract

An experimental study involving interaction of concentrated streamwise wing tip vortices and normal shock fronts was carried out in a Mach 2.49 flow. The interaction scheme involved positioning a vortex-generator wing section upstream of a pitot type normal shock inlet such that the wing tip vortices interacted with the normal shock formed in front of the inlet. The vortex strength was varied by placing the vortex generator wing at different angles of attack while a normal shock was created by adjusting the mass flow rate passing through the inlet. Spark shadowgraphs, laser sheet planar visualizations, and pitot pressure measurements of the flowfield indicated a significant change in the structure of streamwise vortices generated by the vortex generator wing at 5 and 10 degrees angle of attack upon encountering a normal shock discontinuity. Results of the investigation showed that the interactions lead to the formation of an unsteady conical shock wave far upstream of the inlet as well as a highly turbulent flow downstream for both vortices. Pitot pressure measurements using a fast response pressure transducer in conjunction with the spark shadowgraphs revealed a bi-modal feature of the flowfield. The frequency of oscillation of the generated structure was found to be higher for increased vortex strength.

Introduction

The interaction of a concentrated vortex and a shock wave may occur in many instances in the operational environment of supersonic aircraft and missiles. The interaction may be a result of vortices created by the forward components of a supersonic vehicle convecting downstream and interacting with shock waves formed over aft components or shock waves present in front of the air intake system of the vehicle, leading to performance deterioration. In practice, such encounters involve interaction of three-dimensional curved line vortices with non-planar shock fronts. Experimental evidence[1-6] indicates that the flowfield generated by the shock wave/vortex interaction can result in brutal destruction of vortices with large scale turbulent structure similar to those observed during low speed vortex breakdown. Although the aerodynamics implications of the vortex breakdown in external flows are in general undesirable, this phenomenon has been suggested to be a potential means of enhancing the rate of fuel-air mixing in the combustor of a supersonic combustion ramjet (scramjet).

Previous experimental and numerical studies of the shock wave/vortex interaction problem have concentrated on a streamwise vortex interacting with an otherwise planar shock front with emphasis on supersonic vortex breakdown. Although interaction of a streamwise vortex with an oblique shock wave is more likely to occur in practice, prior studies have mainly dealt with interaction of a streamwise vortex with a normal shock wave in an attempt to establish a vortex breakdown limit as a function of vortex swirl rate and flow Mach number. This is due to the severity of the pressure jump imposed on the vortex by a normal shock wave in comparison to that of an oblique shock front. As a result, for a given vortex strength, breakdown of streamwise vortices is more likely to occur during a normal shock

*Associate Professor, Member AIAA
**Graduate Research Fellow, Student Member AIAA
+Graduate Student, Student Member AIAA

wave/vortex interaction than an oblique shock wave/vortex interaction. Moreover, the normal shock wave/vortex interaction may be considered as an axi-symmetric flow while the oblique shock wave/vortex interaction is fully three-dimensional leading to a more complex flow.

The original study in this area appears to be due to Zatoloka et al.[1] who experimentally studied the interaction between a streamwise vortex generated by a swept wing and a normal shock in front of a pitot type inlet. The results of their exploratory investigation indicated that a conical shock forms as a result of the encounter downstream of which a vortex breakdown and a stagnation zone was reported. The experimental study of Ref. 1 only considered a single vortex and no detailed measurements of the flowfield were reported. Moreover, the experimental arrangement was such that the vortex had weakened by crossing an oblique shock front prior to interacting with the main normal shock. The first comprehensive study of the normal shock wave/vortex interaction problem was performed by Delery et al.[2] who placed a vortex generator wing in the subsonic portion of a supersonic nozzle; while a normal shock wave was created by a pitot type inlet placed in the test section. The drawback of this approach to simulate the shock wave/vortex interaction problem was due to the fact that the axial Mach number of the vortex increased during the expansion process in the nozzle while its swirl Mach number remained nearly constant. Consequently, the generated vortices were weak in comparison to those found in practice. The results of their study produced a vortex breakdown limit as a function of vortex swirl rate and Mach number however, no visualizations of the generated flowfield were presented in Ref. 2.

Other experimental studies involving interaction of streamwise vortices with normal shocks were reported by Metwally et al.[3] and Cattafesta and Settles.[4] The vortices of Refs. 3 and 4 were generated by swirl vanes and the strength of these vortices were varied by changing the vane angles. Their results indicated a highly unsteady flow regardless of the vortex strength. A weak interaction, characterized by perturbation of the main shock that bulged forward with a characteristic size on the order of incoming vortex core diameter, and a strong interaction consisting of a much larger bulged shock structure were identified. The results of Refs. 3 and 4 further extended the vortex breakdown curve of Delery et al.[2] to cover a wider range of Mach number.

On the numerical side, a few contributions have dealt with the behavior of streamwise vortices upon encountering an abrupt pressure jump imposed by a normal shock wave. In Ref. 2, numerical solution of the normal shock wave/vortex interaction problem using the steady Euler equations was presented. These results indicated a good agreement with experimental observations in the absence of vortex breakdown and the breakdown limit was well predicted. Reference 3 reported the results of axisymmetric Navier-Stokes computations in support of the experimental data. These simulations predicted a similar structure to the strong interaction, including a stagnation point. Unsteady Navier-Stokes calculations were performed by Kandil et al.[5] for the case of quasi-axisymmetric vortices interacting with normal shocks in an inlet-type configuration which revealed several vortex breakdown modes.

Examination of the normal shock wave/vortex interaction problem (Fig. 1) reveals certain characteristics to be expected during such encounters. Since a planar normal shock wave is only possible for a flow with uniform properties upstream of the shock, any non-uniformity in the flow upstream of the shock wave will lead to a local deformation of the shock front. Consequently, introduction of a rotational vortex of limited spatial extent and non-uniform flow properties upstream of an otherwise planar normal shock will lead to local deformation of the shock which in the absence of vortex breakdown will have a characteristic size on the order of the vortex core diameter. On the other hand, breakdown of supersonic vortices has been experimentally shown to lead to formation of a subsonic conical struc-

ture with a characteristic size which is much larger than the vortex core diameter.[6]

The objective of the present work was to conduct an experimental study simulating the interaction of streamwise wing tip vortices and normal shock waves in a Mach 2.49 flow. The experiments were designed to investigate behavior of vortices of various strengths encountering a severe pressure jump across a normal shock with particular emphasis on supersonic vortex distortion. A fundamental difference between the previous experimental studies of the normal shock wave/vortex interaction and that of the present investigation is the method used to generate the streamwise vortices. The vortices generated in the present study have been shown[7] to have different Mach number characteristics than those of previous work. In particular, the axial Mach number distribution in the core region of wing tip vortices of present work are considerably lower than that of the free stream, a fact that is believed to be of significance in the character of the resulting flowfield.

Test Facility, Instrumentation, and Experimental Set-Up

The experimental study of the interaction between streamwise vortices and normal shock waves was carried out in Polytechnic University's supersonic wind tunnel facility.[8] The facility is an intermittent blowdown wind tunnel with a square test section of 38.1 cm x 38.1 cm and is capable of producing unit Reynolds numbers in the range of 26×10^6 to 22×10^7 per meter over a Mach number range from 1.75 to 4.0. The present experiments were performed at a nominal test section Mach number of 2.49. The stagnation pressure and temperature for these experiments were 0.45 MPa and 290 K respectively, resulting in a unit Reynolds number of 4.3×10^7 per meter.

A generic illustration of the experimental arrangement is shown in Fig. 2. The vortex-generator is a semi-span wing having a diamond shape airfoil section with a chord length of 50.8 mm, a span of 165.1 mm, a half angle of 8^o, and angle of attack capability of $0\text{-}10^o$. Vortices of different intensity could be generated by placing the wing section at various angles of attack. The present study utilized 2 different vortex strengths by placing the wing at 5^o and 10^o angles of attack. Effectiveness of wing tip vortices suitable for interaction studies has been demonstrated in previous studies of similar problems.[6,9] A normal shock, pitot type inlet is placed approximately 152.4 mm, or three vortex-generator chords, downstream of the wing section. The normal shock generator has a square 63.5 mm x 63.5 mm inlet which is 156 mm long and is equipped with optical windows for flow visualization and measurement purposes (Fig. 2). A normal shock wave is created in front of the inlet by an adjustable downstream obstruction in the form of a two-dimensional wedge section which chokes the flow coming out of the inlet.

Quantitative measurements in the interaction zone of the flowfield were conducted by means of a pitot probe equipped with a fast response pressure transducer in order to gain insight into the unsteady behavior of the flowfield. The pitot tube had a circular opening of 1.4 mm which diverged to a larger opening a short distance downstream of the nose to house the miniature pressure transducer. The probe was placed approximately 108 mm downstream of the vortex generator wing section. The pitot pressure measurements were made using a fast response Kulite pressure transducer (Model XCQ-062-50A) which was installed in the probe shaft. The pressure transducer had an outer diameter of 1.6 mm, a useful range of 0-345 kPa, and a natural frequency response of 600 kHz. The amplified output from the transducer was digitized using a LeCroy 12-bit A/D convertor at rates up to 100 kHz. Conventional uncertainty analysis of the measurements indicated an uncertainty value of 0.066 for the Mach number and 0.0042 for the non-dimensional pitot pressure (p_t/p_0).

Shadowgraphs of the flow were taken using a spark light source which provided micro-second range exposure times. Multiple spark shadowgraphs of the flowfield were possible at a

rate of two per second. The output from the spark source was also fed into the data acquisition system to correlate the exact timing of the shadowgraphs with the measured pitot pressure during a typical run. Planar visualization of the flowfield were made using a Ruby Pulsed laser with a pulse duration on the order of 30 ns. A thin (on the order of 2 mm) laser sheet illuminates the segment of interest in the test section to provide planar visualization of the flowfield. For these tests, the flow was seeded using a mixture of water and alcohol (2/3 water and 1/3 alcohol by volume) in the settling chamber prior to the tunnel start. These planar visualizations were performed at several axial locations downstream of the vortex generating wing. Schematic of the laser sheet visualization set-up is shown in Fig. 3.

Measurements of flow properties in the core region of supersonic wing tip vortices by means of conical five-hole and four-hole probes were conducted in a previous study and the results are reported in Ref. 7. These measurements were made for vortices generated by the wing placed at 5^{o} (weak vortex) and 10^{o} (strong vortex) angles of attack at a distance of 113 mm (2.25 chords) downstream of the vortex generator trailing edge. The results indicated a significant deficit in the axial Mach numbers along with "Burger-like" swirl distributions for both vortices.[7] Figures 4 and 5 illustrate the axial and swirl components of the Mach number in the core region of vortices respectively. The above figures indicate tightly wound vortices with viscous core diameters of approximately 4 mm and 5.5 mm for the weak and strong vortices respectively. The axial Mach number distributions show a wake-like profile with a minimum axial Mach number of 1.75 and 1.63 for the weak and strong vortices respectively. Such deficits are believed to play a strong role in the character of the shock wave/vortex interaction problem.

Experimental Results

Results for the weak vortex

The initial experiments were carried out to investigate feasibility of the experimental set-up to effectively simulate the normal shock wave/vortex interaction problem. These experiments included visualization of the generated flowfield in the absence of the vortex to determine the proper blockage needed to create a planar normal shock wave. Figure 6 is a shadowgraph of the flowfield in which a planar normal shock is created by properly adjusting the downstream choke obstruction. The interaction experiments were initiated by placing the vortex generator wing section at an angle of attack of 5^{o} upstream of the normal shock inlet. The strength of this vortex was the weaker of the two vortices considered during previous experiments dealing with the interaction of wing tip vortices and oblique shock fronts.[9] In the experiments of Ref. 9, interaction of this vortex with the strongest attached planar oblique shock at Mach 2.49 did not reveal significant alterations to the structure of the vortex and the vortex was seen to pass smoothly through the oblique shock.

Figure 7 is a shadowgraph of the flowfield taken when the vortex generator is placed upstream of the normal shock inlet. A concentrated wing tip vortex may be seen in the shadowgraph which convects downstream and is seen to pass through the inlet. The above figure indicates that introduction of the vortex upstream of the inlet alters the mass flow rate through it causing the inlet flow to un-choke and the shock wave to be swallowed. As a result, it was necessary to increase the downstream blockage for the interaction experiments involving wing tip vortices. Figure 8a shows a spark shadowgraph of the flowfield generated as a result of the interaction. The above figure indicates a dramatic change in the structure of the flowfield and a strong visual resemblance to the incompressible B-type vortex breakdown. In the shadowgraph of Fig. 8a, the vortex may be seen to expand drastically downstream of a conical shock structure. The forward portion of the conical shock wave is situated approximately 80 mm upstream of the inlet suggesting the strong influence of the subsonic flow

inside the inlet on the character of the resulting flowfield.

The generated flow may be seen to have a strong visual resemblance to the distorted vortex structure observed during the head-on interaction of a streamwise vortex and a wedge[6] and those observed during the strong oblique shock wave/vortex interactions reported in Ref. 9. One notable exception between the present results and those of Ref. 9 is the larger scale of the conical structure observed during the normal shock/vortex interaction in comparison to those observed during the oblique shock wave/vortex interactions. This difference is believed to be due to the larger scale of the subsonic flow downstream of the normal shock which is capable of propagating information upstream as opposed to that observed during the oblique shock/vortex interaction tests. In the present configuration, the entire inlet which has a scale much larger than that of the incoming vortex core diameter is subsonic and is therefore capable of influencing the upstream flow; while the oblique shock/vortex interaction experiments of Ref. 9 revealed a structure containing subsonic flow of limited size which may influence the upstream flow. In Ref. 6, the flow leading to vortex distortion was suggested to consist of two distinct regions; a central subsonic zone consisting of the distorted vortex with its apex situated at the vortex center, and a supersonic region formed between the distorted vortex and the conical shock structure. An interpretation of the flowfield generated during the normal shock wave/vortex interaction based on the vortex distortion model of Ref. 6 is presented in Fig. 8b. Examination of the shadowgraph shown in Fig. 8a and its comparison to that shown in Fig. 7 also indicates that the flow inside the inlet is highly turbulent and remains subsonic.

Multiple spark shadowgraphs of the flow during the normal shock wave/vortex interaction experiments indicated an unsteady behavior of the flowfield leading to formation of conical shock structures of different size. An example of this unsteady flow behavior may be observed by comparing the shadowgraph of Fig. 8a with that shown in Fig. 8c which is taken during the same run but at a later time. However, the subsonic central region containing the burst vortex was limited to the inlet area in all the experiments performed during this study. This observation suggests that interaction of wing tip vortices with normal shock fronts leading to vortex breakdown is strongly governed by the extent of the subsonic region downstream of the undisturbed normal shock wave. Another important facet of the interaction leading to vortex breakdown may be seen by examining Figs. 8a and 8c which indicate a strongly curved shock in the vicinity of the vortex center while outside this region the shock may be seen to be straight. The length scale associated with the curved portion of the conical shock wave is seen to be on the order of the vortex viscous core diameter (about 4 mm for this case) suggesting that supersonic vortex breakdown is largely a viscous phenomenon. This observation is of significant importance when considering inviscid computations of the normal shock wave/vortex interaction as well as supersonic vortex dominated flows with vortex breakdown.

The aforementioned shadowgraphs also indicate a significantly higher turbulence levels downstream of the conical shock structure as a result of shock wave/vortex interaction. Although a universally accepted feature of low speed vortex breakdown is the formation of a highly turbulent region, a fundamental difference between incompressible vortex breakdown and vortex bursting in crossing a shock wave exists. An examination of the quasi-steady state of the flowfield, similar to those seen in Figs. 8a and 8c indicates that the normal shock wave/vortex interaction problem degenerates into the problem of a streamwise vortex crossing a highly curved shock structure with the shock being normal to the axial flow direction at the vortex axis. As a result, the degree of fluctuating turbulent components and Reynolds stresses in the vortex will be subject to amplification in crossing the strong shock wave in a manner similar to those observed during shock wave boundary layer interactions[10-12] as the

vortical structure result from separation of the boundary layer. This is particularly important when applying a low-speed turbulence model in computational solutions of the shock wave/vortex interaction with vortex breakdown.

Planar laser-sheet visualizations of the flowfield during a typical interaction are illustrated in Figs. 9a-9c at three different axial locations. Figure 9a is a slice of the flow upstream of the conical shock structure and represents the state of the undisturbed vortex structure. Figures 9b and 9c on the other hand, represent planar visualizations of the flow at two axial locations downstream of the conical shock. The aforementioned figures clearly illustrate a significant growing of the vortex size with the downstream distance, which is also a known characteristic of the incompressible vortex breakdown.

Further insight into the problem, particularly the unsteady character of the interaction, may be gained by considering the results of pitot pressure measurements. It should be mentioned that these measurements are not capable of providing details of the turbulent properties in the flow. Figure 10 illustrates the time history of the measured pitot pressure for a 50 ms period. In Fig. 10 and subsequent time history plots, t = 0 is arbitrary and represents the start of data acquisition process which is well after establishment of supersonic flow in the test section. The above figure clearly demonstrates a bi-modal character of the flow. One mode corresponds to the case for which the probe is upstream of the burst region (representing pitot pressure measurements of the undisturbed vortex); while the second mode represents the case for which the probe is inside the conical structure (i.e burst vortex). Examination of the standard power spectral density of the pitot pressure measurements at several sampling frequencies indicated a highly repeatable frequency of about 160 Hz associated with the occurrence of the two modes. An example of the normalized power spectral density distribution indicating the frequency distribution of the unsteady motion is shown in Fig. 11.

To associate the observed modes with the state of the flowfield, simultaneous measurements of the pitot pressure and spark shadowgraphs of the flow were obtained. Analysis of this procedure indicated that the first mode representing the case for which the probe is upstream of the burst conical region, is characterized by a higher mean pitot pressure and relatively high amplitude fluctuating pressures. On the other hand, the second mode, representing the case in which the probe is inside the conical structure, had a substantially lower mean value and lower amplitude pitot pressure fluctuations. At least two pieces of evidence exist to support this argument. First, the mode in which the probe is outside the conical region should closely correspond to that of the undisturbed vortex which is argued to be the mode with higher mean pressure shown in Fig. 10. Measurements were performed in the undisturbed vortex core by removing the downstream inlet blockage and preventing the formation of a normal shock. An example of pitot pressure time history for this case covering a period of 15 ms is shown in Fig. 12. Comparison of pressure traces for mode 1 shown in Fig. 10, and measurements in the vortex core illustrated in Fig. 12, clearly demonstrates close agreements in terms of amplitude, frequency, and mean values. The second and stronger evidence supporting the aforementioned argument is obtained by correlating the exact time at which the shadowgraphs were taken with the measured pitot pressure. This is illustrated in Figs. 13a and 13b at two distinct time intervals during the same run. The instant at which the spark light source for the shadowgraphs is activated along with the shadowgraphs corresponding to them are shown in the above figures.

Figure 12 also indicates a relatively high frequency (approximately 1.2 kHz) and amplitude fluctuations about a mean value of $p_t/p_0 = 0.39$ in comparison to that of the empty test section which has a value of 0.50. The lower value of pitot pressure relative to that of the free stream is in agreement with the conical probe measurements of Ref. 7 in the core of the vortex. However, the

fluctuations of pitot pressures were not detected in the measurements of Ref. 7 due to the damping effect of conventional probes with finite tubing length. These fluctuations are believed to be due to the vortex meandering phenomenon and since gradients of flow properties in the vortex core are large,[7] any slight meander of the vortex will produce large amplitude pitot pressure fluctuations. Similar type of vortex meander was observed during the head-on interaction of a wing tip vortex with a wedge in a Mach 3 flow.[6] In contrast to mode 1, the second mode in which the probe is immersed in the conical burst region has significantly lower mean ($p_t/p_0 \sim 0.1$) and fluctuating pressures. Although the exact cause of these observations are not well understood at the present time, a candidate mechanism to explain this behavior may be the formation of a reversed flow and a stagnation region in the burst structure which is a universally accepted characteristic of incompressible vortex breakdown. More detailed measurements of this region using other techniques are needed to substantiate this argument.

Results for the strong vortex

Interaction experiments incorporating stronger wing tip vortices were carried out by placing the vortex generator at an angle of attack of 10 deg. The axial and swirl Mach number distributions for the 10 deg. vortex as reported in Ref. 7. were shown in Figs. 4 and 5 respectively. Interaction of this vortex with a strong oblique shock in a Mach 2.49 flow revealed a significant expansion of the vortex core downstream of a separated shock structure.[9] Successive spark shadowgraphs of the flowfield during a typical run for this strong encounter are presented in Figs. 14a and 14b. The flow may be seen to have a strong visual resemblance to the 5^o case discussed earlier. The length scale associated with the curved portion of the conical shock wave is again seen to be on the order of the vortex viscous core diameter. Similar to the 5 deg. case, the unsteady nature of the flow together with the formation of a conical and highly turbulent region are also apparent.

A notable difference between the strong and weak vortex interactions does however exist. Figure 15 is a time history plot of the measured pitot pressure for a period of 15 ms. An examination of the above figure indicates a higher frequency associated with the two modes and a substantially lower mean pitot pressure in mode 1 relative to the 5 deg. case. The lower mean pitot pressure measured is again consistent with the measurements of Ref. 7 for the stronger vortex. The frequency of occurrence for the two modes has more than doubled for this case (on the order of 375 Hz) while the distinction between the modes are not as clear as the 5^o case. Conversely, the mean value of the measured pitot pressures for mode 2 is approximately the same as the one observed for the weak vortex (0.09 for the strong vortex vs 0.1 for the weak vortex). In summary, interaction experiments involving the strong vortex exhibited many characteristics of the weak vortex case which was discussed earlier.

Study of the pitot pressure history plots for the interaction of weak (Fig. 10) and strong (Fig. 15) vortices reveals another feature of the conical structure. The aforementioned figures indicate an almost instantaneous transition from one mode to the next, as is evident from a sharp increase or decrease of the measured pitot pressures. This trend combined with the shadowgraphs shown in Fig. 13, suggest that the pitot pressure remains constant with the downstream distance starting immediately behind the conical shock for interactions involving both vortices.

Conclusions

An exploratory experimental study involving interaction of concentrated streamwise wing tip vortices and normal shock fronts was carried out in a Mach 2.49 flow. Spark shadowgraphs, laser sheet visualizations, and pitot pressure measurements incorporating a fast response pressure transducer indicate a significant change in the structure of streamwise vortices upon encountering a normal shock wave. These observations

revealed that the interaction leads to the formation of an unsteady conical shock wave far upstream of the inlet as well as a highly turbulent flow downstream. Time accurate measurements of the pitot pressure in conjunction with the spark shadowgraphs revealed a bi-modal feature of the flowfield. Although many features of the interaction experiments incorporating weak and strong vortices were found to be identical, some differences in details of the unsteady flow were observed. Interaction of a strong wing tip vortex with a normal shock indicated higher frequency oscillations than that of the weak vortex. Measurements of pitot pressure in the vortex core in the absence of a shock wave revealed a high frequency oscillations due to the vortex meandering phenomenon.

Acknowledgement

The work was supported by the Air Force Office of Scientific Research under Grant F49620-94-1-0210 and NASA Lewis Research Center under Grant NAG3-1378. The assistance provided by Mr. Lester Orlick and Dr. Svetozar Popovic was greatly appreciated during the experimental study.

References

[1]Zatoloka, V., Ivanyushkin, A. K., and Nikolayev, A. V., "Interference of Vortexes with Shocks in Airscoops. Dissipation of Vortexes," Fluid Mechanics, Soviet Research, Vol. 7, No. 4, July-August 1978, pp. 153-158.

[2]Delery, J., Horowitz, E., Leuchter, O., and Solignac, J. L., "Fundamental Studies on Vortex Flows," La Recherche Aerospatiale (English Edition) (ISSN 0379-380X), No. 2, 1984, pp. 1-24.

[3]Metwally, O., Settles, G., and Horstman, C., "An Experimental Study of Shock Wave/Vortex Interaction," AIAA Paper 89-0082, January 1989.

[4]Cattafesta, L. N., and Settles, G. S., "Experiments on Shock/Vortex Interaction," AIAA Paper 92-0315, January 1992.

[5]Kandil, O. A., Kandil, H. A., and Liu, C. H., "Supersonic Quasi-Axisymmetric Vortex Breakdown," AIAA Paper 91-3311, September 1991.

[6]Kalkhoran, I. M, "Vortex Distortion During Vortex-Surface Interaction in a Mach 3 Stream," AIAA Journal, Vol. 32, No. 1, January 1994, pp. 123-129.

[7]Smart M. K., Kalkhoran, I. M., and Bentson, J., "Measurements of Supersonic Wing Tip Vortices," AIAA Paper 94-2576, June 1994.

[8]Kalkhoran, I. M., Cresci, R. J., and Sforza, P. M., "Development of Polytechnic University's Supersonic Wind Tunnel Facility," AIAA Paper 93-0798, January 1993.

[9]Smart M. K., and Kalkhoran, I. M., "The Effect of Shock Strength on Oblique Shock Wave-Vortex Interaction," AIAA Paper 95-0098, January 1995.

[10]Anyiwo, J. C., and Bushnell, D. M., "Turbulence Amplification in Shock-Wave Boundary-Layer Interaction," AIAA Journal, Vol. 20, No. 7, July 1982, pp. 893-899.

[11]Zang, T. A., Hussaini, M., Y., and Bushnell, D., M., "Numerical Computations of Turbulence Amplification in Shock-Wave Interactions," AIAA Journal, Vol. 22, No. 1, January 1984, pp. 13-21.

[12]Trolier, J., W., and Duffy, R. E., "Turbulence Measurements in Shock-Induced Flows," AIAA Journal, Vol. 23, No. 8, August 1985, pp. 1172-1178.

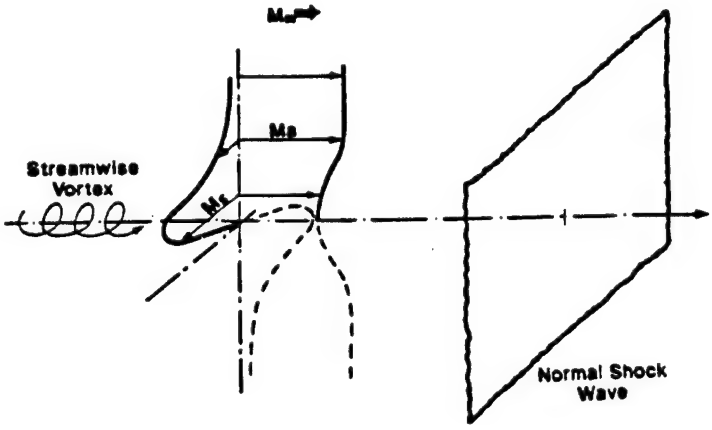

Fig. 1 Schematic representation of the normal shock wave/vortex interaction

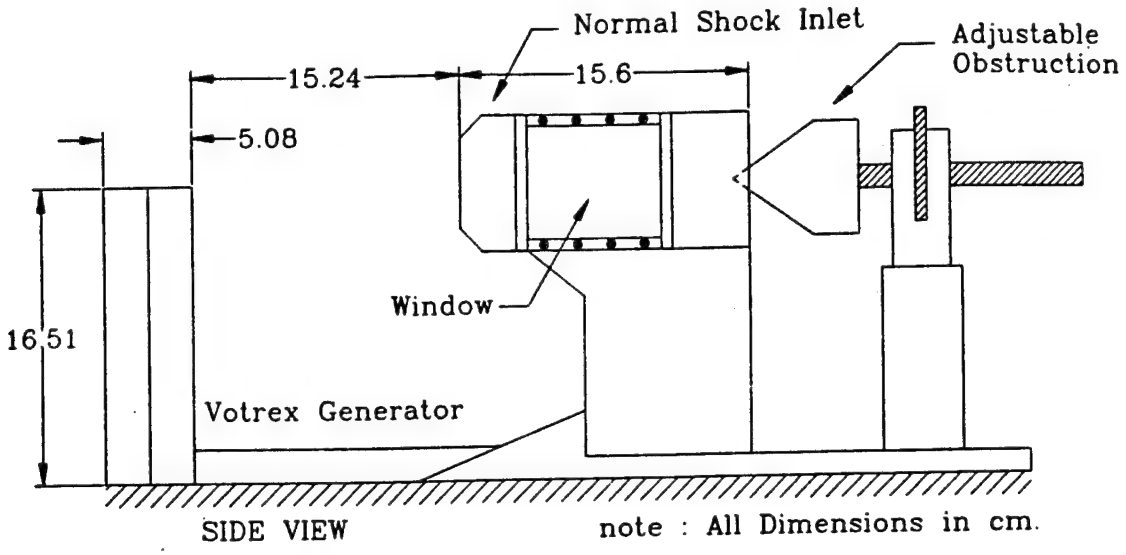

Fig. 2 Schematic of the experimental set-up

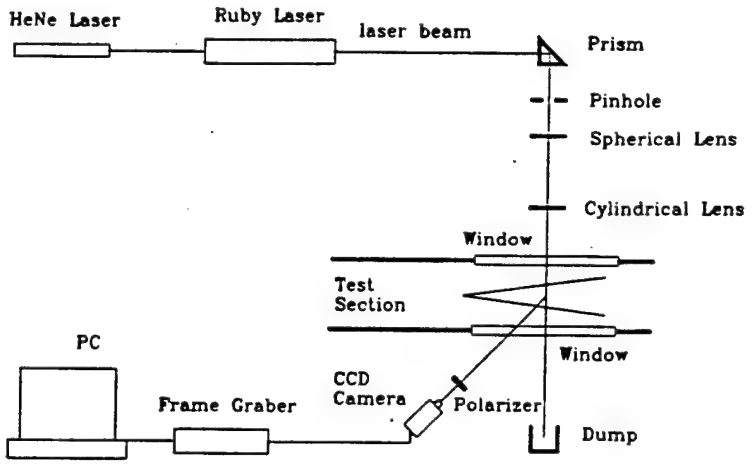

Fig. 3 Schematic of the laser-sheet flow visualization set-up

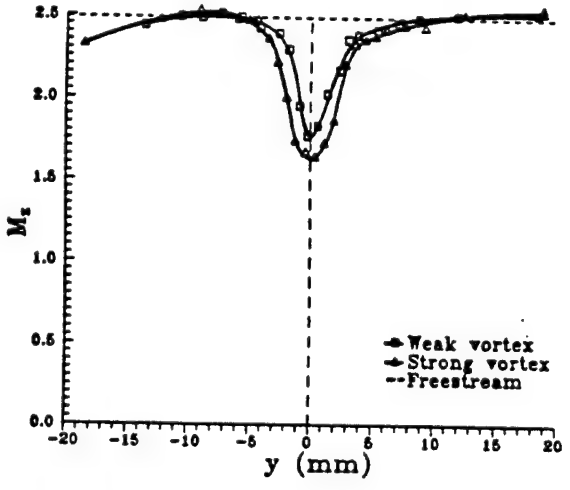

Fig. 4 Distribution of the axial Mach number in the vortex

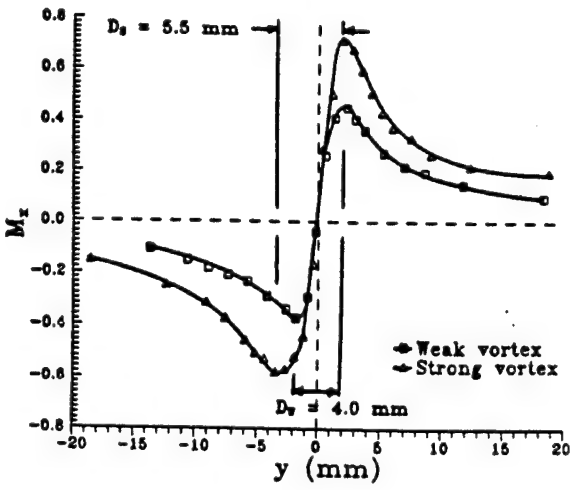

Fig. 5 Distribution of the tangential Mach number in the vortex

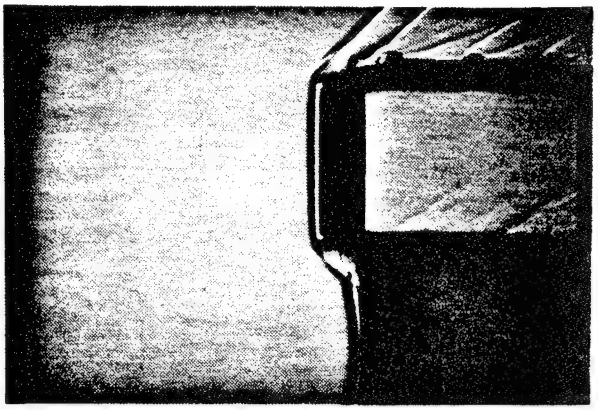

Fig. 6 Shadowgraph of the flow resulting in the formation of a planar normal shock

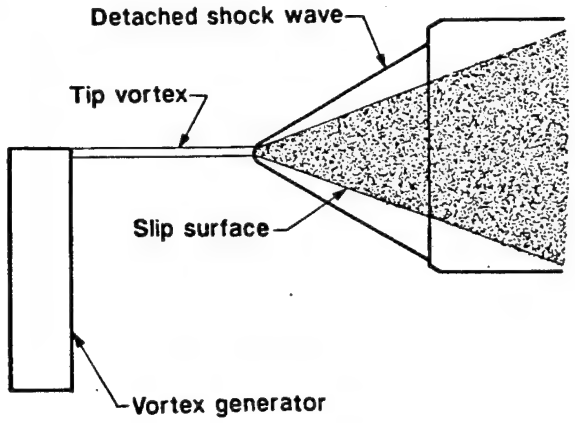

Fig. 8b Interpretation of the shadowgraph observed in Fig. 8a

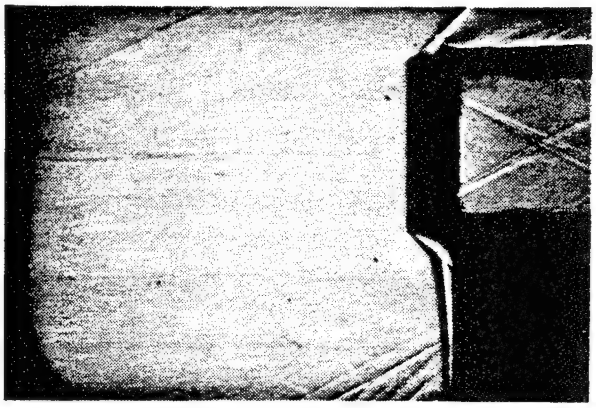

Fig. 7 Shadowgraph of the flow illustrating the vortex passing through the inlet

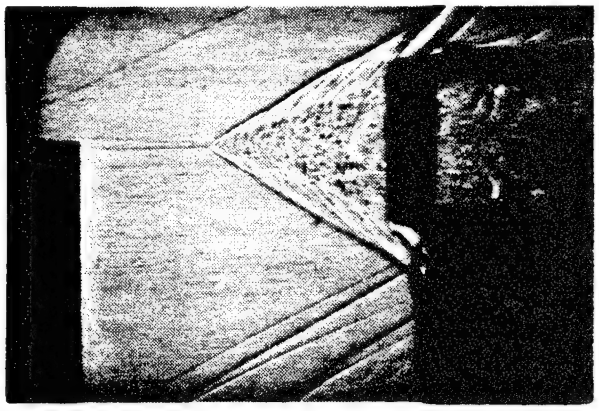

Fig. 8c Shadowgraph of the flow during a weak vortex/shock wave interaction at $t=t_2$

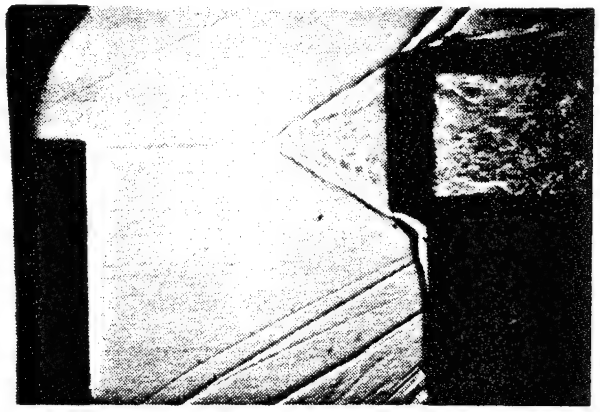

Fig. 8a Shadowgraph of the flow during a weak vortex/shock wave interaction at $t=t_1$

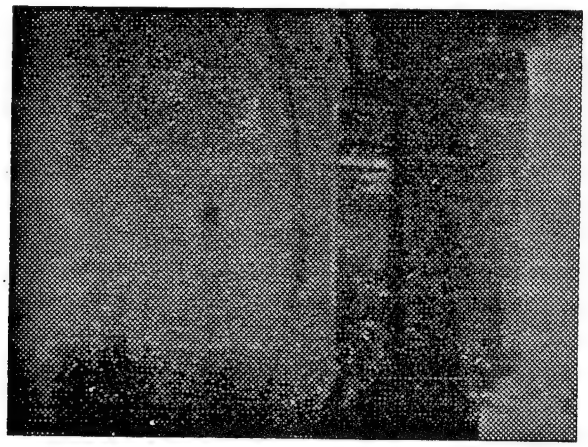

Fig. 9a Laser sheet visualization of the vortex upstream of the conical shock

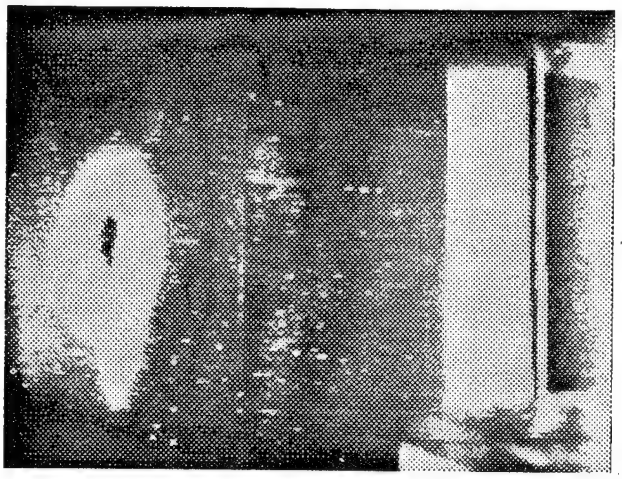

Fig. 9b Laser sheet visualization of the vortex slightly downstream of the conical shock

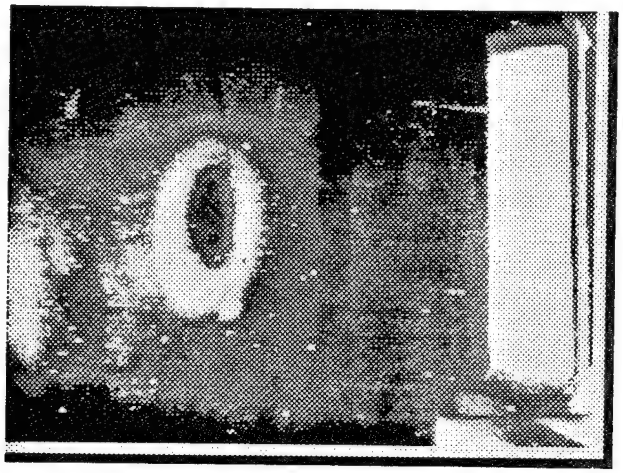

Fig. 9c. Laser sheet visualization of the vortex far downstream of the conical shock

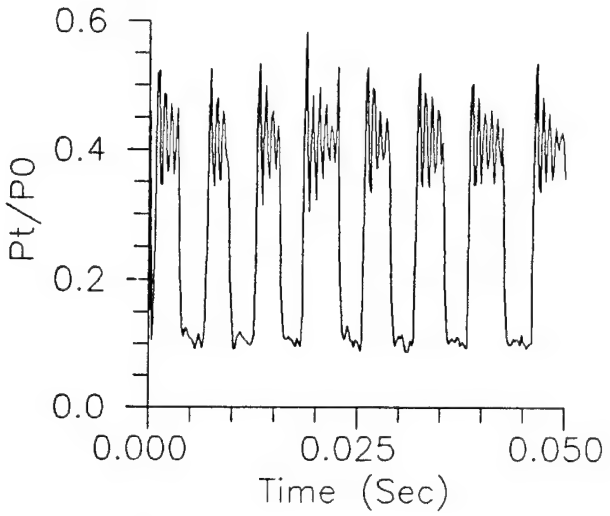

Fig. 10 Time history plot of the pitot pressure during the interaction of the weak vortex

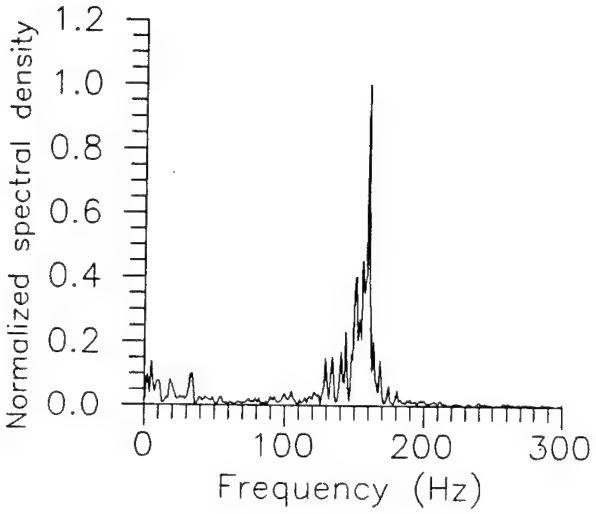

Fig. 11 Power spectral density distribution

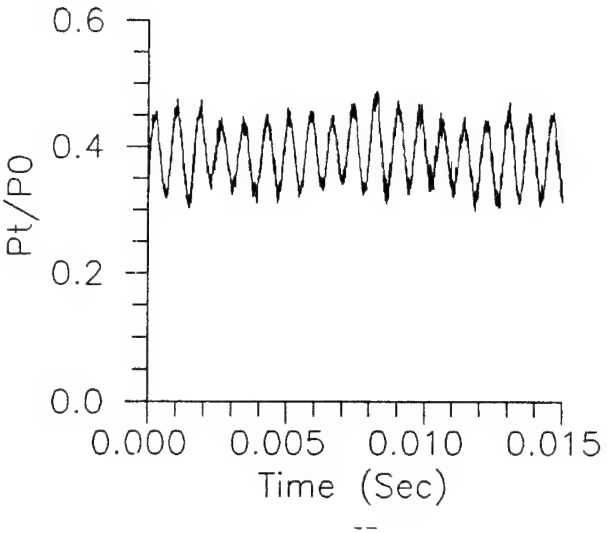

Fig. 12 Time history plot of the pitot pressure in the core of the weak vortex

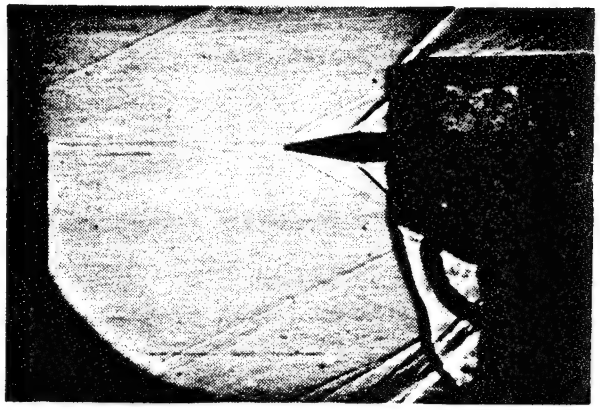

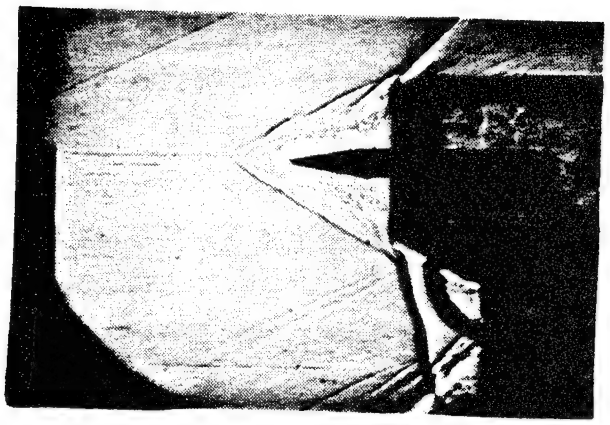

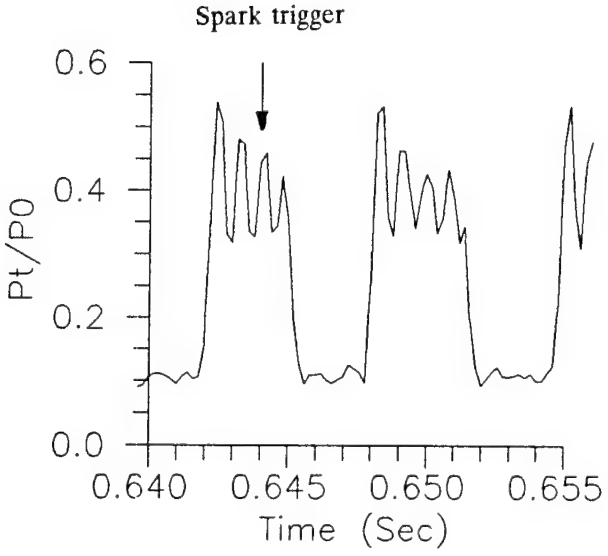

Fig. 13a Shadowgraph of the flow and time history of the measured pitot pressure at $t=t_1$

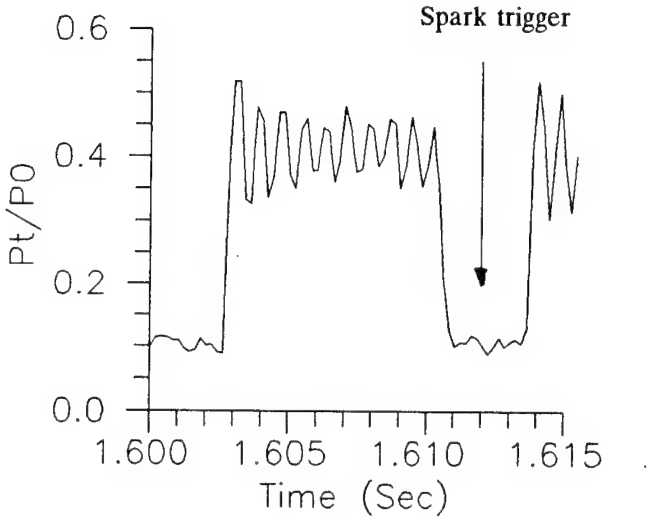

Fig. 13b Shadowgraph of the flow and time history of the measured pitot pressure at $t=t_2$

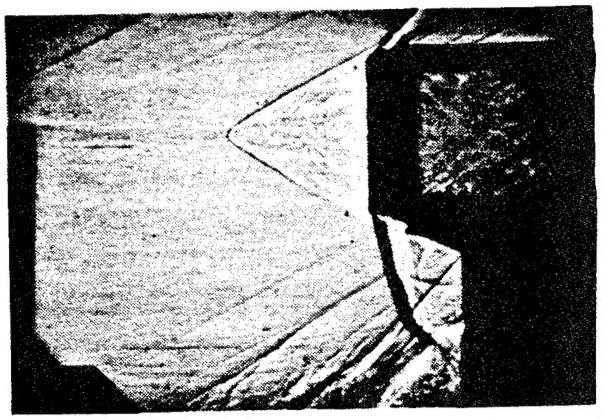

Fig. 14a Shadowgraph of the flow during a strong vortex/shock wave interaction at $t=t_1$

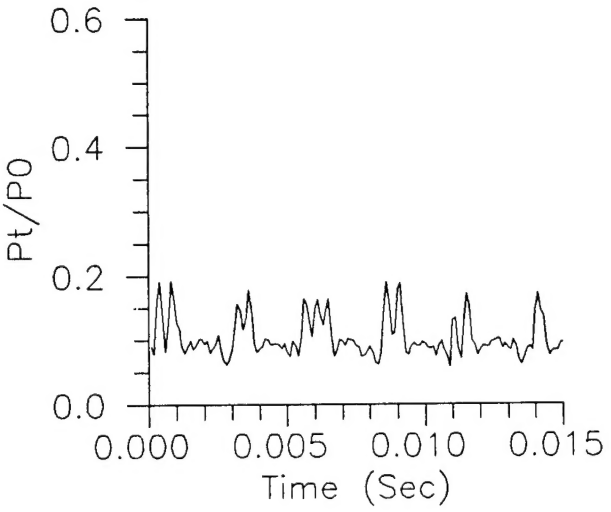

Fig. 15 Time history plot of the pitot pressure during the interaction of the strong vortex

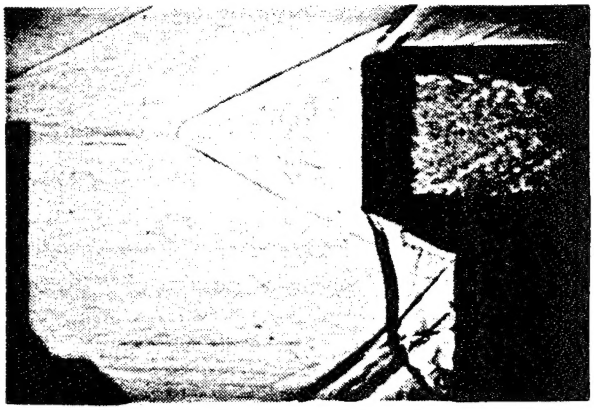

Fig. 14b Shadowgraph of the flow during a strong vortex/shock wave interaction at $t=t_2$

APPENDIX C. JOURNAL PUBLICATIONS

The list of paper accepted for archival publications in the AIAA Journal during the funding period are as follows:

1. Smart, M. K., Kalkhoran, I. M., and Bentson, J., "Measurements of Supersonic Wing Tip Vortices," AIAA Journal In Print.

2. Smart, M. K., and Kalkhoran, I. M., "The Effect of Shock Strength on Oblique Shock Wave Vortex Interaction,", AIAA Journal In Print.

Abstracts of these papers are shown in the following pages.

Measurements of Supersonic Wing Tip Vortices

Michael K. Smart*, Iraj M. Kalkhoran+ and James Bentson**
Polytechnic University, Brooklyn, New York 11201

ABSTRACT

An experimental study of supersonic wing tip vortices has been conducted at Mach 2.49 using small scale 4-hole and 5-hole conical probes. The study was performed 2.25 chords downstream of a semi-span rectangular wing at angles-of-attack of 5.7 and 10.4 degrees. The main objective of the experiments was to determine the Mach number, flow angularity and total pressure distribution in the core region of supersonic wing tip vortices. A secondary aim was to demonstrate the feasibility of calibrating a conical probe using a computational solution to predict the flow characteristics. Results of the present investigation showed that the numerically generated calibration data can be used for pointed nose 4-hole conical probes, but were not sufficiently accurate for conventional 5-hole probes due to nose bluntness effects. A combination of 4-hole conical probe measurements with independent pitot pressure measurements indicated a significant Mach number and total pressure deficit in the core regions of supersonic wing tip vortices, combined with an asymmetric "Burger-like" swirl distribution.

The Effect of Shock Strength On Oblique Shock-Wave/Vortex Interaction

Michael K. Smart* and Iraj M. Kalkhoran+
Polytechnic University, Brooklyn, New York 11201.

ABSTRACT

An experimental study of the interaction between streamwise vortices and two-dimensional oblique shock waves has been conducted at Mach 2.5. The experiments involved positioning an instrumented two-dimensional wedge downstream of a semi-span wing so that the trailing tip vortex from the wing interacted with the oblique shock wave formed over the wedge surface. The experiments were designed to simulate interaction of streamwise vortices with shock waves formed over aerodynamic surfaces or in supersonic inlets. The influence of oblique shock wave intensity on this inherently three-dimensional interaction was examined for vortices of variable strength. Results indicate that the interaction of a moderate strength vortex with an oblique shock wave can lead to the formation of a steady separated shock structure upstream of the oblique shock front. A significant expansion of the vortex core is observed in these cases and the scale of the structure increases with shock wave intensity. In some instances the separated shock structure continues through the oblique shock front to strike the shock generating wedge forming a three-dimensional shock-wave/boundary-layer interaction. The experiments indicate that significant distortion of streamwise vortices can be precipitated by oblique shock fronts with supersonic downstream conditions.